ABSTRACT

Title of Dissertation: CLASSIFICATION OF NORTHERN HEMISPHERE STRATOSPHERIC OZONE AND WATER VAPOR PROFILES BY METEOROLOGICAL REGIME: VALIDATION, CLIMATOLOGY, AND TRENDS

Melanie Beth Follette, Doctor of Philosophy, 2007

Dissertation directed by: Professor Robert D. Hudson
Department of Atmospheric and Oceanic Science

The presence of stratospheric ozone is essential for the survival of life on the Earth's surface. The decrease in the column content of ozone over mid-latitudes from 1979-1991 has previously been attributed to destruction by anthropogenic halogens, and changes in the general circulation. The research presented here shows that a poleward movement of the subtropical and polar upper troposphere fronts is responsible for 35% of this observed decrease.

In Hudson et al. (2003) we showed that the Northern Hemisphere total ozone field could be separated into meteorological regimes, bounded by the subtropical and polar upper troposphere fronts. These regimes were characterized by relatively constant total ozone, tropopause height, and ozonepause height. Negative trends in total ozone within each regime were found for the time period January 1979-May 1991. These trends corresponded to a statistically significant increase in the relative area of the tropical

regime, and decrease in the relative area of the polar regime, indicating a net poleward movement of the subtropical and polar fronts over this time period. This poleward frontal movement was responsible for ~35% of the negative zonal trend in total ozone over this time period and latitude range, the remaining 65% being the result of total ozone changes within the meteorological regimes.

Ozone and water vapor profiles from 1997-2004, from the HALOE and SAGE II satellite-based instruments, were classified by regime. Each regime was characterized by a distinct ozonepause and hygropause height, and profile shape below ~25km, over a wide latitude range (25°-60°N). Therefore, previously reported zonal trends in the lower stratosphere and upper troposphere are a combination of both tropospheric and stratospheric air.

Trends within each regime were calculated for both ozone and water vapor from 1997-2004 and from October 1984-May 1991. The relationship between the observed zonal vertical trends and the trends within each regime were consistent with the idea of meteorological regimes and reinforce the major conclusion of this work. A true understanding of zonal trends in either the column or in the lower stratosphere involves understanding both changes within each regime and changes in the relative weighting of each regime over time.

CLASSIFICATION OF NORTHERN HEMISPHERE STRATOSPHERIC OZONE AND WATER VAPOR PROFILES BY METEOROLOGICAL REGIME: VALIDATION, CLIMATOLOGY, AND TRENDS

by

Melanie Beth Follette

Dissertation submitted to the Faculty of the Graduate School of the
University of Maryland, College Park in partial fulfillment
of the requirements for the degree of
Doctor of Philosophy
2007

Advisory Committee:

Professor Robert D. Hudson, Advisor
Professor Russell Dickerson
Assistant Professor Daniel Kirk-Davidoff
Adjunct Professor Kenneth Pickering
Adjunct Professor Anne Thompson
Professor Christopher Justice

Dedication

To my mother, for her unwavering and unconditional love and support

To my grandmother and grandfather, from whom I learned to love science

Acknowledgements

I would like to express my gratitude to my advisor Dr. Robert Hudson, for his time, patience, guidance, and most importantly, his support throughout my years at Maryland, and to my friend, Dr. Marcos Andrade for his constant help and support.

Table of Contents

List of Tables

List of Figures

Chapter 1: Introduction

Traditionally, temporal trends of ozone in the column and in the vertical have been calculated over latitude bands. However, Hudson et al. (2003) presented clear evidence that the Northern Hemisphere total ozone field can be separated into distinct regimes, the boundaries of which are associated with the subtropical and polar upper troposphere fronts, and in the winter, the polar vortex. These boundaries are not zonal and in fact vary on a daily basis as they meander about their mean latitudes. The upper troposphere fronts are characterized by large gradients in wind speed, temperature, tropopause height, and total ozone (Bluestein 1993; Shalamyanskiy and Romashkina 1980; Shapiro et al. 1982), whereas the regions away from the fronts are characterized by small gradients in tropopause height and total ozone (Defant and Taba 1957; Karol et al. 1987). Therefore, the variability of both total ozone and tropopause height will be smaller within a regime than when calculated over a zonal band. Hudson et al. (2003) defined the boundaries using contours of total ozone. This method of defining the boundary positions is, however, an approximation and can be more exact if the boundary values are allowed to vary with latitude.

If each regime is characterized by relatively constant total ozone and tropopause height, then an average over a zonal band that contains more than one regime will smooth the distinct features found within each regime. This is also true in the vertical. A zonal average taken in the lower stratosphere that contains more than one regime could be averaging both upper tropospheric and lower stratospheric air. However, if classified into meteorological regimes, the lower stratosphere and upper troposphere can be isolated

from one another, allowing for more accurate determination of trends in these regions.

The goals for this work are to:

a) Develop a boundary definition that allows the boundary values to vary with latitude
b) Examine the temporal variability of total ozone between 25° and 60°N within a regime, as well as the contribution made by each regime to the latitude band
c) Examine ozone and water vapor profiles within each regime and calculate climatologies
d) Examine ozone and water vapor trends within each regime

This work is divided into seven chapters. Chapter 2 provides a background on atmospheric structure and circulation as well as the characteristics and distribution of ozone. Chapter 3 describes the method developed to separate the total ozone field into meteorological regimes. Chapter 4 discusses the total ozone within each regime as well as the contribution made by each regime over time. Chapter 5 examines ozone and water vapor profiles within each regime. Chapter 6 presents vertical trends in ozone and water vapor. Conclusions and a description of future work are found in Chapter 7.

Chapter 2: Background

The atmosphere protects life on Earth by absorbing potentially harmful ultraviolet solar radiation. This work will involve the two layers of the atmosphere closest to the Earth's surface: the troposphere, and the stratosphere. This chapter outlines the basic concepts and past literature involved in understanding the theory of meteorological regimes.

2.1 Atmospheric Characteristics – Dynamical

2.1.1 Vertical structure of the atmosphere

The atmosphere consists of four distinct layers, each defined by their unique temperature structure. They are, beginning at the surface of the Earth and increasing with altitude, the troposphere, the stratosphere, the mesosphere, and the thermosphere. The boundaries between these layers are called the tropopause, the stratopause, and the mesopause. The tropopause and its definition will be the only one of these boundaries discussed in detail. A schematic of these layers can be seen in Figure 2.1.

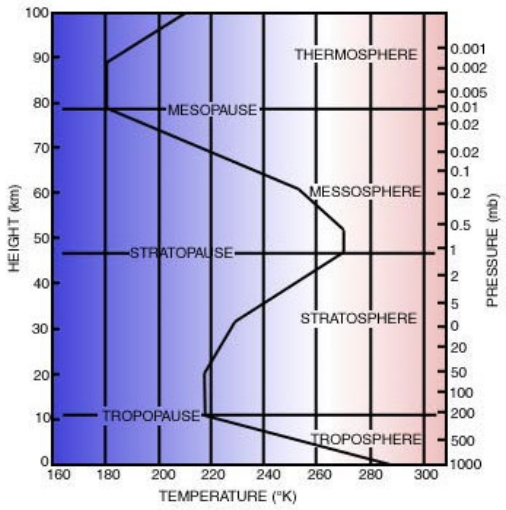

Figure 2.1 Vertical temperature profile of the International Civil Aviation Organization (ICAO) Standard Atmosphere (http://www.met-office.gov.uk/education/secondary/teachers/atmosphere.html#main)

2.1.1.1 The Troposphere

The word troposphere originates from the Greek word "tropos", meaning "turning" or "mixing", referring to the fact that it is characterized by rapid overturning motions. Here, temperature decreases with height at the environmental lapse rate, 6.4 °C for every 1 km increase in height. This is due to both heating from the surface and the adiabatic cooling of air parcels, which is the temperature decrease caused by the expansion of an air parcel as pressure decreases with altitude. The troposphere is more prone to vertical mixing by convective and turbulent transfer. The atmosphere in this region becomes unstable when sensible and latent heat from the surface heat the air above it, making it warmer than the air above.

As stated above, the troposphere is the layer found closest to the Earth's surface, and as such, it is the densest layer. It contains approximately 75% of the mass of the atmosphere, and almost all of the water vapor and aerosols. The inherent turbulence of the atmosphere and abundance of water vapor in this region are the primary reasons why the troposphere is where all of our day-to-day weather occurs.

2.1.1.2 The Stratosphere

The stratosphere reaches from the tropopause to approximately 50 km. It is so named for its stratified temperature profile. In this region, the absorption of incoming solar ultra-violet (UV) radiation by the comparatively large concentration of ozone causes the temperature to increase with altitude, reaching a maximum at the stratopause, leading to very stable conditions. As a result, vertical motions are inhibited, making horizontal motions the dominant factor in this region's chemistry and dynamics.

2.1.1.3 The Tropopause

The tropopause is the boundary region that lies between the turbulent troposphere and the more vertically stable stratosphere. Its height varies with both latitude and season. In the tropics, the tropopause height is approximately 18 km (corresponding to a temperature of ~190 K), whereas at higher latitudes, it can be as low as 8km (~220 K) (Brasseur and Solomon 1984). Thus, despite the warmer temperatures at the surface, the tropopause in the tropics will be much cooler than the tropopause at higher latitudes.

There are several methods to determine the height of the tropopause. Three definitions will be discussed here, the thermal definition, the dynamical definition, and the chemical definition. The 'thermal tropopause' definition utilizes the change in temperature with altitude, or the lapse rate. As described above, the troposphere is characterized by decreasing temperatures with height, whereas temperatures in the stratosphere increase with height. Thus, the tropopause is defined as the lowest height at which the temperature lapse rate decreases to 2 K km^{-1} or less and remains below this value for a depth of at least 2 km (WMO 1957). However, there are disadvantages to this method. The tropopause is not always clearly delineated in the thermal profile, such as in the vicinity of the jet streams (Defant and Taba 1957; Danielsen 1968; Reiter 1975; Hoerling et al. 1991; Bethan et al. 1996), due to the possibility of multiple stable atmospheric layers from the folding of the tropopause. Because of this, the thermal tropopause is most appropriate in the tropics (Seidel et al. 2001; Hoerling et al. 1991).

Many studies use the 'dynamical tropopause', known as a near zero-order discontinuity in potential vorticity between the troposphere and stratosphere (Reed 1955;

Hoerling et al. 1991; Hoinka 1998). Potential vorticity (PV) on an isentropic (constant potential temperature) surface is defined as:

$$PV = -g\frac{(\zeta_\theta + f)}{\frac{\partial p}{\partial \theta}} \tag{2.1}$$

where ζ_θ is the relative vorticity along an isentropic surface, f is the Coriolis parameter ($f = 2\Omega\sin\varphi$), g is gravity, p is pressure, and θ is the potential temperature (Hoskins et al. 1985). Neglecting diabatic and turbulent mixing processes, the potential vorticity of an air parcel is conserved along its trajectory (Shapiro 1980). Thus, PV takes not only the static stability of a parcel into account, similar to the thermal definition, but also the three-dimensional motion of the air. As a result, the vertically stable stratosphere is characterized by comparatively higher values of PV than the troposphere, leading to the near zero-order discontinuity across the tropopause.

In most studies using this method, a 'critical value' of PV is chosen to mark the position of the tropopause, above which all values are considered stratospheric, and below all values considered tropospheric. Many studies have been done to determine the best value; WMO (1986) defined the tropopause by the value of 1.6 potential vorticity units (pvu, 1 pvu = 1 x 10^6 km^2 kg^{-1} s^{-1}). Shapiro (1978, 1980) chose the 10^{-7} K s^{-1} mb^{-1} isopleth of potential vorticity, based on aircraft observations. Hoerling et al. (1991) tested from 2.0 to 5.0 pvu and determined that 3.5 pvu was the best value for automating tropopause height calculations in the extratropics. This result agrees with other estimates (Hoinka et al. 1996; Hoinka 1998; Danielsen 1987). Conventionally, the dynamical tropopause is thought to be best represented by 2.0 pvu (Holton et al. 1995). It should be noted that all of these values will qualitatively delineate the tropopause location.

Ozone, as will explained in more detail later, is a gas that has very different concentrations in the troposphere and stratosphere. Approximately 90% of the ozone in the atmosphere is found in the stratosphere, which therefore has higher mixing ratios than the troposphere. Because of this sharp increase from the troposphere to the stratosphere, ozone is positively correlated with PV, which shows a similar profile, in the lower stratosphere (Danielsen 1968; Danielsen et al. 1970; Danielsen and Hipskind 1980), and can be used to find the position of the tropopause.

Unlike the thermal definition, there is no standard definition for the chemical tropopause. Bethan et al. (1996) defined a tropopause based on the lowest altitude where the ozone profile met the following three criteria,

- The vertical gradient in ozone mixing ratio exceeds 60 ppbv km^{-1} over a depth of approximately 200 m
- The ozone mixing ratio is greater than 80 ppbv
- The ozone mixing ratio immediately above the tropopause is greater than 110 ppbv

The minimum ozone mixing ratio was chosen based on typical ozone/PV ratios around the tropopause. Also, the third criterion was established to exclude layers of stratospheric air intruding into the troposphere. Bethan et al. (1996) examined ~600 ozonesonde and radiosonde measurements over northern Europe. They concluded that when the thermal tropopause was clearly defined, the thermal tropopause and the chemical tropopause agreed well, and the chemical tropopause was approximately 1 km lower in altitude than the thermal 98% of the time. However, they identified instances where there were large differences between the two, and the chemical tropopause marked the more correct

location. These instances were in the vicinity of the jet streams and at high latitudes in winter, when temperatures continued to decrease above the thermally defined tropopause.

2.1.2 General circulation of the atmosphere

Radiation from the sun represents approximately 99.9% of the energy that heats the Earth's surface. This energy can be reflected and scattered by the atmosphere, re-radiated by the atmosphere, or re-radiated by the Earth's surface, such that the planetary heat budget is approximately balanced between incoming and outgoing radiation. It should be emphasized that this happens over time, and the pathways listed can be quite complex (Lutgens and Tarbuck 1998).

Energy from the sun is not distributed uniformly over the Earth's surface. Though the energy budget is balanced globally, the same balance is not maintained at all latitudes. Differences in land-sea surface and the angle of the incoming solar radiation (the solar zenith angle) affect the amount of radiation received by the surface. For example, because of the angle of inclination of the Earth with respect to the ecliptic plane (23.5°), only the mid to low latitudes receive sunlight all year round. However, any object with a temperature above absolute zero emits energy, meaning all latitudes are emitting radiation. Therefore, on annual timescales, lower latitudes (36°N- 36°S) receive more radiation than is lost to space. Figure 2.2 shows the annual radiation balance of the planet as a function of latitude (Ackerman and Knox 2003). This radiation and heat 'surplus' results in higher temperatures at the equator and, subsequently, lower temperatures at the poles (Holton 1992).

In order to maintain a balance, the atmosphere and oceans transport energy and heat away from the equator. In 1735 George Hadley proposed a circulation that was simply one large hemispheric convection cell. The higher temperature tropical air would rise and move poleward where it would eventually cool and sink to the surface, and then return to the tropics. Once there, the air would heat and rise again, thus completing the cell.

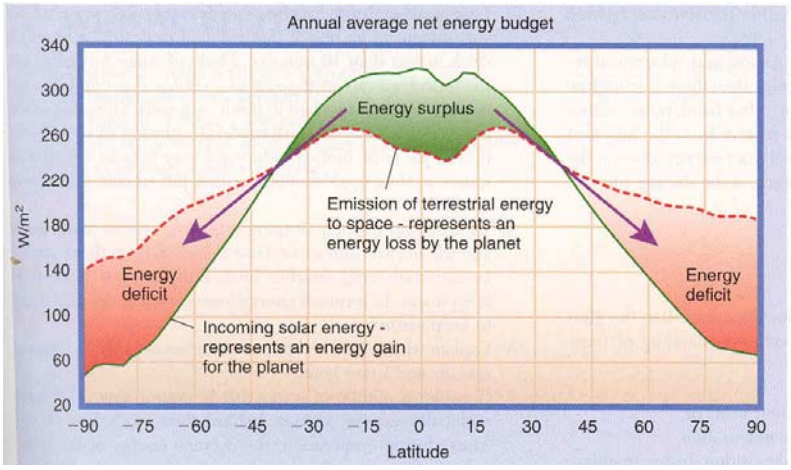

Figure 2.2 The radiation balance of the planet as a function of latitude. (Figure 2.21 and caption from Ackerman and Knox 2003)

However, this circulation did not match observed pressure distributions. Therefore, in the 1920s, the three-cell model was developed. Figure 2.3 shows a diagram of the three-cell model. Similar to Hadley's theory, warm air rises in the tropics and then migrates poleward. However, subsidence occurs long before the air reaches the pole, at around 30°, due to radiative cooling as the air moves poleward and eastward. The eastward component of the motion is due to the Coriolis Effect. This effect is a result of the rotation of Earth about its axis, and deflects moving air to the right in the Northern Hemisphere (to the left in the Southern Hemisphere) (Holton 1992), and whose parameter is defined as

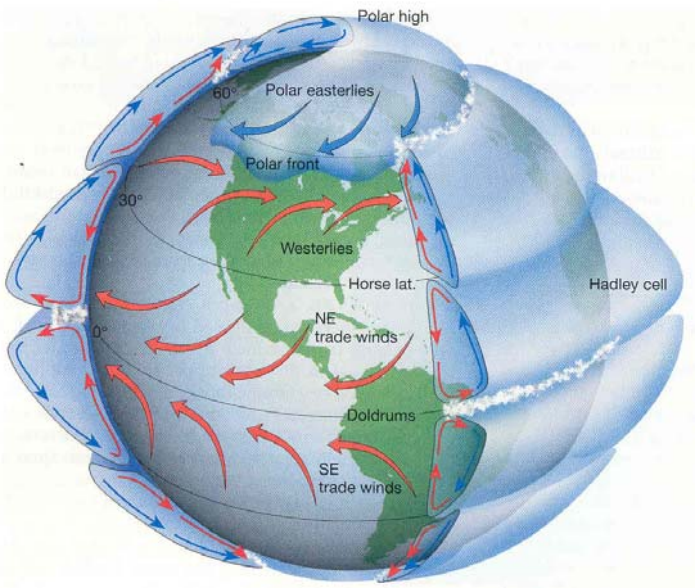

Figure 2.3 Idealized global circulation proposed for the three-cell circulation model of a rotating earth. (Figure 7-5 and caption from Lutgens and Tarbuck 1998)

$$f = 2\Omega\sin\varphi \tag{2.2}$$

where f is the Coriolis parameter, Ω is the angular velocity of the Earth, and φ is the latitude. From this equation we can see that the Coriolis effect increases with latitude. Therefore, by the time air has reached ~30°, it is in a more west-to-east direction (in the Northern Hemisphere) than north-to-south. As the air rises and travels towards the pole it becomes relatively dry, due to the release of moisture. The air experiences additional drying due to the effect of adiabatic compression during its descent. It is worthwhile to note that this region of subsidence is the location of many of the world's deserts. Once this subsiding air reaches the surface, it spreads both poleward and equatorward. The Coriolis force deflects the equatorward flow to form the trade winds, which flow from the northeast to the southwest in the Northern Hemisphere. Once the air reaches the equator, it warms and rises, and completes the first of the three cells, appropriately named the Hadley cell.

The poleward surface flow is also deflected by the Coriolis force to form the mid-latitude westerlies, which are weaker and more sporadic than the trade winds. This is due to the eastward migration of cyclones and anticyclones. This surface flow forms one branch of the Ferrell cell, which extends from ~30° to ~60°. This cell is unique because it is thermally indirect. In other words, it is characterized by subsiding air on the equatorward side of the cell, and rising air at the poleward side. Whereas the Hadley and polar cells are driven by radiative heating, the Ferrell cell is eddy-driven (Holton 1992).

The third cell is the polar cell. This cell extends from ~60° to ~90°. Cold, dense air subsides at the pole and travels eastward and equatorward to form the polar easterlies at the surface. This cold air meets the warmer air from the mid-latitude westerlies and forms a region known as the polar front.

2.1.3 Upper troposphere fronts and jet streams

A front is defined as a boundary between two air masses. It is usually an elongated zone of strong temperature gradient and relatively high static stability. A jet is defined as an intense (minimum wind speed of 30 m s^{-1}), narrow quasi-horizontal or horizontal current of wind that is associated with strong vertical shear (greater than 5-10 m s^{-1} km^{-1}) (Bluestein 1993). They are sometimes discussed together as "jet-front systems."

Both phenomena are characterized by strong temperature gradients and strong vertical shear because of the thermal wind relation. The thermal wind relates the hydrostatic and geostrophic balances such that horizontal gradients of temperature must

be accompanied by vertical gradients of wind in the atmosphere. The u_g component can be written in pressure coordinates as,

$$\frac{\partial u_g}{\partial p} = \frac{R}{fp}\left(\frac{\partial T}{\partial y}\right)_p \tag{2.3}$$

where p is pressure, R is the dry air gas constant (287.05 J kg^{-1} K^{-1}), T is temperature, and f is the Coriolis parameter. This relationship also tells us that as the temperature gradient increases, so does the wind velocity. This increase in wind velocity can also be viewed from the point of conservation of angular momentum. Angular momentum is the product of mass, the perpendicular distance from the axis of rotation, and the tangential velocity. Therefore, a parcel of air moving poleward on a level surface will experience a decrease in the distance from the axis of rotation, and must increase its eastward zonal velocity to conserve angular momentum (Hartmann 1994).

Both hemispheres contain two permanent upper-troposphere fronts, the subtropical and polar fronts, which are associated with the subtropical and polar jet streams, respectively. These fronts are vital to the balance of the Earth's energy budget as they transport energy poleward through Rossby wave breaking. In addition, this flow aloft is largely responsible for surface weather patterns and storm tracks. Therefore, resolving the location and evolution of these systems is vital to both day-to-day weather prediction and climate variability. Each front will be described in more detail below, in addition to the Northern Hemisphere polar vortex.

2.1.3.1 The subtropical front

The subtropical jet stream is a westerly jet near 200 mb, and is usually located between 25° and 35° (Shalamyanskiy and Romashnika 1980; Bluestein 1993) though at

various times of the year it can migrate to higher latitudes. The horizontal (or quasihorizontal) zone of temperature gradient below the subtropical jet is referred to as the subtropical front (Bluestein 1993). This temperature gradient is relatively shallow compared to that of the polar front. Thus, it can appear and disappear on standard isobaric chart levels and as result, can be difficult to isolate (Djuric 1994). However, on average the subtropical front appears continuous around the globe. It is also worthwhile to note that the subtropical jet is thermally driven. Referring back to the three-cell model above, the Hadley cell circulation is a result of radiative heating and thermal convection in the tropics; this air is then driven poleward (Lee and Kim 2003).

2.1.3.2 The polar front

The polar front is a slanting, narrow transition layer associated with the polar jet stream (Djuric 1994). This layer is deeper than that of the subtropical front, and the associated jet stream is stronger because of the larger low-level temperature gradients and vertical wind shear, in accordance with the thermal wind relation given above. When this front becomes very narrow, it becomes a discontinuity in several meteorological variables such as temperature, humidity, and wind speed and direction.

The polar jet is usually found at approximately 300 mb (Shalamyanskiy and Romashkina 1980; Bluestein 1993). Unlike the subtropical jet, the polar jet is not thermally driven. The polar jet is located in the poleward branch of the thermally indirect Ferrell cell. Recall from the discussion above, that the flow in this region aloft and at the surface is poleward and westerly, and is not result of radiative heating resulting in convection. The polar jet is driven by baroclinic eddies. Lee and Kim (2003) reported

several two-layer quasigeostrophic model studies that demonstrated baroclinic eddies were capable of spontaneously generating a jet, even in the absence of a pre-existing jet.

2.1.3.3 The polar vortex

The polar vortex is a persistent, wintertime phenomena found in the mid to upper troposphere and stratosphere of both the Northern and Southern Hemispheres. It is a large-scale cyclonic circulation pattern characterized by circumpolar winds and cold temperatures in the interior of the region (Nash et al. 1996). It has been conclusively shown that the high winds and high PV associated with the polar vortex form a coherent air mass with a distinctly different chemical composition than the surrounding air masses (Nash et al. 1996 and references therein). Within the polar vortex, heavy ozone depletion takes places as a result of heterogeneous chemistry on polar stratospheric clouds (PSCs). This depletion is not as severe as in the Antarctic due to the increased wave activity and higher temperatures found in the Northern Hemisphere (Solomon 1999).

2.1.3.4 Upper-troposphere fronts and tropopause height

There is a feature of these fronts that is essential to this work; the tropopause height changes across a front. More specifically, as the front is crossed from the equatorward side to the poleward side, there will be a decrease in tropopause height. This can be seen by examining the thermal wind relation for the component of the geostrophic wind normal and to the left of the temperature gradient (Bluestein 1993),

$$-\frac{\partial u_g}{\partial p} = -\frac{1}{f_o}\frac{\partial}{\partial y}\left(\frac{RT}{p}\right)_p \tag{2.4}$$

where all the terms have been defined previously. Also consider the equation for potential temperature, θ,

$$\theta = T\left(\frac{p_o}{p}\right)^{R/C_p} \tag{2.5}$$

where C_p is the specific heat of air and p_o is the surface pressure (1000 mb). By substituting eq. (2.5) into (2.4), and taking a partial derivative with respect to pressure we obtain,

$$\frac{\partial^2 u_g}{\partial p^2} = \frac{1}{f_o}\frac{\partial}{\partial y}\left(\frac{RT}{p}\frac{1}{\theta}\frac{\partial \theta}{\partial p}\right)_p \tag{2.6}$$

Considering

$$\sigma = -\frac{RT}{p}\frac{\partial \ln\theta}{\partial p} \tag{2.7}$$

it follows that

$$\frac{\partial^2 u_g}{\partial p^2} = -\frac{1}{f_o}\frac{\partial \sigma}{\partial y} \tag{2.8}$$

At the jet wind maximum,

$$\frac{\partial^2 u_g}{\partial p^2} < 0 \tag{2.9}$$

Considering both eqs. (2.8) and (2.9), one can see that $\frac{\partial \sigma}{\partial y} > 0$. Therefore the static stability parameter must increase toward the "cold" side of the jet (Bluestein 1993). Remembering that the stratosphere is more stable than the troposphere, this equation implies a decrease in the altitude of the tropopause on the cold side of the front. This feature has been observed and reported in the literature (Reed 1955; Defant and Taba 1957; Danielsen 1968; Shapiro 1978, 1980, 1985; Keyser and Shapiro 1986; Shapiro et

al. 1987). Therefore, the highest tropopause heights will be found equatorward of the subtropical front, and the lowest poleward of the polar front. Defant and Taba (1957) plotted all available soundings for January 1, 1956 and constructed a tropopause map for this day using the thermal definition for the tropopause described above. They found that the fronts stood out clearly in the gradient of tropopause height. Figure 2.4 shows the hemispheric tropopause map taken from their study. From this figure one can observe high tropopause heights in the tropics, a sharp gradient representing the subtropical front, lower tropopause heights between the two fronts, another sharp gradient representing the polar front, and the lowest tropopause heights near the poles. They then used the two upper-troposphere fronts as boundaries to separate the hemisphere into five regions: polar, polar-front jet, middle, subtropical jet, and subtropical. When they examined the soundings within each region, they observed that the polar, middle, and subtropical groups each had distinct tropopause heights and temperatures that varied little within their respective region. Next, they calculated a mean-meridional cross section of temperature, shown in Figure 2.5 to demonstrate the threefold structure of the tropopause. Later, Shapiro et al. (1987) used data from the Arctic Gas and Aerosol Sampling Program (AGASP) to analyze a possible arctic tropopause fold and polar vortex migration from January 12-14, 1985. Figure 2.6a shows the 500 mb geopotential height field for 0000 UTC January 20, 1985 taken from their study. This figure shows a deep intrusion of polar vortex air over Minnesota. The cross section analyses of potential temperature and wind speed, shown in Figure 2.6b, displays the vertical structure along the line AA' from Figure 2.6a. The cross-section shows two fronts, along with their associated jet streams. Again the threefold structure of the tropopause (shown as the heavy solid line) is evident

from this figure. Based on many case studies of multiple tropopause folding events, Shapiro et al. (1987) proposed a meridional model of the tropopause, shown in Figure 2.7. This model is a good schematic for the tropopause height change across a front.

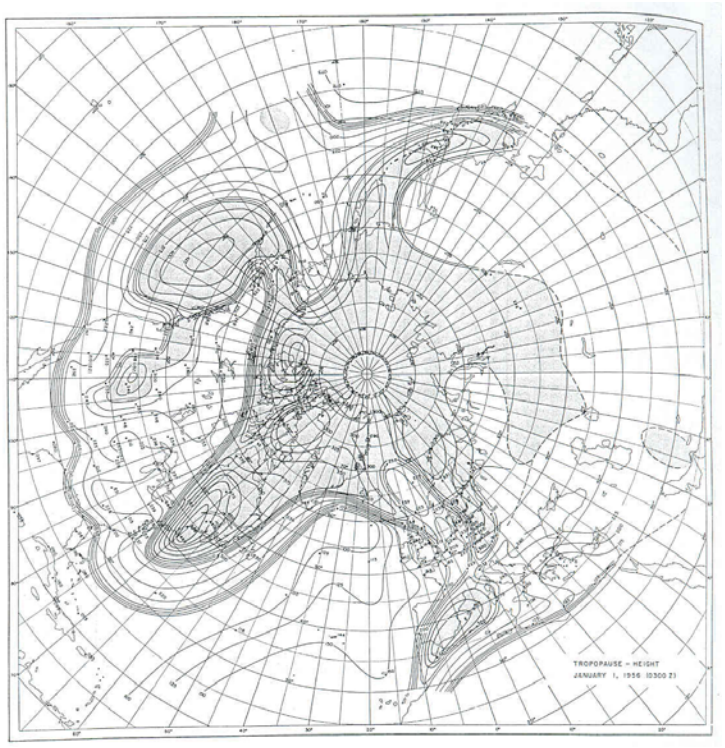

Figure 2.4 Map of Northern Hemisphere tropopause heights (in mb) for 0300Z January 1, 1956. Tropopause breaklines are shown by concentrations of isolines. Dashed lines show approximate breakline continuation. (Figure 2 and caption from Defant and Taba 1957)

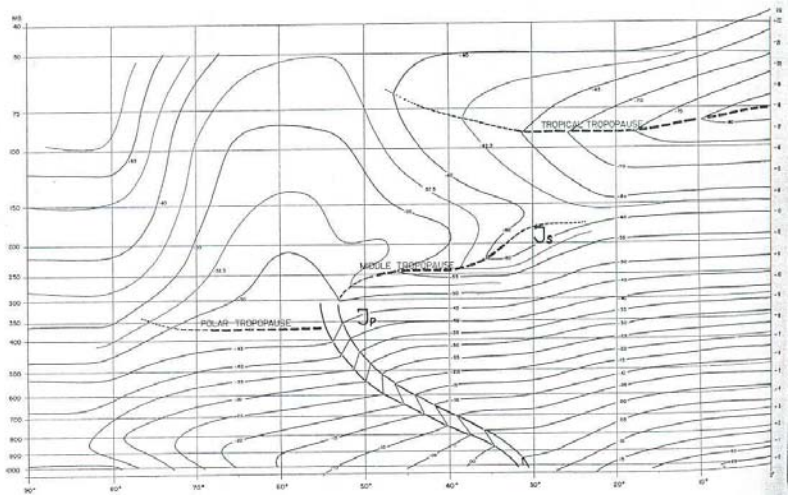

Figure 2.5 Mean meridional temperature cross-section for January 1, 1956. I_p = location of polarfront jet, I_s = location of subtropical jet. (Figure 12 and caption from Defant and Taba 1957)

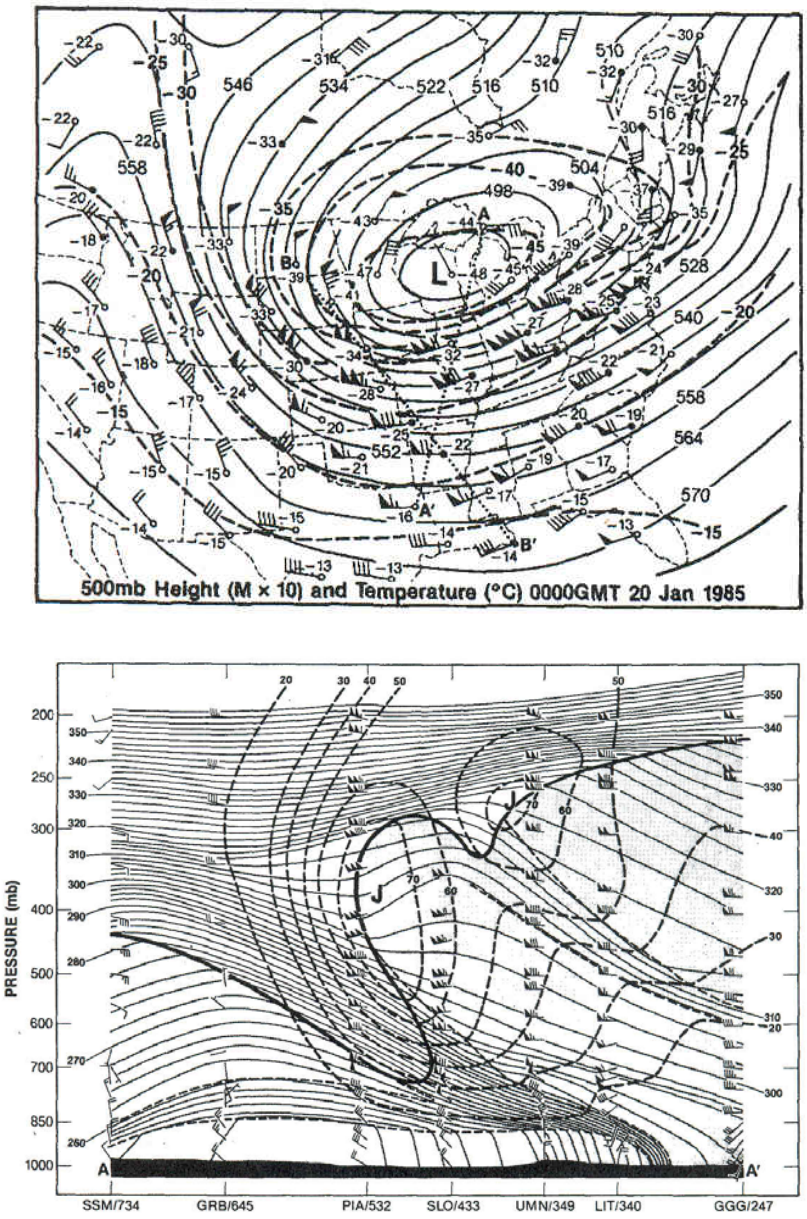

Figure 2.6 a) 500 mb height (dm, solid lines) and temperature (°C, dashed lines) field for 0000 UTC January 20, 1985. Wind vector flags and barbs are as follows: flag = 25 m s^{-1}, full barb = 10 m s^{-1}, half barb = 2.5 m s^{-1}. AA‘ projection line shown as dashed line. (Figure 7 from Shapiro et al. 1987). b) Cross section analysis of potential temperature (K, solid lines) and wind speed (m s^{-1}, heavy dashed lines) for the projection line AA’ from a). Heavy solid line indicates the tropopause (10^{-7} K s^{-1} mb^{-1} isopleth of potential vorticity). Thin dashed lines mark tropospheric frontal boundaries. Wind vectors same as in a). (Figure 9 from Shapiro et al. 1987)

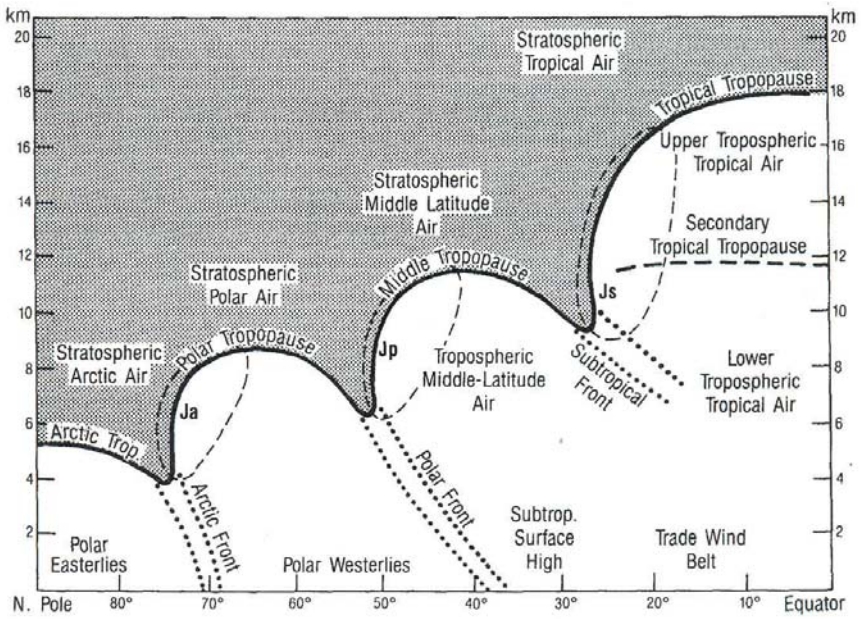

Figure 2.7 Model of the threefold structure of the tropopause. The stratosphere is shown as stippled region. Principle frontal zones, air masses, and wind systems labeled. The 40 m s^{-1} isotach shown as thin dashed circle to indicate cores of primary jet streams, arctic – Ja, polar – Jp, and subtropical – Js. (Figure 17 from Shapiro et al. 1987)

2.2 Atmospheric Characteristics – Chemical

The Earth's atmosphere is made up mostly of nitrogen (N_2, ~78%) and oxygen (O_2, ~21%). Other important trace species that are important to Earth's climate include water vapor, carbon dioxide, methane, nitrous oxide, and ozone. These species and others make up the last 1%. Because of its relevance to this work, in this section we focus on ozone.

2.2.1 Characteristics

Ozone (O_3) is a key species in the chemistry and radiative processes of the atmosphere. It is also crucial to the biosphere. Ozone absorbs shortwave UV radiation in the UVB (λ=280-320 nm), and UVC (220-280 nm) that would otherwise be harmful to

human life (Staehelin et al. 2001). Its distribution throughout the atmosphere is not uniform. Barring heavy tropospheric pollution, approximately 90% of ozone resides in the stratosphere, or in other words, from the height of the tropopause to ~50 km, where the stratopause is usually located. Ozone in the mid to upper stratosphere is in photochemical equilibrium (Brasseur and Solomon 1984) as a result of the Chapman cycle (Finlayson-Pitts and Pitts 2000):

$$O_2 + h\nu\ (\lambda < 242\ \text{nm}) \rightarrow 2O \tag{2.10}$$

$$O + O_2 \xrightarrow{M} O_3 \tag{2.11}$$

$$O + O_3 \rightarrow 2O_2 \tag{2.12}$$

$$O_3 + h\nu\ (\lambda < 336\ \text{nm}) \rightarrow O(^1D) + O_2 \tag{2.13}$$

$$O_3 + h\nu\ (\lambda \leq 1000\ \text{nm}) \rightarrow O(^3P) + O_2 \tag{2.14}$$

The Chapman cycle is dependent on incoming short-wave solar radiation, which is subsequently absorbed by ozone in the mid and upper stratosphere. It is for this reason that ozone in the lower stratosphere has a relatively long chemical lifetime of several weeks (Brasseur and Solomon 1984) compared to the timescale of transport (~1 day) (Salby and Callaghan 1993).

Often, ozone is expressed in terms of its column amount. This is the amount of ozone between the surface of the Earth and the top of the atmosphere. For the purposes of this work, this quantity will be referred to as total ozone. A standard way to express the amount of ozone in the atmosphere, and total ozone, is in Dobson Units (DU). One Dobson unit (1 DU = 1 matm cm, or 2.69×10^{16} O_3 molec cm^{-2}) refers to a layer of ozone 0.01 millimeters thick when compressed to standard temperature and pressure (0°C and 1

atm). Therefore, a total ozone value of 300 DU would, if compressed to standard temperature and pressure, form a slab approximately 3mm thick.

2.2.2 Distribution

A two-dimensional picture of total ozone in the Northern Hemisphere will look like Figure 2.8. The lowest values are found in the tropics, and the largest values at the pole. This is a result of the Brewer-Dobson circulation. Based on observations of water vapor, Brewer (1949) proposed a stratospheric circulation that was characterized by rising motion only in the tropics, and descending motion in the extratropics. Dobson (1956) observed maximum total ozone values at high latitude, despite the fact that the region of maximum ozone production was the tropical upper stratosphere. He suggested that downward and poleward transport were needed to explain this. It should be noted

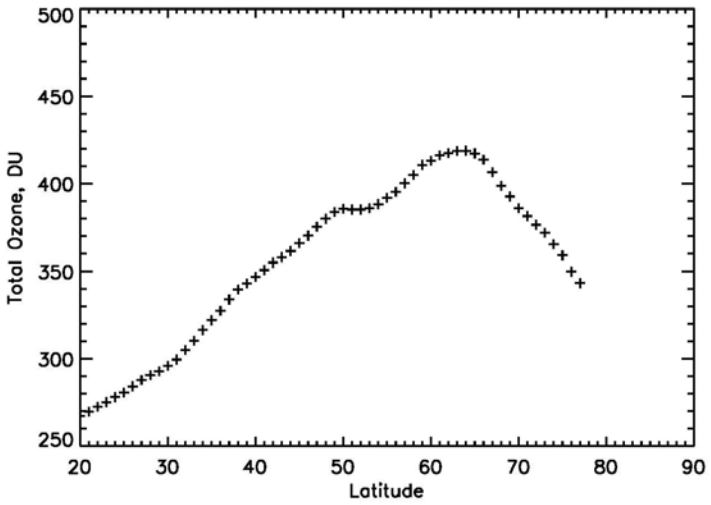

Figure 2.8 One-degree zonally averaged total ozone for March 11, 1990. Total ozone measurements taken from Nimbus-7 TOMS.

again that Figure 2.8 is a two-dimensional picture. Figure 2.9 shows the Northern Hemisphere total ozone field for March 11, 1990, taken from the Total Ozone Mapping Spectrometer (TOMS). Looking at this figure it is clear that the total ozone field is not

two-dimensional, and in fact has little zonal character. Thus, on a given day, other factors are contributing to how total ozone is distributed.

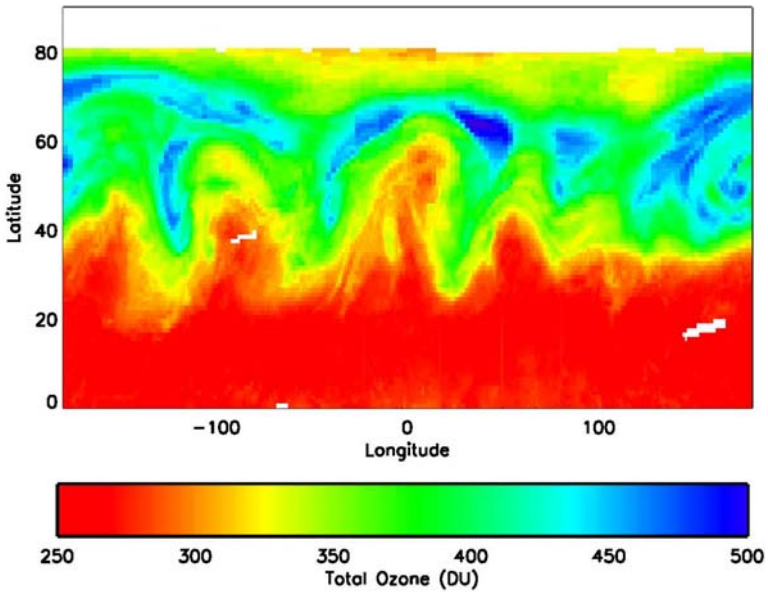

Figure 2.9 Total ozone field taken from Nimbus-7 TOMS for March 11, 1990.

As stated above, almost all the ozone in the atmosphere is located in the stratosphere between the tropopause and ~50km. Since the mid to upper stratosphere is in photochemical equilibrium, day-to-day changes in total ozone are dominated by how much ozone is in the mid to lower stratosphere, and this is in turn affected by the height of the tropopause.

The relationship between total ozone and tropopause height has been observed in various studies. Petzoldt et al. (1994) noted the positive correlation between temperature and ozone mixing ratio up until ~25km. In the lower stratosphere, upward/downward motion transports lower/higher ozone values to higher/lower altitudes. At the same time, the temperature decreases/increases adiabatically. Hoinka et al. (1996) compared total ozone measurements made by a Dobson photo spectrometer at Hohenpeissenberg, Germany with tropopause pressure from rawinsondes measurements from nearby

Munich. They also compared total ozone from TOMS and various tropopause height estimates from the European Centre for Medium-Range Weather Forecasts (ECMWF) analysis. They concluded that 50% of the variations in ozone could be explained by the tropopause pressure. In addition, they calculated that a one-kilometer change in tropopause height was associated with a change in total ozone of 13 DU. Similar results were obtained by Schubert and Munteanu (1988). They compared total ozone from TOMS and tropopause pressure from the National Meteorological Center (NMC) and concluded that 40-60% of the variance in middle latitude total ozone could be explained by changes in tropopause pressure. Steinbrecht et al. (1998) ascribed 30% of a decreasing trend in total ozone at Hohenpeissenberg to an increasing trend in tropopause height, and also computed a 16 DU decrease in total ozone with a one-kilometer increase in tropopause height. Varotsos et al. (2004) examined total ozone and temperature profiles over Athens and attributed a quarter of the decreasing total ozone trend to tropopause variations. They calculated the change in total ozone per kilometer to be 10 DU.

In the discussion above, it was shown through dynamical calculation and the results of experimental studies that the tropopause height changes across an upper troposphere front. Therefore, if changes in total ozone are correlated with changes in tropopause height, they will also be related to movement of the upper troposphere fronts. G. M. B. Dobson was one of the first to observe a connection between variations in total ozone and pressure changes in 1926. He observed high total ozone episodes when the region was under “maritime polar” air, and lower total ozone when a “warm sector of tropical air” neared the region (Dobson et al. 1929).

Shalamyanskiy and Romanshkina (1980) analyzed aircraft measurements and ground based data from the Russian ozone network. The aircraft paths intersected the polar and subtropical fronts 32 times between 1974 and 1977. They observed large gradients in total ozone when they were in the region of a front, and otherwise observed smaller gradients in both the zonal and meridional directions. They suggested that the instantaneous meridional cross section was not a smooth transition from the equator to the pole, as seen in Figure 2.4, but resembled more of a step-wise function, with the "steps" referring to the upper-troposphere fronts.

To ascertain whether this phenomenon extended to the entire hemisphere, for every day in 1975 and 1976 Shalamyanskiy and Romashkina (1980) assigned the 300 mb and 200 mb geopotential height surfaces to represent the altitudes of the polar and subtropical fronts, respectively. On each of these charts, they took the isohypses that best represented the levels of maximum wind speed to represent the positions of the fronts. These were used to separate the hemisphere into three air masses. The total ozone measurements were then plotted onto these charts and in turn, sorted into one of the three air masses. They found that the Northern Hemisphere could be divided into three regions, each with different ozone contents (Shalamyanskiy and Romashkina 1980). They also noted that the isohypses clearly separated the air masses, irrespective of the wind speed. In other words, even in regions where the wind speed was low, there was still a clear distinction between the total ozone values in the neighboring air masses. Later, Karol et al. (1987) performed a similar analysis, separating both temperature and ozone data using the isohypses best representing maximum wind on the 200 mb and 300 mb surfaces. They found that the variability of ozone within an air mass was a factor of 2

to 3 less than for the corresponding latitude zone. This indicated that the total ozone field was fairly homogeneous within each air mass (Karol et al. 1987).

Shapiro et al. (1982) compared aircraft measurements of wind speed, rawinsonde measurements, and total ozone data from TOMS for two case studies. In both cases the ozone isopleths were nearly parallel to the wind direction in the vicinity of the strongest gradient in wind speed. In addition, the ozone gradient was proportional to the wind speed, i.e. the strongest gradient in total ozone was found in the region of the strongest jet stream winds (Shapiro et al. 1980). Because of this Shapiro et al. (1980) recommended that total ozone data be used to nowcast both the position and intensity of the upper troposphere fronts.

In summary, the upper troposphere frontal regions are characterized by large gradients in wind speed, temperature, tropopause height, and total ozone. The regions away from the upper troposphere fronts are characterized by small gradients in tropopause height and total ozone. In addition, ozone in the lower stratosphere has a long chemical lifetime relative to its dynamical lifetime. This makes total ozone an excellent dynamical tracer on synoptic timescales (Danielsen 1968; Danielsen et al. 1970; Shapiro et al. 1982; Salby and Callaghan 1993; Wohltmann et al. 2005). I will therefore be using the gradients in the total ozone field to locate the positions of the upper troposphere fronts. The method I use will be described in detail in the next chapter.

Chapter 3: Method and Validation

As reviewed in the previous chapter, Shalamyanskiy and Romashkina (1980), Shapiro et al. (1982), and Karol et al. (1987) observed gradients in total ozone associated with the upper-troposphere fronts. Shalamyanskiy and Romashkina (1980) and Karol et al. (1987) used the isohype of maximum wind on the 200 mb and 300 mb geopotential height surfaces to delineate the positions of the subtropical and polar front, respectively. Hudson et al. (2003) used the TOMS total ozone field to locate the positions of these fronts.

3.1 Data

The TOMS instruments provide daily high-resolution global maps of total ozone. They measure backscattered solar ultraviolet (UV) radiation in six 1-nm bands; these bands differ for every instrument. Total ozone is retrieved by comparing measured radiances and radiances derived from radiative transfer calculations as a function of total ozone, viewing geometry, surface pressure, surface reflectivity, and latitude (McPeters et al. 1996, 1998, Herman et al. 1996). This work uses version 8, which uses two wavelengths (317.5 nm and 331.2 nm) to derive total ozone. Four other wavelengths are used for diagnostics and error correction. Error analysis done on the data suggests that the algorithm is capable of producing total ozone with rms error of about 2% (Wellemeyer et al. 2004, and references therein). However, these errors are at a maximum at high solar zenith angles and in the presence of heavy aerosol loading.

Data from several TOMS instruments were used in this work. Table 3.1 lists some general features of the satellites that bore these instruments. Both the Nimbus-7 and Earth Probe (EP) TOMS satellites were launched into near polar sun-synchronous orbits. The Meteor-3 satellite orbit precessed relative to the Earth-sun line with a period of 212 days. Thus, the equator crossing time changed within that period (Herman et al. 1996).

Satellite	**Start Date**	**End Date**	**Altitude** (km)	**Inclination** (degrees)	**Orbit period** (min)	**Equator crossing time** (local time)
Nimbus-7	Nov 01, 1978	May 05, 1993	995	104.9	104	Noon
Meteor-3	Aug 15, 1991	Dec 27, 1994	1200	82.5	109	N/A
Earth Probe	Jul 25, 1996	Present	739*	98.4*	100	11:16

***** EP/TOMS was initially launched into a 98°, 500 km orbit to obtain higher resolution data. The failure of the ADEOS TOMS instrument led to the increase in the orbit altitude to provide more global coverage.
Table 3.1 Basic characteristics of satellites that hosted the TOMS instruments used in this work

The level-3 daily gridded total ozone dataset was used. These data are on a 1° latitude by 1.25° longitude grid. The potential vorticity data used here were obtained from National Centers for Environmental Prediction / National Center for Atmospheric Research (NCEP/NCAR) reanalysis data set (Kalnay et al. 1996, Kistler et al. 2001). This dataset is an assimilation of interpolated observational and model data to obtain a "best estimate of the evolving state of the atmosphere" (Kalnay et al. 1996). It is a global data set with 2.5° latitude by 2.5° longitude resolution. It has synoptic fields for 0Z, 6Z, 12Z, and 18Z. Because the TOMS data are at local noon, the reanalysis data were interpolated in time to produce a "TOMS-centered" dataset (Andrade 2004).

3.2 The Boundary as an Ozone Contour

Similar to Shalamyanskiy and Romashkina (1980) and Karol et al. (1987), Hudson et al. (2003) divided the Northern Hemisphere into meteorological regimes separated by the upper troposphere fronts:

1) Tropical regime – area between the equator and the subtropical front
2) Midlatitude regime – area between the subtropical front and the polar front
3) Polar regime – area between the polar front and the polar vortex (or if the vortex is not present, the pole)
4) Arctic regime – the area within the polar vortex

Assuming, based on observations, that the variability within a regime is small compared to the frontal regions, a simple schematic of the total ozone as a function of latitude can be made. This schematic is shown in Figure 3.1 (Figure 4 of Hudson et al. 2003). On it, the subtropical and polar frontal positions have been shown as the midpoint along their respective ozone gradients. This is in fact the approximation made in Hudson et al. (2003). They define a front as the ozone contour that represents the numerical average of the ozone values on either side of the front.

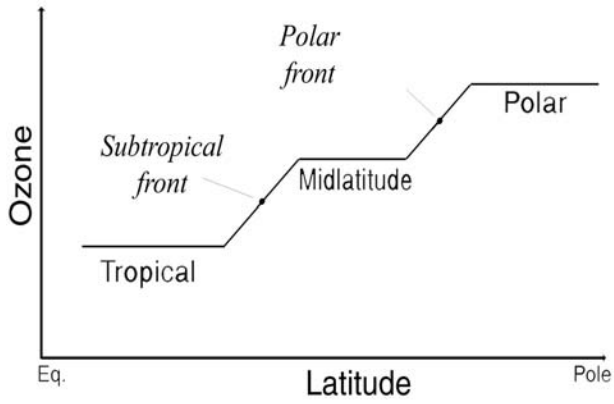

Figure 3.1 Schematic showing total ozone as a function of latitude, including the subtropical and polar fronts. (Figure 4 and caption from Hudson et al. 2003)

Before describing the method used to define these values, one must first delineate the polar vortex boundary. As explained in Chapter 2, the polar vortex is characterized by

ozone loss through heterogeneous chemical processes. Ozone depletion in the Arctic is not as extensive as that of the Antarctic due to increased wave activity and higher temperatures in the Northern Hemisphere (Solomon 1999). However, we earlier stated that total ozone is a dynamical tracer because its chemical lifetime is greater than its transport lifetime on synoptic timescales. This is not necessarily the case inside the polar vortex, where ozone depletion due to chemistry can occur rapidly (Solomon 1999). Therefore, for the purposes of this analysis, the polar vortex becomes a source of noise. In order to define the polar vortex boundary, spatial gradients of PV were calculated on the 550 K isentropic surface. Next the PV value that best represented the region of maximum gradient was chosen as the boundary. This process was repeated for every day such that each day will have a unique PV-defined polar vortex boundary. A five-day running average was used instead of the actual value in order to reduce noise. After other isentropic values were tested and other sensitivity analyses completed, it was concluded that this definition was robust and reliable (Andrade 2004).

An additional aspect that must be explained is the latitude interval chosen for this analysis. The latitude range chosen was 25°-60°N. As stated above, the TOMS instruments use solar backscattered radiation, and thus cannot take measurements when there is no sunlight. A poleward limit of 60°N ensures that data will be available year-round. The region 25°-60°N represents a band in which each regime is represented adequately. Choosing a lower latitude limit would, for example, cause the tropical regime to dominate, leading to possible uncertainties in the boundary values (Andrade 2004).

An iterative method was developed in order to calculate the *ozone* value that best represented each front, hereafter called a "*boundary* value". Based on the work done by Karol et al. (1987), two boundary value climatologies, one for each front, were developed using data from ground-based instruments, rocketsondes, and ozonesondes from the former Soviet Union network (Andrade 2004). The two climatologies are shown in Figure 3.2. The subtropical and polar boundary values, indicated by the red and blue stars, respectively, served as the first guess for the iterative method. The contours for these two values, in addition to the polar vortex boundary, were used to separate the Northern Hemisphere total ozone field into regimes as defined above. As explained in Chapter 2, these frontal regions are characterized by a gradient in total ozone, and are therefore considered to be a transition region between meteorological regimes. In order to exclude values that fall within this transition region, the boundary region was widened by two pixels in both latitude and longitude. The area-weighted mean total ozone between 25°-60°N for the tropical, midlatitude, and polar regimes was then calculated. New boundary values were calculated by taking the numerical average of the mean total ozone on either side of the front such that the new

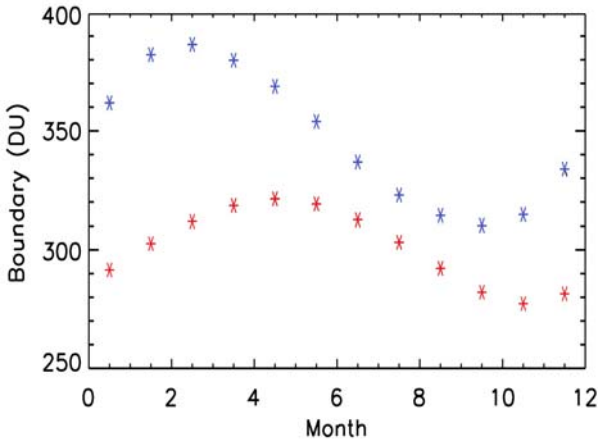

Figure 3.2 Monthly total ozone values for the boundary of the subtropical front (red stars) and the polar front (blue stars) adapted from the Karol et al. (1987) data (Andrade 2004).

subtropical boundary value was the average of the tropical and midlatitude regimes, and the new polar boundary value was the average of the midlatitude and polar regimes. The polar vortex boundary remained the same throughout the iterative process.

These new boundary values were then used to separate the total ozone field, the boundaries were widened, the mean total ozone between 25°-60°N for each regime was calculated, and new boundary values were calculated by taking the average of the regime means. This process was repeated until convergence, which was reached when the new boundary values were within 5 DU of the iteration before. This process is summarized in Figure 3.3. In this way, subtropical and polar boundary values were obtained for every

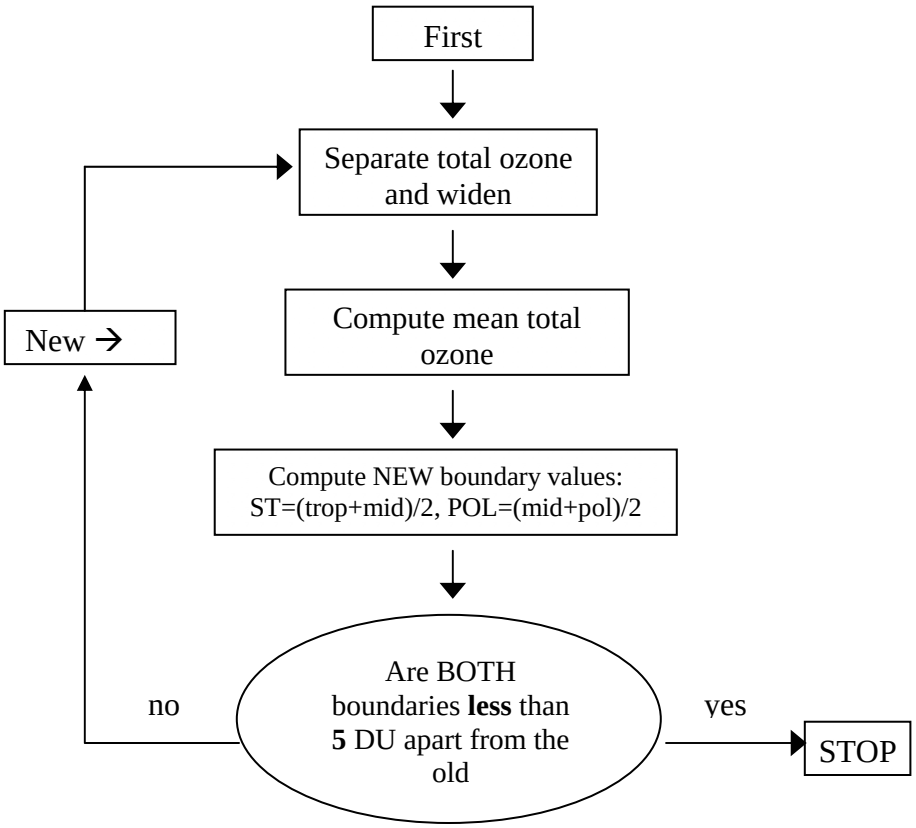

Figure 3.3 Flow chart of the method used to derive the subtropical and polar boundary values from the TOMS data.

day TOMS data were available. In practice, a 30-day running mean of these daily values is used to reduce noise from the daily data. Figure 3.4 shows the total ozone field from Nimbus-7 TOMS for March 11, 1990 (Figure 1 from Hudson et al. 2003). The solid blue and yellow lines represent the subtropical and polar boundaries, respectively, calculated for this day. The solid red line marks the edge of the polar vortex.

Once the boundaries were obtained, Hudson et al. (2003) examined the total ozone within each regime to look for reduced variability away from the front. Figure 3.5 shows a picture similar to Figure 2.8, with the one degree zonal averages within each regime for March 11, 1990 also plotted. Relatively constant (with respect to the un-separated zonal data) total ozone values are observed within a regime. This picture is

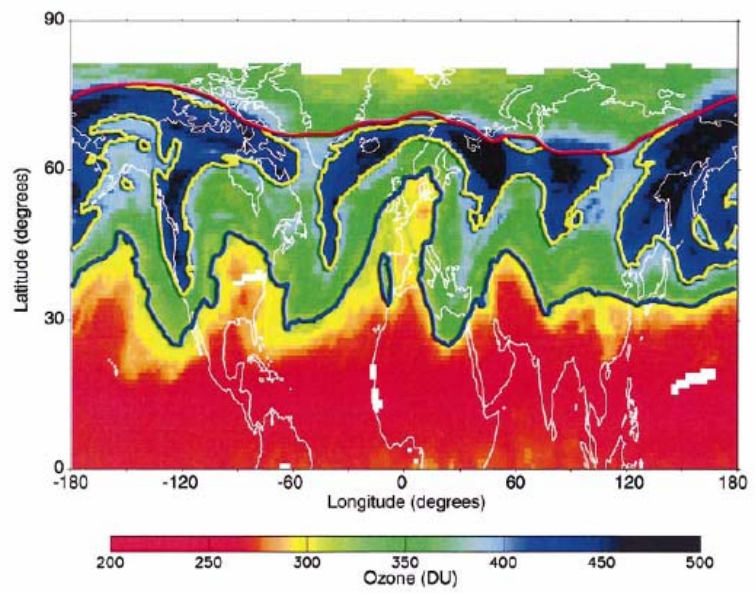

Figure 3.4 Total ozone field from Nimbus-7 TOMS on March 11, 1990. The solid yellow and blue lines represent the polar and subtropical upper tropospheric fronts, respectively. The red line indicates the edge of the polar vortex derived from the sharpest gradient in PV on the 550 K isentropic surface. (Figure 1 from Hudson et al. 2003)

consistent with what previous studies have observed (Shalamyanskiy and Romashkina 1980; Shapiro et al. 1982; Karol et al. 1987). The small total ozone variability seen within a regime should restrict the shape of the ozone profile, given that day-to-day variability in total ozone is dominated by the lower stratosphere. To examine this, Hudson et al. (2003) separated ozonesondes from 1985-1990 into regimes. Figure 3.6 shows twenty profiles, selected at random, for each regime. Each regime does show a distinct lower stratospheric profile shape and ozone-tropopause height.

Given that total ozone is a dynamical tracer and correlates well with tropopause height, one would expect to see relatively constant thermal tropopause heights as observed by Defant and Taba (1957). Figure 3.7 (Figure 8 of Hudson et al. 2003) shows the total ozone field over North America for March 11, 1990. On this figure, the subtropical and polar fronts are shown as blue and yellow lines, respectively, in addition to the rawinsonde measurements for that day, indicated by white circles. Colored crosses in these circles indicate into which regime the measurement fell. Red crosses indicate tropical, green indicate midlatitude, and blue indicate polar. Measurements that fell too close to the boundary were not included in the analysis for reasons stated above, and thus are left as white circles. Figure

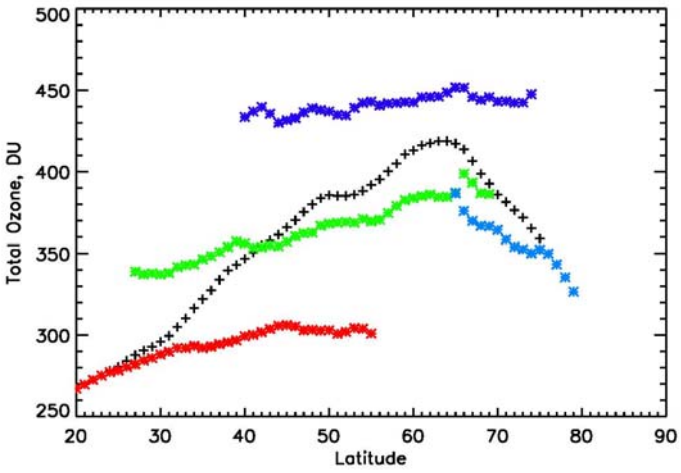

Figure 3.5 One-degree zonal averages within each regime for March 11, 1990. Tropical - red stars, midlatitude - green stars, polar - blue stars, and arctic – light blue stars. The unclassified data is shown as black pluses, as in Figure

3.8 (Figure 9 from Hudson et al. 2003) shows the rawinsonde measurements indicated by crosses in Figure 3.7. As expected, unique tropopause heights and profile shapes are seen for each regime. It should be emphasized that this also supports the previous findings of Shalamyanskiy and Romashkina (1980), Shapiro et al. (1982), and Karol et al. (1987), that the ozone boundary and the meteorological boundary are one and the same. Further, Andrade (2004) examined regions of high winds on the 200 mb surface from the NCEP/NCAR reanalysis dataset for September 5, 1990. When these high wind regions were compared with boundaries derived from the total ozone field, they agreed well. That is, high total ozone gradients corresponded to high winds, and weaker gradients corresponded to weaker winds, similar to the findings of Shapiro et al. (1982).

The above experiments indicate defining the ozone boundary as the numerical average of the neighboring regimes' mean total ozone is a good assumption. However,

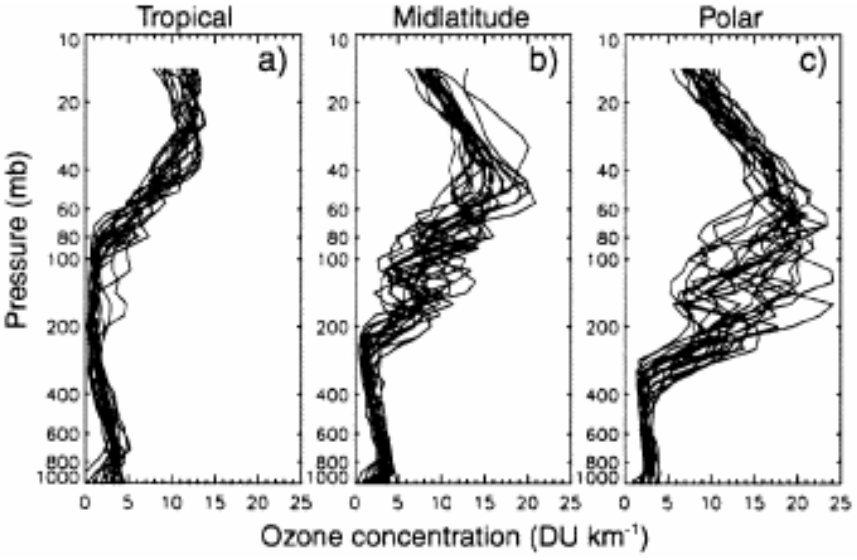

Figure 3.6 Twenty randomly selected March ozonesonde ozone profiles for each regime from the period 1985 to 1990 for the a) tropical, b) midlatitude, and c) polar regimes. (Figure 10 from Hudson et al. 2003)

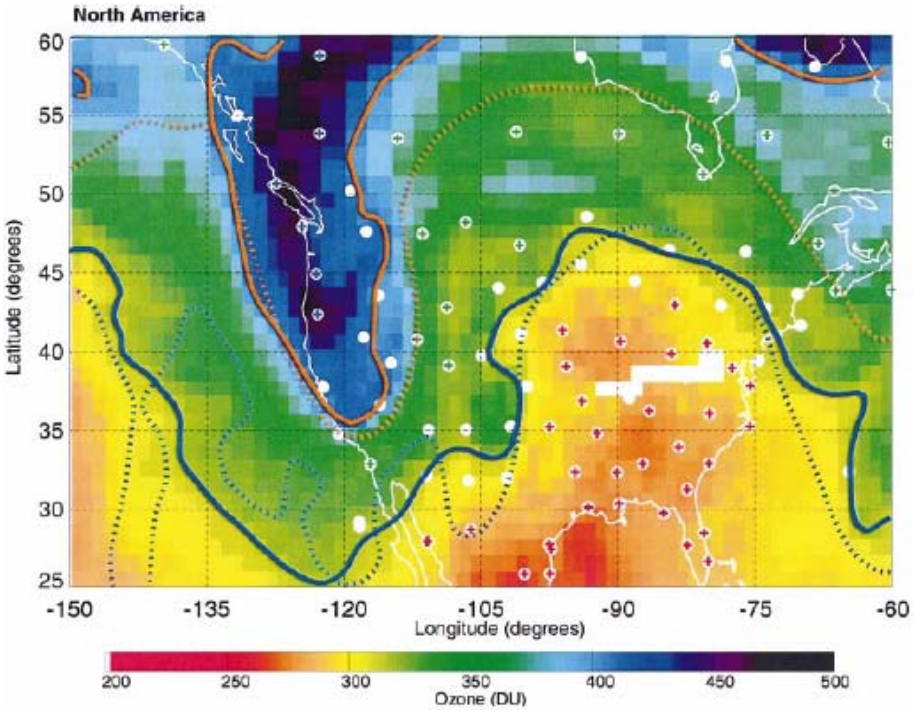

Figure 3.7 Nimbus-7 TOMS total ozone field over North America on March 11, 1990, between 25° and 60°N. The yellow and blue solid lines represent the positions of the polar and subtropical front, respectively. The white circles indicate the positions of rawinsonde measurements. Crosses in the white circles identify a measurement as within a particular regime: red crosses are tropical, green are midlatitude, and blue are polar. The white circles without crosses are rawinsonde measurements that fell within two pixels in latitude and longitude of the frontal boundaries and were not used in the analysis. (Figure 8 and caption from Hudson et al. 2003)

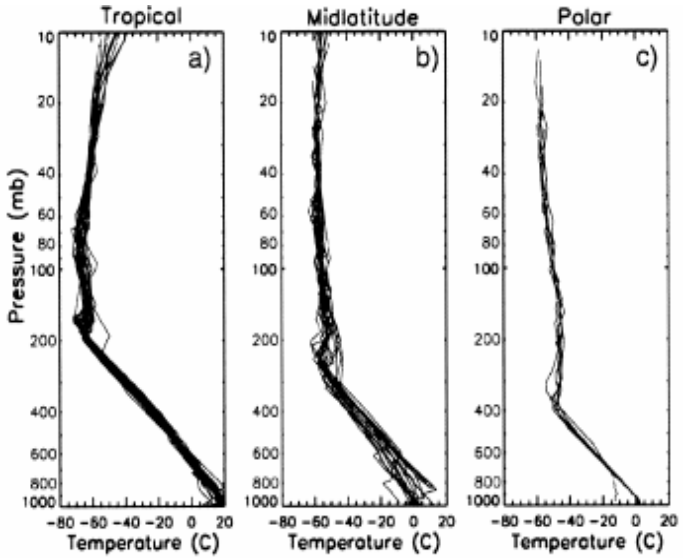

Figure 3.8 Temperature vs. pressure profiles from the rawinsonde measurements for the filled circles shown in Figure 3.7. They are (a) tropical, (b) midlatitude, and (c) polar. (Figure 9 of Hudson et al. 2003)

this definition can be carried further. Looking again at Figure 3.5, one notices a latitude dependence within each regime. Thus, a numerical average between regimes will be different at different latitudes and using one total ozone value to delineate a front will underestimate/overestimate the value at high/low latitudes. For example, the ozone contours used for this day are 329 and 409 DU for the subtropical and polar boundaries, respectively. However, the subtropical boundary value will not fit the definition above for 30°N, where the value given is obviously higher than the numerical average. Therefore, in order to carry the definition through fully, the boundary values must be allowed to vary with latitude.

3.3 The Latitudinally Varying Boundary

To begin, the previously calculated boundary values are used as a first guess. The boundaries are widened by two pixels as before, and one-degree zonal averages are calculated. Figure 3.9 shows an example of this for March 11, 1990. Instead of computing the area-weighted mean total ozone for each regime as before, the new boundary values are calculated for every latitude that two regimes overlap. These new boundary values are shown as black stars in Figure 3.9. Thus, the boundary is no longer a single value, but a set of values that are a function of latitude. Looking again at the subtropical boundary values shown in Figure 3.9, a gap is seen from 43°-48°N. Based on the observation that total ozone within a regime changes slowly with latitude, the points on either side of the gap were used as endpoints, and a slope was calculated between them. Boundary values for the gap were interpolated along this slope.

These latitudinally varying boundary values were then used to separate the total ozone field, and the procedure was repeated until convergence. It should be noted that after the first iteration, which used the ozone contours, the boundaries were only widened by one pixel in latitude and longitude. This is because the boundaries are now calculated for every one-degree band, rather than for the whole hemisphere as before, and widening the boundaries by two pixels was found to exclude too much data. However, it was still maintained as the first guess in order to begin with the 'strictest' initialization, in terms of the total ozone within each regime.

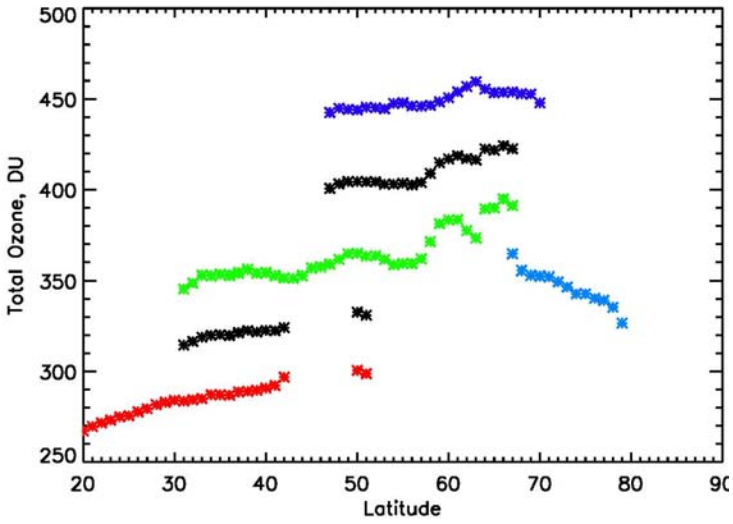

Figure 3.9 One-degree zonal averages within each regime for March 11, 1990. Colors and symbols the same as in figure 3.5. The black stars are the new boundary values calculated by taking the numerical averages of the mean total ozone on either side of the boundary.

After each iteration was complete, the relative area of each regime between 25°-60°N was calculated. The relative area of a regime is defined by the area of a regime divided by the total area between 25°-60°N, such that the sum of the relative areas of all present regimes will equal one. It can be written as:

$$R_{regime} = \frac{A_{regime}}{A_{25°-60°N}} \tag{3.1}$$

where A_{regime} is the area of the polar, midlatitude, tropical, or arctic regimes, R_{regime} is the relative area of the same regime, and $A_{25°\text{-}60°N}$ is the total area between 25°-60°N. When the relative area of each regime had changed less than 5%, convergence was reached. The 5% convergence criterion was chosen based on the resolution of the TOMS data, which are 1° latitude by 1.25° longitude. In each iteration, any change in the area of a regime, for a given latitude band, will have a minimum value given by the area of a pixel. This error due to the pixel size varies from 2-4% of the regime areas, depending on latitude. The slightly more conservative criterion of 5% was chosen to allow for any additional error arising from variance in the ozone data within a regime. If by the fifth iteration convergence was not reached, the day was not used. In addition, if more than 50% of the Northern Hemisphere total ozone data were missing, the day was not used. As a result, some months, whether because of non-convergence, or lack of data, did not have enough data. Any month with less than 15 days of data was eliminated from the analysis. The Meteor 3 time period was most affected by this criterion.

Figure 3.10 shows the Nimbus-7 TOMS image for March 11, 1990 with both sets of boundaries, the boundaries as ozone contours (dashed lines), and the final latitudinally varying boundaries (solid lines). The red and blue lines represent the polar and subtropical upper troposphere fronts, respectively. The black line marks the edge of the polar vortex. To make sure relatively constant total ozone within each regime is seen, we again calculate one-degree zonal averages within each regime based on the new boundaries. These are shown in Figure 3.11, along with the unclassified data. Although

the latitude dependence in each regime has increased, relatively constant total ozone within each regime is seen, despite large overlaps in latitude.

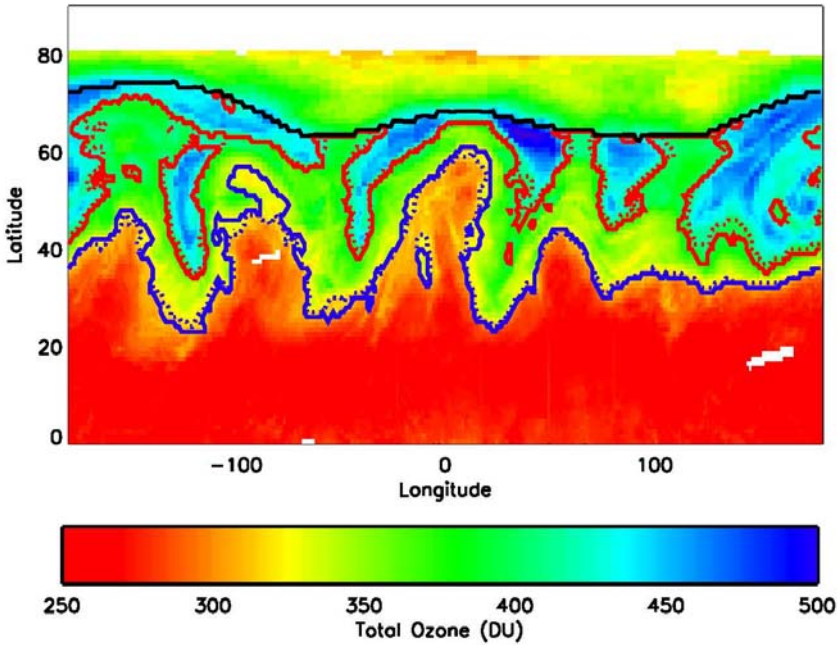

Figure 3.10 Total ozone field from Nimbus-7 TOMS on March 11, 1990. The solid blue and red lines represent the polar and subtropical upper tropospheric fronts, respectively, derived from the latitudinally dependent boundaries. The dashed lines indicate the fronts using the ozone contour method. The black line indicates the edge of the polar vortex derived from the sharpest gradient in PV 550 K isentropic surface.

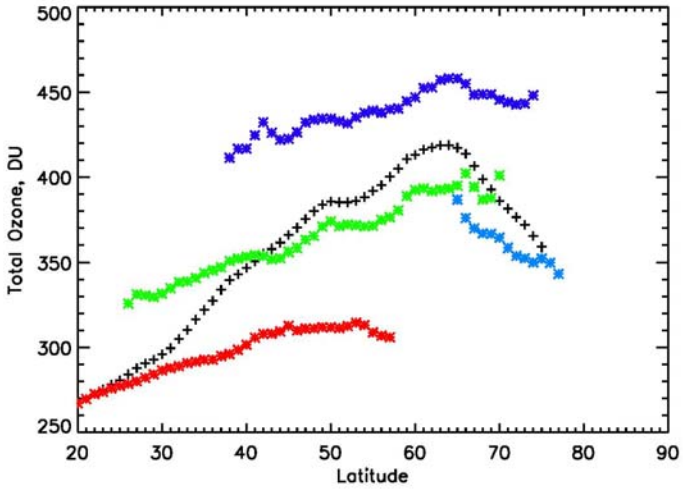

Figure 3.11 One-degree zonal averages within each regime, and the unclassified data, for March 11, 1990 after separation by the new latitudinally-dependent boundaries. Colors and symbols the same as Figure 3.5.

3.4 Method Comparison

Looking at Figure 3.10, it is apparent that the boundaries calculated by the two methods differ. The boundaries differ most at the northernmost and southernmost reaches of their latitudinal extent. For example, the newer boundaries increase the latitude range of the tropical and polar regimes, with respect to the ozone contour boundaries. The best agreement appears near the middle of a boundary's latitudinal extent. This is expected, given the initial ozone contour definition and, as discussed above, their under- and overestimation at high and low latitudes, respectively. Both sets of boundaries, however, do show the same synoptic features. To further demonstrate this, Figure 3.12a-d shows four days in 1986: March 15, June 15, September 15, and December 15. The same synoptic features are seen, regardless of month chosen.

As described above, Andrade (2004) performed an extensive validation of the ozone contour method. In that analysis, upper-level winds from the NCEP reanalysis, rawinsondes, and ozone profiles from the SAGE II instrument (to be described in a later chapter) were used to prove that the total ozone field could be broken up into meteorological regimes. Since the two boundaries agree synoptically throughout the year, the validation should hold for the latitudinally varying boundary values as well. As mentioned above, when profiles are classified by regime, the boundary is typically widened to avoid including any profiles that might fall too close to the boundary. A more detailed explanation of this will be given later. When the boundary is widened, the sensitivity to its exact position decreases. Therefore, we would expect that the results of the rawinsonde and ozonesonde classification, where the boundary was widened by two pixels in latitude and longitude, to be the same for both methods. Chapter 5 will explain

and show the results of classifying ozone and water vapor profiles using the new boundaries.

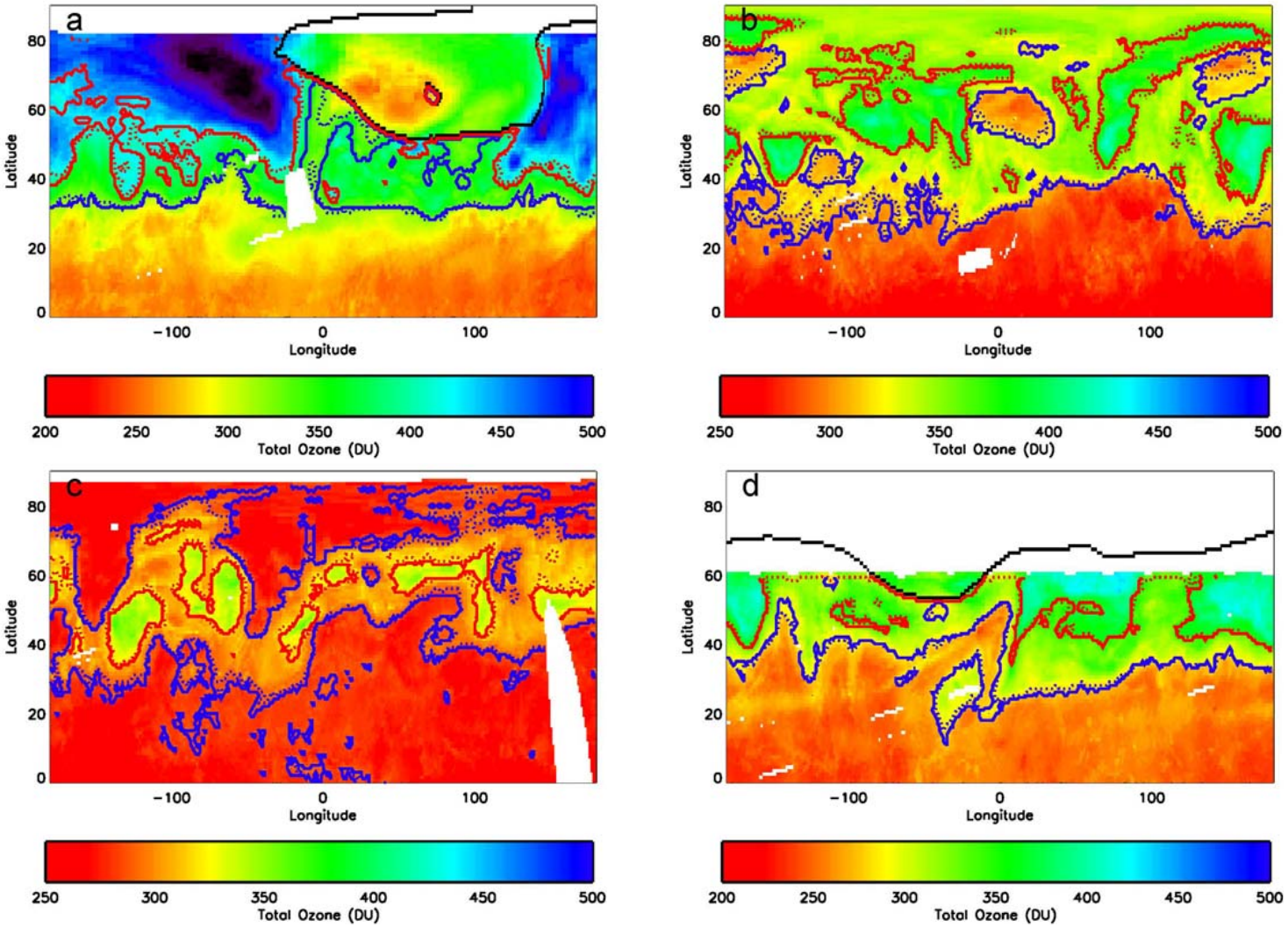

Figure 3.12 Total ozone field from Nimbus-7 TOMS on a) March 15, 1986, b) June 15, 1986, c) September 15, 1986, d) December 15, 1986. The boundaries from the two different methods are as in Figure 3.10.

Chapter 4: Results – Total Ozone

In the previous chapter, the method used to separate the total ozone field into meteorological regimes was described. This chapter will now examine the temporal variability of these regimes throughout most of the TOMS period. Referring back to Table 3.1, the analysis will extend from January 1979 to December 2003, with a gap between January 1995 and August 1996. It should be noted that the Nimbus-7 and Meteor-3 instrument periods overlap. In this case, Nimbus-7 data is used, because the Meteor-3 algorithm has had problems with extreme geometries, such as at high solar zenith angles (Herman et al. 1996). Also, while EP-TOMS data extends through 2005, because of a hardware problem, north of 50°N this data has a possible negative bias up to ~4%[1]. Thus, the TOMS data processing team advises against using the data after 2002 for trend analysis. Recently, it was communicated that the 2003 data is going to be re-released, and it differs little from the 2003 data currently available (S. Frith, personal communication). As stated earlier, all analyses are done for the latitude band 25° - 60°N.

The total mass of ozone (M), between 25° and 60°N, can be written as:

$$M = cA\Omega_0 = cA_T\Omega_T + cA_M\Omega_M + cA_P\Omega_P + cA_A\Omega_A \quad (4.1)$$

where c is a constant of proportionality, A is the total area between 25° and 60°N, Ω_0 is the total ozone over the same latitude band, hereafter referred to as the "zonal" total ozone, A_T, A_M, A_P, and A_A are the areas of the tropical, midlatitude, polar, and arctic

[1] "Because of continuing changes in the optical properties of the front scan mirror that are not well understood, we are now seeing a latitude dependent error that cannot be corrected by a simple calibration correction. The calibration appears to be stable near the equator. But by 50 degrees latitude, there is now a -2% to -4% error in TOMS, a bit larger in the northern hemisphere than in the southern hemisphere. Because of this error, data since 2002 should NOT be used for trend analysis**."** From http://toms.gsfc.nasa.gov/news/news.html#aug01

regimes, respectively, and Ω_T, Ω_M, Ω_P, and Ω_A are the corresponding mean area-weighted total ozone values. If both sides of Equation 4.1 are divided by cA, an equation for the zonal total ozone in terms of total ozone, and the relative areas of each regime (R_x), as defined above, is obtained.

$$\Omega_0 = R_T\Omega_T + R_M\Omega_M + R_P\Omega_P + R_A\Omega_A \quad (4.2)$$

Looking at this equation, it is apparent that changes in zonal total ozone are a result of both changes in total ozone within a regime and changes in the relative areas of each regime over time. The temporal variability of both will be examined below, in addition to the contribution made by each regime to a zonal trend in total ozone.

4.1 Total Ozone

Area-weighted mean total ozone was calculated for each regime, for the latitude band 25° - 60°N, for every day that TOMS data was available. For this analysis, all of the data in this latitude band was used. If a pixel was designated as a boundary pixel, then half of it was assigned to one regime, and half to the other. Because all of the data is used, the mean total ozone within each regime will include values that would otherwise be classified as being in the transition zone between regimes. However, in order to compare these results with those that have used zonal averages, all of the data must be used.

Figure 4.1 shows the monthly mean total ozone within each regime, and for the zonal data; note the different scales used. All show strong seasonal cycles, with the polar having the largest amplitude. The arctic is not seen below 60°N from about May to October. In order to examine the temporal variability of total ozone, monthly

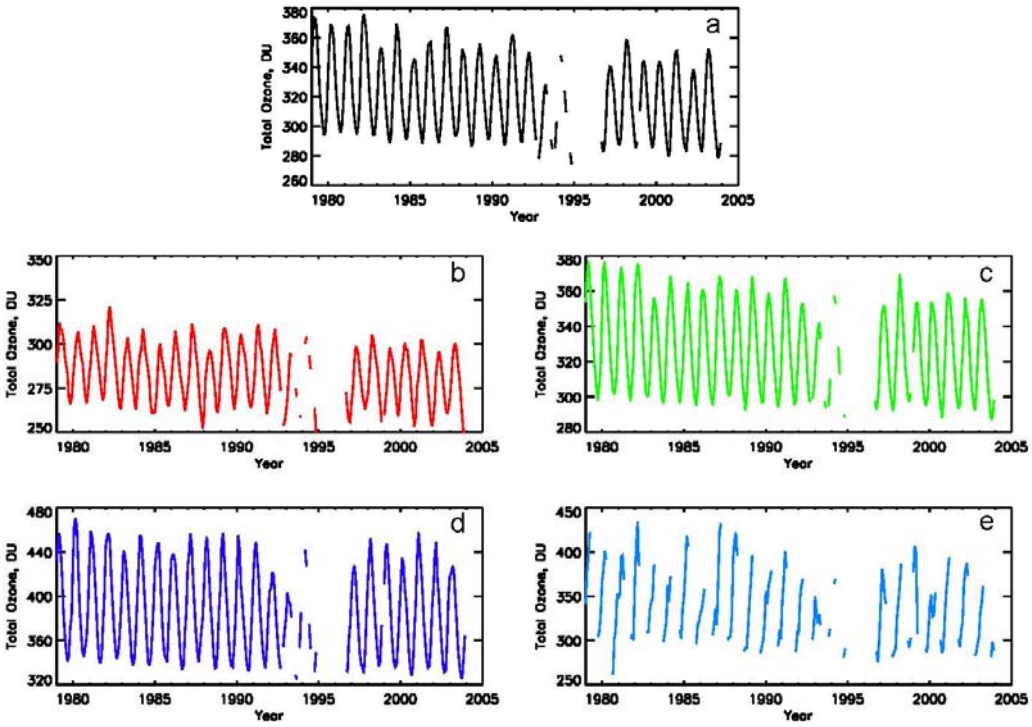

Figure 4.1 Monthly mean total ozone values for the a) zonal data, b) tropical regime, c) midlatitude regime, d) polar regime, and e) arctic regime for 25°-60°N, 1979- 2004. Note the different scales.

climatologies were subtracted from the data. The climatologies were calculated over the time period 1979-2004, and can be seen in Figure 4.2. Earlier, the Brewer-Dobson circulation was discussed as the reason why total ozone was greatest at high latitudes, rather than the tropics, where maximum ozone production takes place. This circulation is also responsible for the seasonal cycle of the polar regime seen in Figure 4.2. The Brewer-Dobson circulation is strongest in the winter and spring, leading to increased transport of ozone poleward, and greater subsidence at higher latitudes. The midlatitude seasonal cycle lags the polar by about one month. The tropical cycle also lags the midlatitude by about a month, its maximum being a mix of subsidence at the higher-latitude reaches of the regime, and maximum ozone production in spring/summer. These monthly climatologies are also listed in Table 4.1, along with the climatological standard

Month	Tropical Regime			Midlatitude Regime			Polar Regime		
	Mean total ozone (DU)	Error of the mean (DU)	Persistence (Days)	Mean total ozone (DU)	Error of the mean (DU)	Persistence (Days)	Mean total ozone (DU)	Error of the mean (DU)	Persistence (Days)
Jan	273	2	4.6	336	4	6.2	417	11	11.7
Feb	283	3	6.2	353	3	4.4	440	5	5.9
Mar	296	2	5.8	361	2	3.4	444	5	5.8
Apr	303	1	3.4	358	2	3.7	429	5	7.9
May	303	1	4.3	347	2	6.4	406	6	12.6
Jun	297	2	6.9	335	4	12.7	382	6	16.4
Jul	290	1	6.7	319	4	16.7	360	5	16.1
Aug	284	2	9.7	308	2	11.1	344	3	7.1
Sep	276	2	11.8	299	1	5.3	336	2	4.5
Oct	266	2	11.4	295	1	2.2	339	5	7.4
Nov	260	1	3.5	300	2	5.6	361	7	9.7
Dec	263	2	6.3	314	3	6.2	386	6	6.5

Table 4.1 Climatological total ozone, error of the mean, and persistence

error of the mean, and the persistence. The standard error of the mean, hereafter referred to as simply the error of the mean (σ_{EM}), is given as

$$\sigma_{EM} = \frac{\sigma}{\sqrt{n/p}} \tag{4.3}$$

where σ is the standard deviation, n is the number of data points in that month, and p is the persistence. The persistence is defined as

$$p = \frac{1-\rho}{1+\rho} \tag{4.4}$$

where ρ is the lag-1 correlation of the data. The climatological error of the mean of the tropical and midlatitude regimes is on the order of 2 DU. The polar regime shows higher values with a maximum of 10 DU in January. The persistence is indicative of how many data points in a row are considered to be dependent. Not surprisingly, the largest values are seen in the early summer to early fall, when the weather patterns are more stable.

Figure 4.3 shows the monthly total ozone trends for 1979-2004. The error bars on

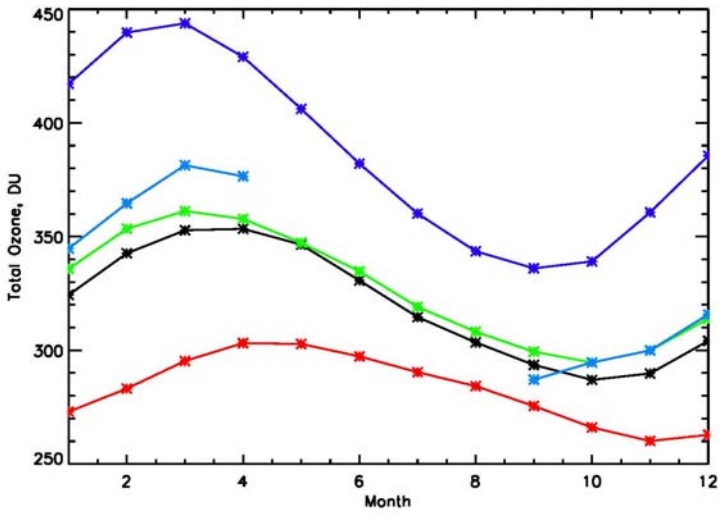

Figure 4.2 Monthly total ozone climatology, calculated from 1979-2004, between 25° and 60°N. The zonal, tropical, midlatitude, polar, and arctic are represented by the black, red, green, blue, and light blue lines, respectively.

each point represent the 2σ error from the simple linear fit applied. The most negative trends in total ozone are found in the polar and midlatitude regimes in January. This agrees reasonably well with past measurements of seasonal ozone trends (WMO 2003), although most studies found the minimum trend in February or March (Stolarski et al. 1992; Hood et al. 1999). However, these studies included the polar vortex in their calculations, and their results will therefore differ slightly from those presented here. The three regime monthly trends appear to be slightly out of phase, similar to their seasonal cycles. The minimum in the monthly trend in the tropical regime is in March.

The monthly mean total ozone residuals, calculated by subtracting the monthly climatology shown in Figure 4.2 from the monthly means seen in Figure 4.1, are shown in Figure 4.4. Again, note the different scales. The zonal data and the data within each regime all show decreasing total ozone with time. Upon further examination, it is apparent that some features present in the zonal data are not present in all regimes. For example, the negative anomaly at the beginning of 1999 is present in the zonal data, as well as the tropical and the midlatitude, although weaker in the midlatitude. However, this feature is not seen in the polar regime. This suggests that the regimes contribute to the zonal mean differently at various times, a point that will be examined further on.

The time period from January 1979 to May 1991 and September 1996 to December 2003 were chosen to examine the contributions made by each regime to a zonal trend in total ozone. The former is a period when the chlorine loading in the stratosphere varied almost linearly with time (Solomon 1999). The latter begins after the gap in the TOMS data. In order to examine trends and trend errors, a multiple linear regression of the form

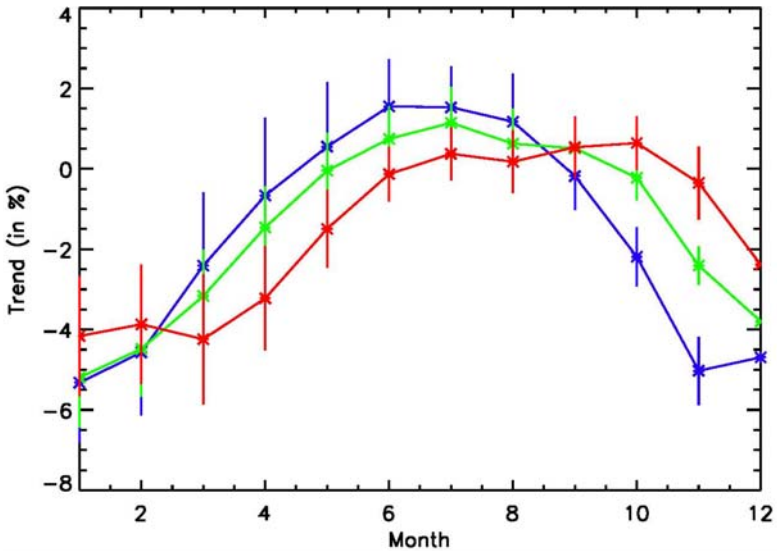

Figure 4.3 Monthly total ozone trends, calculated from 1979-2004, between 25° and 60°N. Colors are the same as in Figure 4.2.

$$O_3(t) = a_0 + \sum_{\omega=1}^{4} (a_i \sin(\omega t) + b_i \cos(\omega t)) + QBO1 + QBO2 + SFX + Cl + AER \qquad (4.5)$$

was applied to the data shown in Figure 4.1, where a_0, a_i, and b_i, are all constants to be determined from the regression. The summation term in this equation represents the seasonal cycle out to four harmonics. QBO1, QBO2, SFX, Cl, and AER are of the form $\alpha X(t) + \sum_{\omega=1}^{2} X(t)(\alpha_i \sin(\omega t) + \beta_i \cos(\omega t))$ and represent the quasi-biennial oscillation (QBO), solar flux, chlorine loading, and aerosols, respectively. The resulting slopes, trends, fit errors from this regression analysis, and mean values over this time period are listed in Table 4.2. The slopes are obtained by taking the constant from the linear chlorine loading term above (α). The fit errors were calculated using a bootstrap method similar to the method used in Stolarski and Frith (2006). The residuals are grouped and rearranged in 12-month increments. The linear regression is then applied to the residuals, and new residuals and constants are calculated. This process is repeated until a sufficient

sample size is obtained. The values acquired for the constants are then used to compute a cross-correlation matrix, from which the fit error is derived.

The zonal total ozone trend of -3.1 %/decade, from January 1979 - May 1991, between 25° and 60°N reported in Table 4.2 agrees well with previous estimates (Staehelin et al. 2001; WMO 1999). As expected, all of the regime total trends are negative in sign. The least negative trend is seen in the tropical regime, and the most negative trend in the polar regime, also agreeing with previous analyses of total ozone trends that have reported the largest ozone depletion at higher latitudes, and the smallest at low latitudes (Stolarski et al. 1992). All trends listed in Table 4.2 are statistically significant, with the exception of the arctic regime. The means, trends, and trend errors

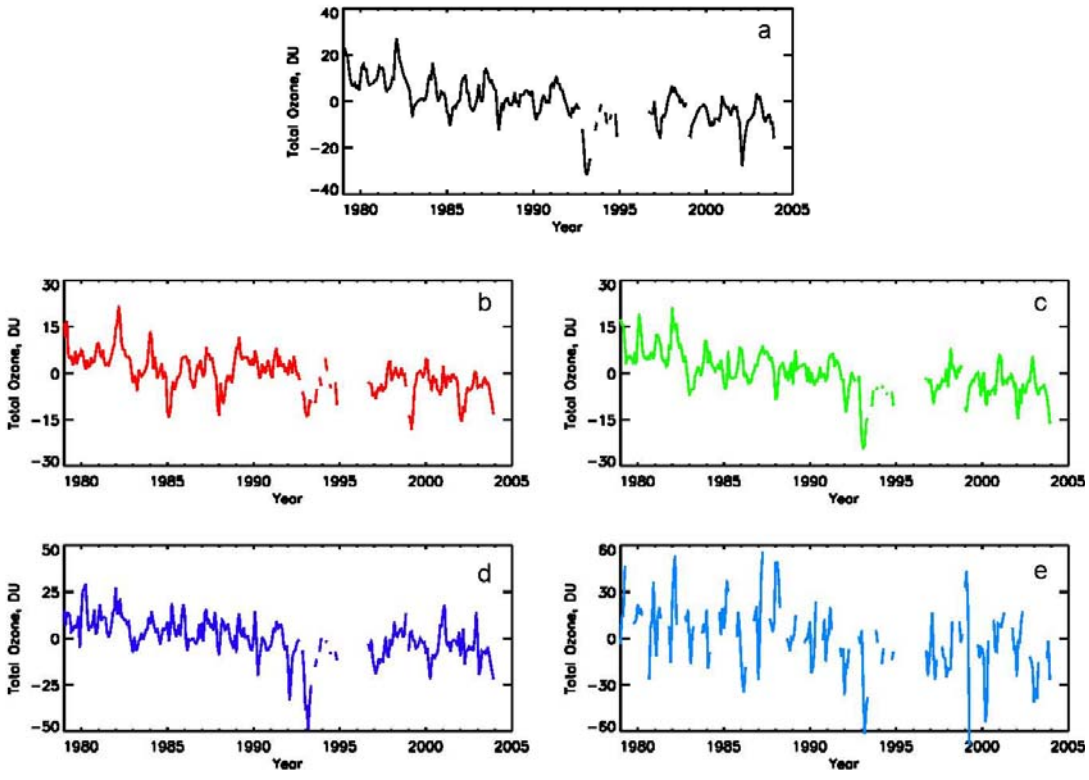

Figure 4.4 Same as Figure 4.1, except the monthly climatology shown in Figure 4.2 has been removed. Note the different scales.

for September 1996 to December 2003 are found in Table 4.3. Again, all of the trends, with the exception of the arctic, are negative and statistically significant. The errors for this time period are larger due to the shorter time period over which the analysis was over. Looking at the similarity between the total ozone trend in the polar regime and the zonal data, one could hypothesize that the polar regime was largely responsible for the zonal trend. However, before concluding this fact, the temporal variability of the relative areas of each regime must also be examined.

Regime	Mean (DU)	Trend (DU/dec)	Trend (%/dec)
Zonal	325	-10.2 ± 2.0	-3.1 ± 0.7
Tropical	286	-3.9 ± 1.4	-1.4 ± 1.0
Midlatitude	332	-7.6 ± 1.6	-2.3 ± 0.5
Polar	394	-11.9 ± 3.1	-3.0 ± 0.7
Arctic	215	-5.2 ± 9.0	-1.5 ± 1.2

Table 4.2 Slopes, trends, and errors (2σ) for the total ozone data for January 1979 to May 1991

Regime	Mean (DU)	Trend (DU/dec)	Trend (%/dec)
Zonal	314	-11.3 ± 3.0	-3.6 ± 2.1
Tropical	278	-8.3 ± 1.4	-3.0 ± 1.2
Midlatitude	323	-8.5 ± 3.6	-2.6 ± 1.3
Polar	383	-18.2 ± 4.8	-4.7 ± 2.4
Arctic	352	30 ± 24	8.7 ± 11.2

Table 4.3 Slopes, trends, and errors (2σ) for the total ozone data for September 1996 to December 2003

4.2 Relative Areas

Figure 4.5 shows the monthly mean relative areas for each regime between 25° and 60°N. The tropical relative area appears to be increasing over this time period, while the polar area is decreasing. This implies that the subtropical and polar upper troposphere fronts have moved northward over this time period. This will be explored in more detail below. Looking further at Figure 4.5, it is apparent that the midlatitude regime is the largest of the regimes throughout most of the TOMS period. The polar regime appears to make up about 15-20% of the area between 25° and 60°N. The arctic,

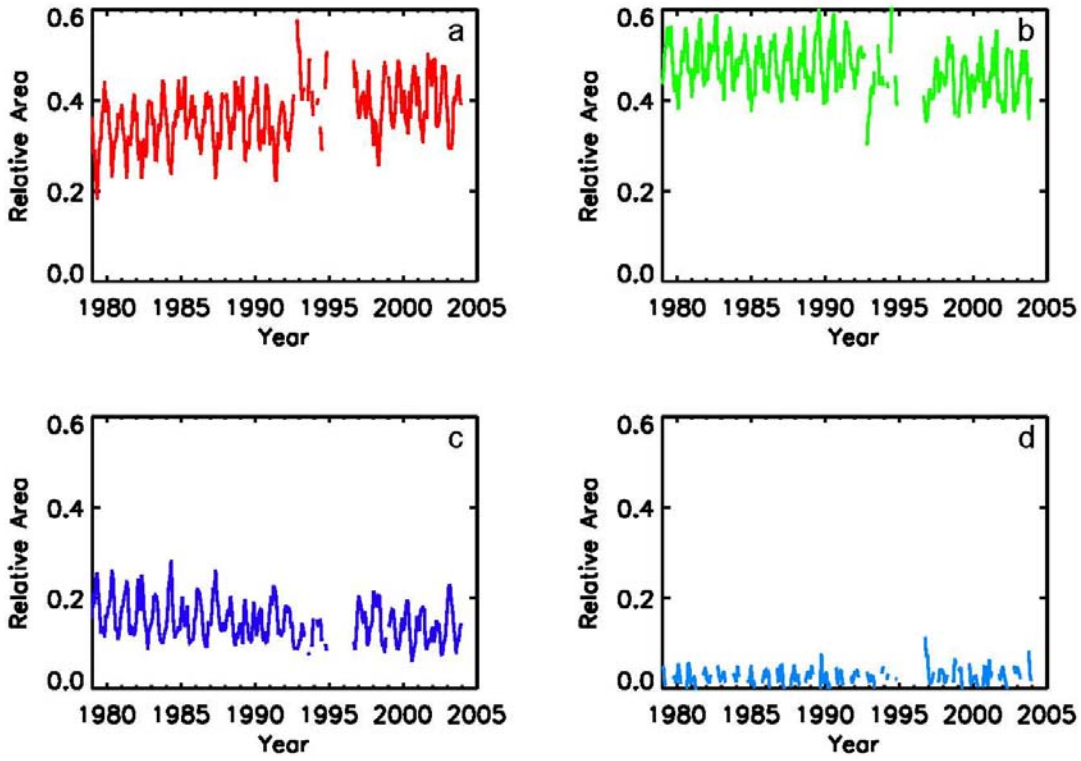

Figure 4.5 Monthly mean relative area values for the a) tropical regime, b) midlatitude regime, c) polar regime, and d) arctic regime for 25°-60°N, 1979- 2004.

which is not present a good portion of the year, is the smallest of the regimes. In addition, while a seasonal cycle is visible in the data seen in Figure 4.5, the relative areas appear to have more interannual variability.

Figure 4.6 displays the climatological monthly relative area means, calculated from 1979 – 2004. The seasonal cycles seen here are much weaker than those of total ozone. In addition, the seasonal cycles of the polar and tropical regimes appear to be out-of-phase. For example, when the tropical relative area is at a minimum, as in May, the polar relative area is at a maximum. This indicates upper troposphere fronts move together and are dependent on one another. The midlatitude and polar regimes are nearly in phase, having maximums in spring, and in the case of the polar, a minimum in fall. The secondary maximum in the midlatitude regime in fall should be viewed with caution. As can be seen in Table 4.1, in fall the difference in total ozone between regimes is at a

minimum. Therefore, an increase in tropospheric pollution could raise the column amount enough for otherwise tropical air to be classified as midlatitude (Hudson et al. 2003), thus increasing the midlatitude relative area at the expense of tropical. Further evidence and discussion of this will be in Chapter 5.

Figure 4.7 shows the monthly relative area trends from 1979-2004. The error bars on each point represent the 2σ error from the simple linear fit applied. Unlike total ozone, the relative area monthly trends do not appear to show a seasonal pattern. The tropical regime shows statistically significant positive trends in every month, with the exception of January and June. In addition, the polar regime shows negative trends, although again, some months are not statistically significant. The midlatitude shows mostly small negative relative area trends throughout the year.

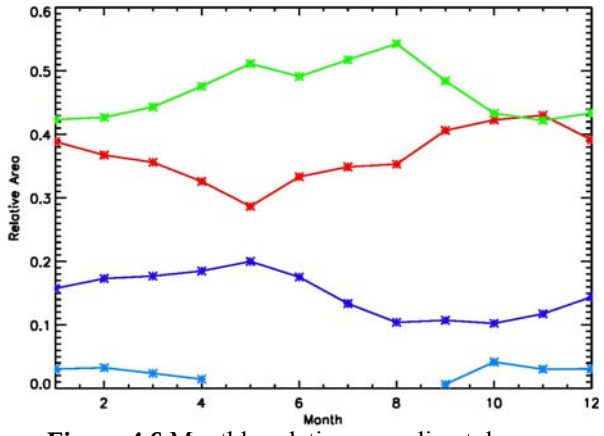

Figure 4.6 Monthly relative area climatology, calculated from 1979-2004. Colors as in Figure 4.2.

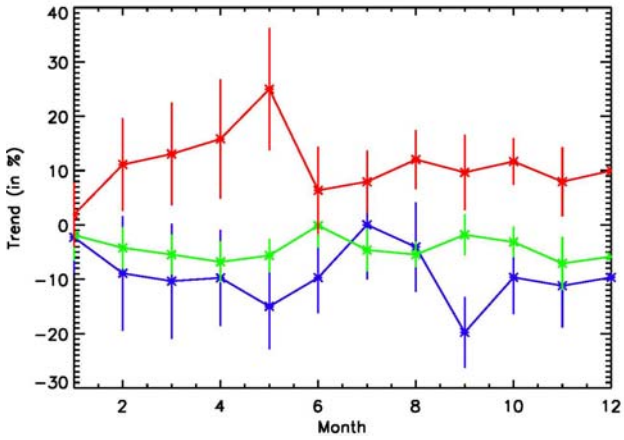

Figure 4.7 Monthly relative area trends, calculated from 1979-2004, between 25° and 60°N. Colors are the same as in Figure 4.2.

Table 4.4 shows the climatological monthly means, errors of the mean, and the persistence for the relative area data. The error of the mean for each regime varies little from month to month. The

Month	Tropical Regime			Midlatitude Regime			Polar Regime		
	Mean area	Error of the mean	Persistence (Days)	Mean area	Error of the mean	Persistence (Days)	Mean area	Error of the mean	Persistence (Days)
Jan	0.39	0.02	2.8	0.43	0.02	3.8	0.16	0.02	4.5
Feb	0.37	0.02	3.4	0.43	0.02	3.9	0.17	0.01	3.4
Mar	0.35	0.02	3.0	0.45	0.02	3.8	0.18	0.02	4.6
Apr	0.32	0.02	3.4	0.48	0.02	4.1	0.19	0.02	4.0
May	0.28	0.02	3.5	0.51	0.02	4.0	0.21	0.01	3.4
Jun	0.32	0.02	4.1	0.50	0.02	4.4	0.18	0.01	3.4
Jul	0.34	0.02	3.1	0.52	0.02	3.6	0.14	0.01	3.8
Aug	0.35	0.02	3.3	0.55	0.02	3.2	0.11	0.01	2.5
Sep	0.40	0.02	3.4	0.49	0.03	3.6	0.11	0.01	2.6
Oct	0.42	0.02	2.5	0.44	0.02	2.9	0.11	0.01	2.7
Nov	0.43	0.02	2.9	0.42	0.02	3.1	0.12	0.01	3.4
Dec	0.39	0.02	2.8	0.43	0.02	3.0	0.14	0.02	4.5

Table 4.4 Climatological relative area, error of the mean, and persistence

persistence of each regime, in each month, is on the order of 2-4 days. This is what would be expected of a quantity that would change on synoptic timescales.

The climatologies shown in Figure 4.6 and listed in Table 4.4 were subtracted from the monthly mean relative areas in order to investigate temporal variability. The residuals are shown in Figure 4.8. The same decrease in tropical area and increase in polar area is seen. The statistical time series model (Equation 4.5) that was used to analyze the total ozone was used to calculate trends and trend errors over the time periods January 1979 to May 1991, and September 1996 to 2004. The results are summarized in Tables 4.5 and 4.6. Over the earlier time period, the relative area of the tropical regime increased by approximately 10%, while the polar decreased by about 15%. Looking at the later period, only the tropical regime barely shows a statistically significant trend.

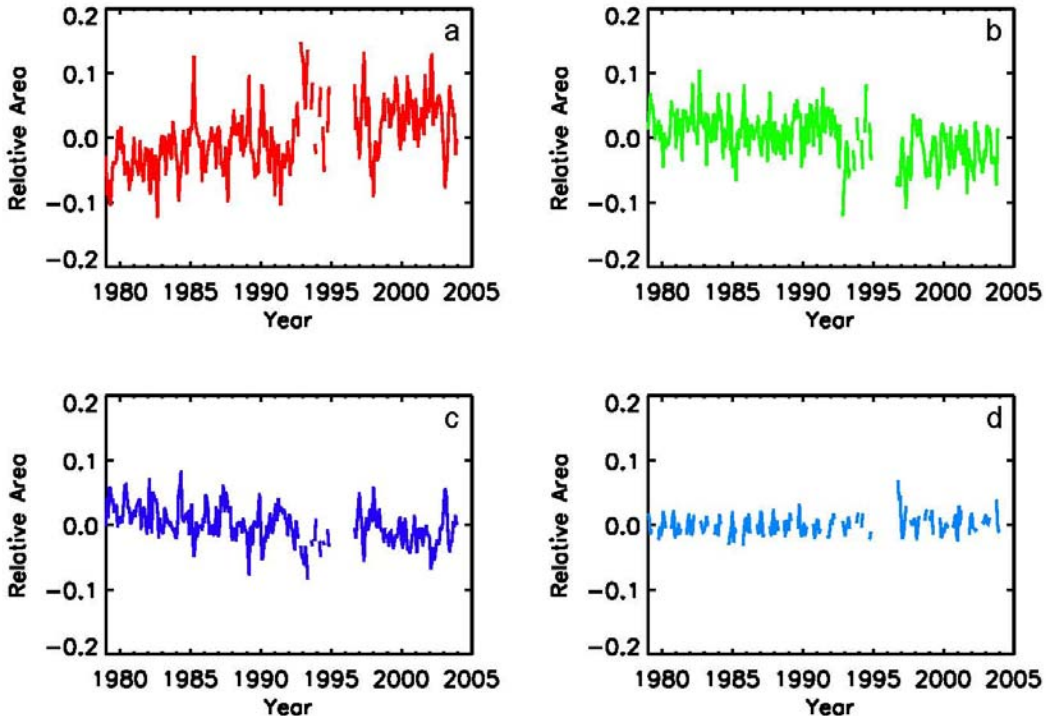

Figure 4.8 Same as Figure 4.5, except the monthly climatology shown in Figure 4.6 has been removed.

The rest of the relative area trends are not statistically significant. As such, the remainder of the relative areas discussion will focus on the earlier period. The relative areas of the

Regime	Mean	Trend per decade ($\times 10^{-2}$)	Trend (%/decade)
Tropical	0.35	2.9 ± 1.3	8.4 ± 3.0
Midlatitude	0.48	-0.4 ± 1.0	-1.0 ± 2.2
Polar	0.16	-2.6 ± 1.1	-16.7 ± 4.2
Arctic	0.02	0.0 ± 0.5	-3.7 ± 0.0

Table 4.5 Slopes, trends, and errors (2σ) for the relative area data for January 1979 to May 1991

Regime	Mean	Trend per decade ($\times 10^{-2}$)	Trend (%/decade)
Tropical	0.40	3.1 ± 2.6	7.8 ± 7.0
Midlatitude	0.44	-2.8 ± 3.0	-6.4 ± 6.7
Polar	0.14	-1.0 ± 0.2	-7.5 ± 14
Arctic	0.03	-2.2 ± 3.0	-73 ± 100

Table 4.6 Slopes, trends, and errors (2σ) for the relative area data for September 1996 to December 2003

midlatitude and arctic regimes show no statistically significant trends. As stated above, these changes in relative area imply a net poleward movement of the subtropical and polar upper troposphere fronts. In fact, the relative areas can be used to calculate the mean latitudes of the upper troposphere fronts over this time period. A linear fit of the resulting mean latitudes from January 1979 – May 1991 yields a poleward shift of 1.1 degrees per decade for the subtropical front, and 1.2 degrees per decade for the polar front. When the same procedure was repeated for the entire period studied, 1979-2004, the trend for the subtropical front was one degree per decade, and the trend for the polar front was 0.5 degrees per decade. It should be noted that significant portions of the polar regime, and therefore the polar front, can migrate north of 60°N at certain times of the year. Portions of the subtropical front can exhibit similar behavior, especially in late summer and early fall. Hence, these estimates of net frontal movement given above

cannot be representative of the entire front. However, Fu et al. (2006) presented an analysis of global measurements of atmospheric temperature based on satellite-borne microwave sounding unit (MSU) data and concluded that the jet streams in both the Northern and Southern Hemispheres moved poleward approximately one degree over the period 1979-2005.

4.3 Net Contributions

The contribution to the zonal trend made by each regime can be examined by taking each term on the right-hand side of Equation 4.5. This is seen in Figure 4.9. The contribution made by the tropical regime is increasing with time, while the contributions of the midlatitude and polar regimes are decreasing. Relative to the other regimes, the

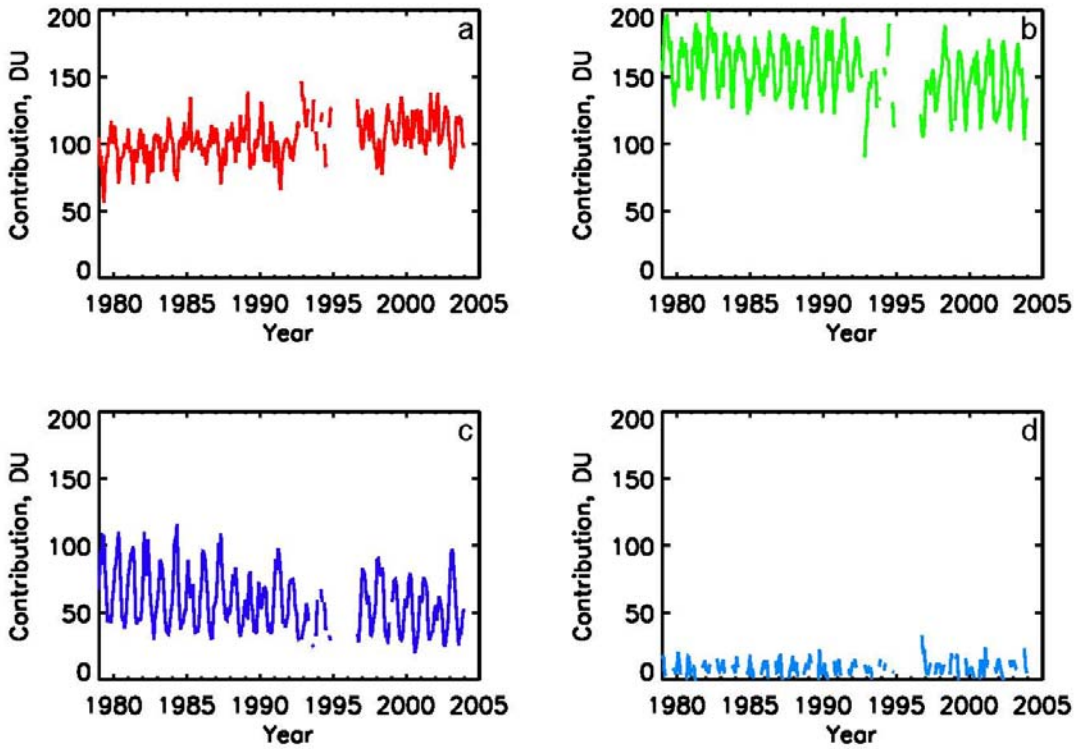

Figure 4.9 Monthly mean mass contribution in DU for the a) tropical regime, b) midlatitude regime, c) polar regime, and d) arctic regime for 25°-60°N, 1979- 2004.

arctic contributes little to the zonal trend between 25° and 60°N. Again examining the time period from January 1979 to May 1991, the net contributions made by each regime can be calculated. The polar and midlatitude regimes show net losses of 16.7 and 10.0 DU, respectively. The tropical and arctic regimes show net gains of 11.8 and 0.1 DU, respectively. The sum of these changes is a loss of 14.8 DU, which agrees well with the loss in the zonal ozone data of 14.9 DU over the same period. The same calculations were done for the period from September 1996 – December 2003, but their associated errors were too large, and therefore most of the calculated contributions were not statistically significant.

Referring back to the discussion of the total ozone trends within each regime, the polar regime was observed to have a trend similar to the zonal trend. However, Figure 4.9 shows that the polar regime contributes the least (except for the arctic) to the zonal total ozone between 25° and 60°N. In addition, the net contribution of the tropical regime is positive, despite its statistically significant negative trend in total ozone. This implies that the area of the tropical regime is increasing faster than the rate of decay of its mean ozone. Since the tropical regime contains the lowest values of total ozone, an increase in the relative area of this regime will bring lower values of total ozone over time, further contributing to the negative zonal trend.

Based on this analysis, I conclude that the downward trend from January 1979 – May 1991 in zonal total ozone is a result of:

1) A net reduction of total ozone within each meteorological regime
2) A change in the relative weighting of the regimes over time, due to a net northward movement of the subtropical and polar upper troposphere fronts.

4.4 Trend Validation

The use of ozone boundaries calculated using the total ozone field has, at times, been criticized by various members of the scientific community. The major criticism has involved the boundary's susceptibility to long-term trends in ozone. It has been contended that a latitudinally-dependent long-term chemical trend in ozone could affect the calculation of the ozone boundaries, and consequently bias trends. However, as explained in Chapter 3, the boundaries are calculated on a daily basis, and are therefore only susceptible to chemistry that happens on timescales shorter than a day.

In order to estimate the robustness of the boundaries for trend analysis, I conducted an experiment using two runs from the NASA Goddard Space Flight Center's (GSFC) 3D Full Chemistry and Transport Model (FCTM, Douglass et al. 1996). The transport in this model is calculated off-line, such that the chemical constituents have no influence over the model dynamics. The resolution of the model was 5° longitude by 4° latitude, with 28 levels in the vertical. The vertical resolution is approximately 2 km below 60 mb, and about 3.5 km above. Both heterogeneous and gas-phase chemistry are included. The wind fields were derived using data from the NASA GSFC Data Assimilation Office (DAO).

Ozone data from two FCTM runs were used. The first was a 50-yr run, from February 1973 to December 2022. This run had observed aerosol and source gas concentrations, hereafter called the "CL" run. The second run was from January 1979 to December 2010, and was the same as the first, except source gases were held to their 1979 value, hereafter referred to as the "XCL" run. The actual time period used for this

experiment was 1983 – 2003. The XCL run required several years spin-up time (A. Douglass, personal communication), and corresponding time periods were desired.

Given that the dynamics is run off-line, the boundaries should be the same for both model runs. The data from both runs was vertically integrated to compute total ozone fields, and the method described in Chapter 3 was applied. The convergence criterion was increased from 5% to 20% to allow for the increase in pixel size. A first test of the boundaries is to examine the relative areas of each regime. Figure 4.10 shows four days in 1994, when ozone in the CL run should be heavily depleted due to chlorine chemistry (Solomon 1999). The solid lines indicate the boundary calculated for the CL run, and the dashed lines for the XCL run. Both are plotted onto total ozone from the CL run. The boundaries agree very well. To establish consistency throughout the period, Figure 4.11 shows several days in 2003. Again, excellent agreement is obtained.

To test for trend bias, trends were calculated using a simple linear fit for the total ozone and relative areas of each regime, for both runs. The results are summarized in Table 4.7. All trends are in percent per decade, and all uncertainties are 2σ. Two time periods were examined: January 1983 – May 1991, and January 1983 – December 2003. The first was chosen because it was a period of maximum ozone depletion, in addition to being relatively clean in terms of atmospheric aerosols. Looking at the trends, the ozone depletion is obvious in the CL run. The relative area trends between the two runs agree within error, and neither shows a significant trend over this time period. The second time period was chosen to establish any long-term drift in the relative areas over the entire time period. Again, the relative areas of the two runs agree within error, and show no significant trend. Therefore, no biases in the relative area trends as a result of long-term

changes in ozone were found, and thus the trends reported here can be considered reliable and robust.

	Tropical		Midlatitude		Polar	
	CL	XCL	CL	XCL	CL	XCL
	Jan 1983 – May 1991					
Total ozone	-1.7 ± 1.0	-0.2 ± 1.0	-1.6 ± 1.4	0.3 ± 1.4	-2.8 ± 2.4	-0.4 ± 2.2
Relative Area	4.5 ± 7.6	3.7 ± 7.0	-0.2 ± 7.8	-0.5 ± 7.4	-7.9 ± 9.8	-5.4 ± 10.0
	Jan 1983 – Dec 2003					
Total ozone	-1.4 ± 0.4	-0.1 ± 0.4	-1.5 ± 0.4	-0.0 ± 0.4	-1.8 ± 0.8	0.0 ± 0.6
Relative Area	0.8 ± 2.0	-1.0 ± 1.8	0.7 ± 2.0	1.0 ± 2.0	-2.7 ± 2.8	0.4 ± 3.0

*All trends reported in %/decade
*All uncertainties are 2σ

Table 4.7 Total ozone and relative area trends calculated for the CL and XCL FCTM runs

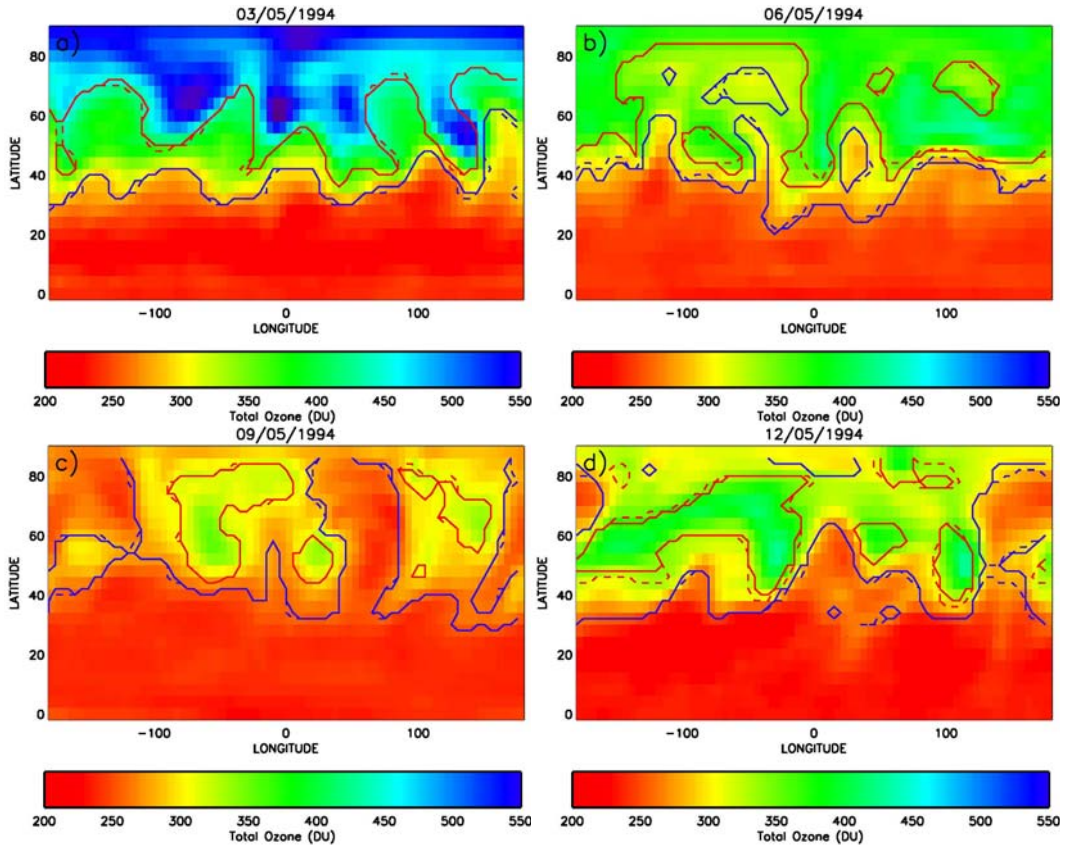

Figure 4.10 Total ozone fields derived from the FCTM data CL run for a) March 5, 1994, b) June 5, 1994, c) September 5, 1994, d) December 5, 1994. The blue and red lines represent the positions of the subtropical and polar fronts, respectively. The solid lines are the boundaries calculated from the CL run, and the dashed lines are the boundaries calculated for the XCL run.

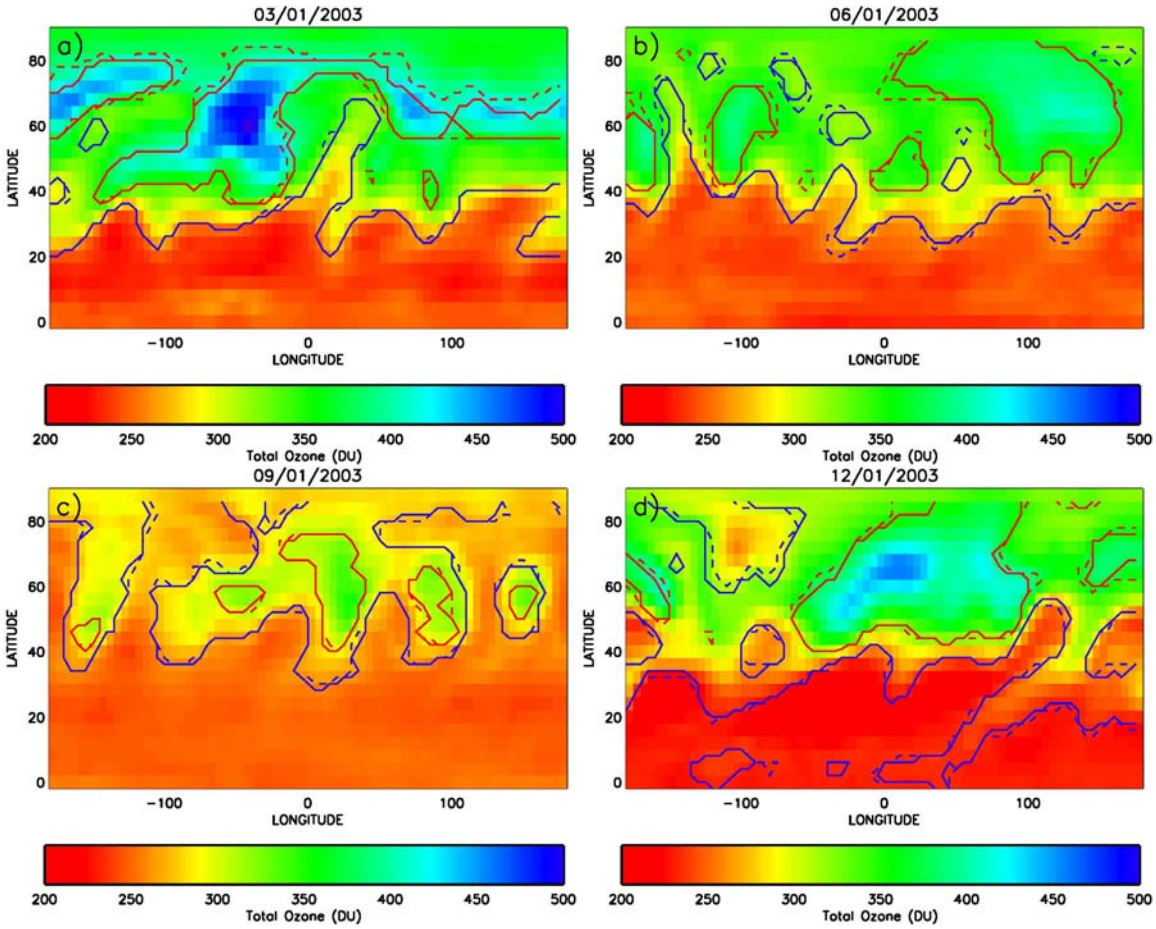

Figure 4.11 Same as Figure 4.10 except for a) March 1, 2003, b) June 1, 2003, c) September 1, 2003, d) December 1, 2003.

4.5 Dynamical Contributions to Zonal Trends

The zonal total ozone trend, -3.1 %/decade for January 1979-May 1991 between 25° and 60°N, has been reported and examined in the literature (Staehelin 2001; WMO 1999). It has previously been interpreted to be the result of increased heterogeneous chemistry on aerosols in the lower stratosphere (Solomon et al. 1996, 1998; Staehelin 2001). However, other studies have explored dynamical influences on total ozone trends, such as changes in the solar cycle, ozone mini-hole frequency, mean meridional

circulation, QBO, North Atlantic Oscillation (NAO), and combinations of these parameters.

Solar radiation emitted by the sun varies at different timescales and at different wavelengths. The most prominent variation in terms of ozone is the ~11 year solar cycle (WMO 2003). Incoming solar UV radiation between 200 and 400 nm is responsible for photochemical ozone formation and destruction in the stratosphere (Brasseur 1993). The Mg-II index closely follows the 180-200 nm wavelength range (Heath and Schlesinger 1986) that controls the formation of the oxygen atom in the upper stratosphere, which then combines with O_2 to form ozone. The amount of radiation from solar maximum to solar minimum can vary by as much as 6-7% at these wavelengths. This variability can result in a 2% change in total ozone and a 5-7% change in ozone mixing ratio in the upper stratosphere (2.0 - 0.7 mb) over the course of a solar cycle (Chandra and McPeters 1997).

The seasonal cycle for zonal total ozone was shown in Figure 4.2. As discussed earlier, it has a maximum in the spring and a minimum in the fall. This is a result of the yearly strengthening and weakening of the Brewer-Dobson circulation, which transports high-ozone air poleward from the tropics, where it is chemically produced. Thus, changes in the strength of this circulation can result in more or less ozone being transported poleward in a given winter, and as a result, affect total ozone trends (WMO 2003). Fusco and Salby (1999) and Randel et al. (2002) use the vertical component of the Eliassen-Palm (EP) flux as a proxy for the meridional wave activity responsible for driving the Brewer-Dobson circulation (Holton et al. 1995). In practice, the eddy heat flux, $\overline{v'T'}$, is used as the proxy for ozone transport, as it is directly proportional to the

divergence of the EP flux (Fusco and Salby 1999; Randel et al 2002; Dhomse et al. 2006).

Fusco and Salby (1999) and later Salby and Callaghan (2004) examined the contributions made by anomalous forcing of the residual circulation. They used two components: interannual changes in upward EP flux, and interannual changes in the QBO. The QBO was used because it has an influence on total ozone at low and high latitudes (Baldwin et al. 2001). It introduces a secondary circulation that transports more or less ozone poleward depending on its phase (Dhomse et al. 2006). The QBO also controls the winds in the tropics, thus determining where planetary waves are absorbed, and thereby further affecting ozone transport (Salby and Callaghan 2004). A proxy often used is the equatorial wind at 10 mb. These dynamic influences were correlated with the wintertime ozone tendency from TOMS, given as

$$\Delta \left\langle \overline{O_3} \right\rangle^{Mar-Nov} = \left\langle \overline{O_3} \right\rangle^{Mar} - \left\langle \overline{O_3} \right\rangle^{Nov} \tag{4.6}$$

which accounts for most of the interannual anomaly in springtime ozone (Salby and Callaghan 2002, 2004). Their analysis also accounts for photochemical changes in total ozone by using what they called an ozone depleting factor (ODF) that takes chlorine and aerosols into account. The anomalous forcing and photochemical effects, and the wintertime ozone tendency were found to have a correlation of 0.95 from 1979-1998. Using the calculated sensitivity of ozone tendency to changes in anomalous forcing, they recreated the ozone trend with 70% of its original magnitude. Randel et al. (2002) performed a similar analysis using only the vertical component of the EP flux and the monthly ozone tendency. The monthly ozone tendency was regressed onto $\overline{v'T'}$, and this was used to recalculate a trend in ozone in order to estimate the effect of wave forcing. It

was found that changes in EP flux explain approximately 20% of the trend in total ozone between 35° and 60°N from 1979 to 1992, and about 30% from 1979 to 2000.

Ozone "mini-holes" are localized regions of anomalously low total ozone that form and dissipate on synoptic timescales. These occur most frequently over Europe in the winter months, sometimes resulting in anomalies as low as 200 DU lower than the zonal mean at the time (James 1998). They are associated with the passage of intense anticyclones and are the result of Rossby wave-breaking (McCormack and Hood 1997). Ozone is not destroyed by this process; rather it is rearranged, so the decreases seen over mini-holes as a result of divergence above an anticyclone will result in an increase in total ozone somewhere else (McCormack and Hood 1997; Hood et al. 2001). These events can therefore lower zonal monthly total ozone averages, and an increase in the frequency of these events can affect both local and zonal total ozone trends. McCormack and Hood (1997) reported that the frequency of ozone mini-holes appeared to be increasing with time from 1979-1993. Later, Hood et al. (1999) attributed 40% of the changes in total ozone in February to increases in the frequency of Rossby wave-breaking events. Reid et al. (2001) also observed an increase in mini-hole frequency over Europe from 1979-1993. Brönnimann and Hood (2003) reported an increase in low ozone events over northwestern Europe from 1990-2000, with respect to the earlier time period studied, 1952-1963.

As stated above, ozone mini-holes are associated with the passage of anticyclones, and are thus associated with mid-latitude storm tracks (James 1998). Therefore, an increase in the frequency of mini-holes at northern latitudes implies an increase in the frequency in the prevalence of these storm tracks. McCabe et al. (2001)

analyzed cyclone statistics from 1959-1997. They found an increase in the cyclone frequency at high latitudes (60°-90°N) and a decrease in cyclone frequency at mid-latitudes (30°-60°N). This suggests a net northward movement of these storm tracks over time. Surface cyclones and anticyclones tend to follow the flow aloft (Bluestein 1993), which also steers the upper-troposphere fronts. Therefore these findings support the conclusion that the upper-troposphere fronts have moved poleward over this time period.

Planetary wave activity can also affect the NAO (Dhomse et al. 2006). The NAO is the year-to-year variation in the strengths and positions of the permanent high pressure system over the Azores and low pressure system over Greenland. A high NAO index year corresponds to increased westerlies and mild weather for Europe. In a low NAO index year, the westerlies are suppressed and storm tracks tend to track southerly, leading to cold European winters. The NAO index shows a continued increase from the 1960's to the 1990's, leading to more northerly storm tracks (Appenzeller et al. 2000), and thus a poleward movement of the upper troposphere fronts.

Many studies use different combinations of these parameters to attempt to deduce the contribution made by dynamics to trends in total ozone. Krzyścin et al. (2001) used many dynamical proxies to estimate the dynamical contribution to the ground-based total ozone trend between 35° and 60°N for 1970-1997. Solar cycle, El Nino Southern Oscillation (ENSO), QBO, PV variations, NAO, and various other prevalent patterns were used, and accounted for ~70-80% of the observed trend. Reinsel et al. (2005) showed that the Arctic Oscillation (AO) and EP flux index series had a considerable influence on total ozone from 1978-2002 at latitudes poleward of 40°N. Hood and Soukharev (2005) found that a regression analysis containing solar, QBO, EP flux, and

PV variations explained approximately 50% of the trend in ozone for Northern Hemisphere latitudes north of 40°N from 1979 to 2002. Hadjinicolau et al. (2005) examined the dynamically-driven trends in total ozone using a three-dimensional chemical transport model. The transport was derived from winds from the European Centre for Medium-Range Weather Forecasts (ECMWF) analysis. They concluded that over the period 1979-1993, the dynamically-driven model trend accounted for 30% of the observed trend and from 1994 to 2000, it accounted for 100% of the trend.

As stated in Chapter 2, the upper troposphere fronts are related to planetary Rossby waves. Their movement will therefore be linked to several of the dynamical processes described above. The trends in the relative areas of each regime can be used to estimate the contribution to the zonal trend made by the movement of the upper troposphere fronts. If the portion of the zonal trend arising from changes in the total ozone within each regime is separated from the portion of the trend arising from changes in the relative areas, then a crude estimate of the role of the two can be obtained. Equation 4.1 is differentiated to yield:

$$\frac{d\Omega}{dt} = \frac{d\Omega_T}{dt} R_T + \frac{dR_T}{dt} \Omega_T + \frac{d\Omega_M}{dt} R_M + \frac{dR_M}{dt} \Omega_M + \frac{d\Omega_P}{dt} R_P + \frac{dR_P}{dt} \Omega_P + \frac{d\Omega_A}{dt} R_A + \frac{dR_A}{dt} \Omega_A \quad (4.7)$$

The variation of zonal total ozone with time is now represented by two terms, one in which the total ozone is fixed, and the area changes (representing frontal movement), and one in which the areas remains constant, and the total ozone within each regime changes (Hudson et al. 2006). The mean values and slopes used to calculate each term are found in Tables 4.2 and 4.5, and therefore include the effects of the solar cycle and QBO. The results can be found in Table 4.8. The sum of the area-changing terms in Equation 4.7 is -3.6 DU, and the sum of the terms indicating changes within the regimes is -7.0 DU.

Thus, from this analysis 35% of the zonal trend in total ozone from January 1979 to May 1991, between 25° and 60°N, can be ascribed to movement of the upper troposphere fronts. The remaining 65% could have both chemical and dynamical origins. For example, ozone depletion by heterogeneous chemistry and an overall weakening of the Brewer Dobson circulation over this time period would cause a negative total ozone trend within a regime. These estimates agree well with the previous studies described above. This analysis was also performed on the period 1996-2004, but the errors in the regression constants became much larger, and no significant conclusion could be drawn for this time period.

This analysis shows that changes in zonal total ozone at mid-latitudes are a combination of changes in total ozone within each regime and changes in the relative weighting of these regimes brought about by movement of the subtropical and polar upper troposphere fronts. The rest of this work will focus on the effect this has on the vertical profiles of both ozone and water vapor.

Regime	$\Omega_X \frac{dR_X}{dt}$	$R_X \frac{d\Omega_X}{dt}$
Tropical	8.4	-1.3
Midlatitude	-1.3	-3.6
Polar	-10.6	-1.7
Arctic	-1.2	-0.1
Total	-3.6	-7.0

Table 4.8 Terms in Equation 4.7, calculated from January 1979 – May 1991

Chapter 5: Results – Vertical Profiles

Hudson et al. (2003) showed that when Northern Hemisphere rawinsonde and ozonesonde data were divided into meteorological regimes, similar profile shapes were seen within each regime. This can be observed by looking again at Figures 3.6 and 3.8 (taken from Hudson et al. 2003). Each regime is characterized by a unique tropopause height in both the thermal and ozone profile. However, it should be noted that, as described in Chapter 2, the thermally defined tropopause and the ozone-defined tropopause do not always agree. Bethan et al. (1996) showed that in the mid-latitudes, 98% of the time the ozone tropopause (hereinafter referred to as the *ozonepause*) was approximately 1 km lower than the thermal tropopause, when the latter was well-defined. Figures 3.6 and 3.8 were created using the ozone contour method of defining the boundary, a method that has since been improved upon, as described in Chapter 3. The same results, in terms of separation into meteorological regimes, are expected to be seen using the latitudinally varying boundaries. Ozone profiles from the Halogen Occultation Experiment (HALOE) and Stratospheric Aerosol and Gas Experiment II (SAGE II) satellite instruments were used to examine this.

5.1 HALOE

The HALOE instrument has been widely used to study the chemistry of the stratosphere because of its global coverage, its coincident measurements of several key chemical species, and its relatively long time period (1991-2005). It was aboard the Upper Air Research Satellite (UARS) and was launched on September 15, 1991 into a

585 km, 57° inclination orbit. The UARS satellite contained ten instruments designed to collectively measure both ozone and those chemical species that affect ozone chemistry. In addition, solar input and stratospheric temperature and winds were measured. The HALOE instrument started taking observations on October 11, 1991 after a brief period of outgassing, and ended on November 21, 2005. The experiment was devised to observe not only ozone but also several other species that have direct effects on ozone levels, namely hydrochloric acid (HCl), hydrogen fluoride (HF), methane (CH_4), water vapor (H_2O), nitrogen dioxide (NO_2), and nitrous oxide (NO), in order to gain a better understanding of the chemistry and dynamics of middle-atmosphere processes (Russell et al. 1993). Vertical profiles of these constituents are measured along with aerosol extinction and temperature versus pressure.

HALOE is a limb-scanning solar occultation instrument. Figure 5.1 shows a schematic of this technique. A vertical scan is obtained by tracking the sun through the atmosphere. Vertical profiles are inferred by measuring solar energy absorption through the atmosphere in selected spectral bands, as well as the unattenuated solar signal. Measurements made using the solar occultation technique have a higher sensitivity than nadir measurements because there is 30-60% more absorber in the limb (Russell et al. 1993). In

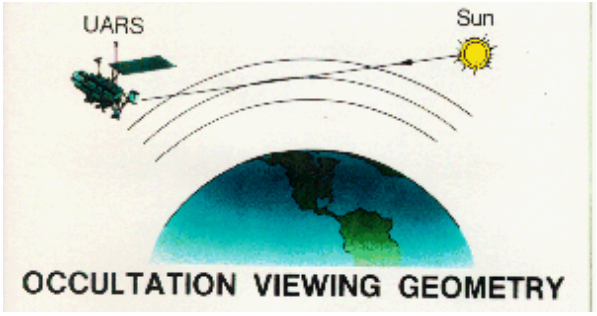

Figure 5.1 Schematic of the solar occultation technique used by the HALOE instrument. Taken from http://www.nasa.gov/centers/langley/science/HALOE_retires.html

addition, because of the limb geometry and the exponential decrease of density with altitude, most absorption occurs at or near the tangent point. Another advantage of this method is that each measurement is a ratio of the attenuation inside and outside of the atmosphere. This makes the instrument somewhat self-calibrating, reduces drift errors, and makes it especially good for trend analysis.

The satellite orbit precesses, covering from ~80°N – 80°S over a year. The latitude coverage for the year 2000 is shown in Figure 5.2. Due to the nature of the satellite's orbit, the maximum sampling for each day is 15 sunrise and 15 sunset measurements, most of the time in opposite hemispheres. During an occultation event, all of the chemical species listed above are measured. Depending on the channel, the altitude range sampled is from 15 to ~60-130 km, with a vertical resolution of about 2.3 km, and a horizontal resolution of ~200 km (SPARC, 2000).

Both broadband and gas filter channels are used to measure selected segments of the infrared spectral range from 2.45 μm to 10.04 μm (Russell et al. 1993). First, the

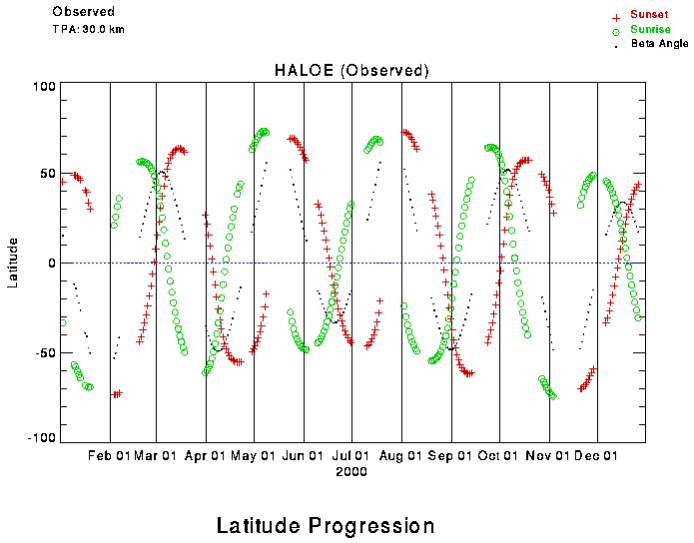

Figure 5.2 Latitude coverage by the HALOE instrument for the year 2000, taken from the HALOE website at http://haloedata.larc.nasa.gov.

exoatmospheric and atmospheric-attenuated measurements are ratioed to calculate the atmospheric transmission over a specific spectral band. However, transmission is a function of temperature, pressure, and mixing ratio. In order to infer the temperature versus pressure profile, this process is first done over a spectral band where the gas mixing ratio is known. For this case, carbon dioxide (CO_2) over the 2.8-μm band is used. Using the temperature versus pressure profile, the mixing ratios of other chemical species over their respective bands can be inferred. For ozone (9.6 μm), water vapor (6.6 μm), CO_2, and NO_2, a broadband radiometer approach can be used because these gases can be spectrally isolated (Russell et al. 1993). The remaining chemical species are inferred using the more complicated gas filter technique, which will not be discussed here, as the primary species of interest are ozone and water vapor.

Validations have been done on the various versions of the HALOE ozone data (Brühl et al. 1996; Bhatt et al. 1999). The HALOE version 19 level 3 data, used here, has been interpolated to the HALOE pressure grid. This data has also been screened for cirrus cloud contamination using the method described in Hervig and McHugh (1999). The sunrise and sunset data have been combined and show differences less than 5% above 100 mb (Brühl et al. 1996). In the lower stratosphere, the major systematic and random uncertainties in the ozone data are between 9 and 25%, and between 9 and 20% for the upper stratosphere (Brühl et al. 1996; Grooβ and Russell 2005). Bhatt et al. (1999) found agreement with coincident ozonesonde measurements better than 10% down to 200 mb, and better than 20% down to 300 mb in the extratropics. In the tropics and subtropics, the agreement was better than 10% down to 100mb.

5.2 SAGE II

The SAGE II instrument was launched aboard the Earth Radiation Budget Satellite (ERBS), and was operational from October 5, 1984 to August 26, 2005. SAGE II (hereafter referred to as SAGE) is a seven-channel sun photometer that uses solar occultation to infer vertical profiles of ozone, water vapor, NO_2, and aerosol extinction at several wavelengths from 0.385-1.02 μm. Similar to HALOE, SAGE was launched into a 610 km, 57° inclination precessing orbit that covers from ~70°S-70°N, and takes a maximum of 15 sunrise and 15 sunset measurements per day (Cunnold et al. 1989). The vertical resolution is 1 km (Chu et al. 1989), and the horizontal extent along the line of sight is 200 km by 2.5 km for a 1-km retrieved layer (WMO 1998).

SAGE employs an onion-peeling inversion algorithm to calculate ozone concentrations. Solar radiance is reduced into transmittance functions over the seven wavelength regions, and used to calculate a vertical extinction profile for ozone, which is the product of its number density and its absorption cross section. The ozone profiles are retrieved using the irradiance measurements in the 0.6-μm channel. The exoatmospheric and atmospheric attenuated transmittance are measured and ratioed over each spectral band and instrumental field of view (Chu et al. 1989). The retrieval algorithm first ascertains the position of the measurement relative to both the sun and the atmosphere. Next the algorithm removes any interference by Rayleigh scattering from the measurement. By excluding water vapor, six reduced equations for optical depth are obtained. The contributions from NO_2, and then aerosols are then removed. A vertical profile inversion is then applied iteratively to obtain the vertical extinction profile.

There are four main sources of error in the SAGE profiles: 1) measurement errors, 2) errors in the temperature measurements, and therefore errors in the density, used to determine the contribution from Rayleigh scattering, 3) uncertainty in the reference altitude, and 4) uncertainty in the removal of the NO_2 and aerosol contributions (Chu et al. 1989). For ozone, the dominant source of error is the measurement error, but the total random error for a 1-km vertical resolution is less than 7% between 2 km above the tropopause and 43 km (Cunnold et al. 1989). Better than 10% agreement between SAGE version 6.1 ozone measurements and coincident ozonesonde measurements was found down to the tropopause (Wang et al. 2002). In addition, Randall et al. (2003) found that HALOE v19 and SAGE v6.1 ozone profiles agree within 5%, and Morris et al. (2002) report virtually no drift in the HALOE v19 ozone observations with respect to SAGE II v6.0. Version 6.2 of the SAGE data is used here. This data differs little from the version before[1], v6.1.

5.3 Method

Every profile measured by HALOE and SAGE has an associated latitude, longitude, time, and date. These were used to locate the corresponding location on the TOMS image for that day in order to classify the profile into meteorological regimes. Both retrieval algorithms assume a homogeneous atmosphere for their calculations (Chu et al. 1993). However, the region around the front represents a discontinuity in tropopause height that will not be accounted for in the retrieval. For this reason, the subtropical, polar, and arctic boundaries were widened. For the present analysis, the

[1]"For the most part, the ozone density profiles have changed on the order of 0.5% from version 6.1. The changes may be larger above 50 km and are due primarily to the correction of an altitude registration problem in our NCEP gridding algorithm." Taken from http://www-sage2.larc.nasa.gov/data/v6_data/

boundaries are widened by one pixel in latitude and longitude. However, when the ozone gradient weakens, from about June to October, the boundaries can become broader. Therefore widening the boundary by one pixel may not be sufficient to eliminate all of the profiles that should be classified as being in the boundary between regimes. However, widening the boundaries by two pixels eliminated too many data points. Thus, one pixel was chosen as a compromise between classification accuracy and number of data points. Misclassification could also occur because of different measurement times. TOMS measurements are made at local noon, whereas both SAGE and HALOE measurement are made at local sunrise or sunset. For example, in the case of sunrise measurements, the total ozone field that is measured by TOMS could have shifted with respect to the total ozone field at sunrise that day. This source of error will depend on the time of year, as weather patterns are more persistent and slower in summer and fall.

Ozone profiles from SAGE and HALOE, from 25°-60°N, were classified into meteorological regimes for every day that there were profiles and TOMS data available from January 1997 to December 2003. This time period was chosen for several reasons. As stated above, HALOE began taking measurements in 1991, and SAGE began in 1984. However, due to the eruption of Mount Pinatubo in June 1991, measurements below 25 km for HALOE (WMO 1998), and below 20 km for SAGE (Wang et al. 2002) until the end of 1993 are contaminated by aerosols. Corrections have been applied for this time period for both instruments (Bhatt et al. 1999; Wang et al. 2002), but as this is the region of interest for this work, these time periods were not analyzed. In addition, Nimbus-7 TOMS data ceased in May 1993, and the Meteor-3 data has many months missing due to

lack of data and non-convergence, as discussed in Chapter 4. Thus, January 1997, the beginning of the EP TOMS data period, was chosen as the starting point.

5.4 Ozone Profile Separation – One day

When classified by meteorological regime, ozone profiles should exhibit similar tropopause heights. Figure 5.3 shows the TOMS total ozone field for January 8, 2001 in addition to the subtropical, polar, and arctic boundaries, shown as blue, red, and black lines, respectively. Each "X" on this figure represents a sunset HALOE event for this day, and has been assigned a number from 01 through 15. The color of each X corresponds to its classification: blue - polar; purple - midlatitude; red - tropical; black - boundary. Each HALOE measurement is approximately 24 degrees of longitude apart. The profiles for this day can be seen in Figure 5.4. Only those that fell within a regime are colored and listed on the figure. All three regimes are seen on this day, in addition to several profiles that have been eliminated because they fell too close to the boundary. Profiles 05 through 08 are of particular interest. Here two tropical profiles are surrounded by a midlatitude profile to the east and west. In order to examine these profiles closely Figures 5.5a-c show the individual profiles that have been classified as polar, midlatitude, and tropical, respectively. The three tropical profiles in Figure 5.5c have similar shapes, show ozonepause heights at around 15-16 km, and ozone mixing ratio maxima around 37 km. Figure 5.5b shows the two midlatitude ozone profiles on either side of the 06 and 07 tropical profiles. These too also show similar profile shapes and ozone maxima around 37 km. Unfortunately, the profiles stop around 12 km, making it difficult to determine approximate ozonepause heights. However, these two profiles

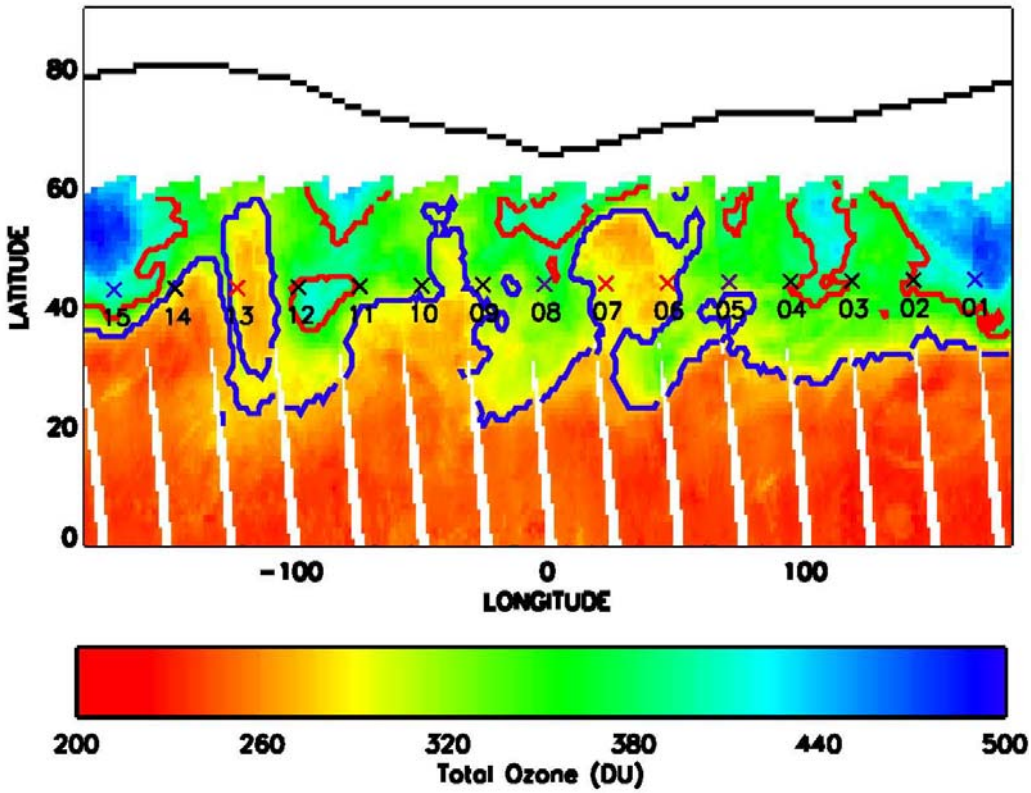

Figure 5.3 EP TOMS total ozone field for January 8, 2001. The subtropical, polar, and arctic boundaries are shown as blue, red, and black lines, respectively. Each X represents a HALOE sunset measurement for this day, and has been numbered 01 through 15. The color of each X corresponds to its classification: red – tropical, purple – midlatitude, blue – polar, and black – boundary.

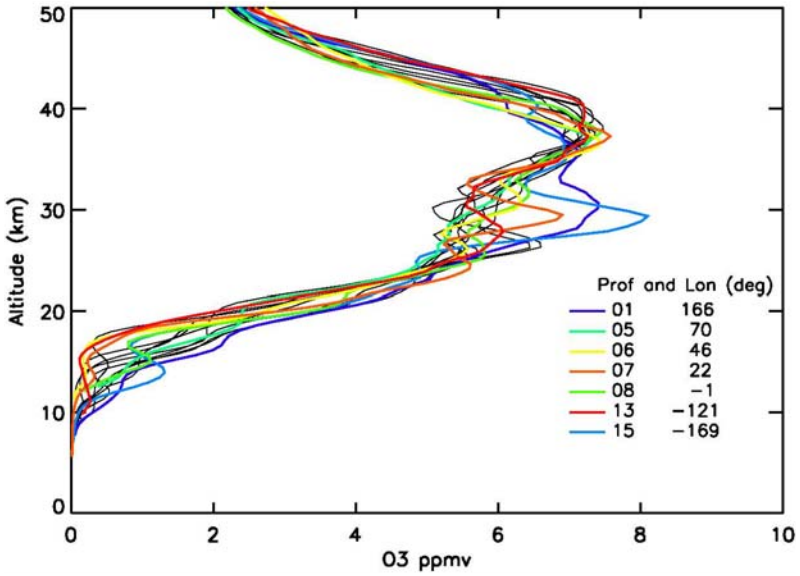

Figure 5.4 HALOE ozone profiles that correspond to the X's on Figure 5.3 for January 8, 2001. Profiles that were classified into a meteorological regime are shown in color and listed on the figure. Profiles that fell within a pixel of the boundary are shown in black.

have distinctly different lower stratospheric profile shapes from the two tropical profiles between them. In fact, profiles 06 and 07 show more similarity with profile 13, 140 degrees longitude away. The polar profiles for this day are seen in Figure 5.5a and display ozonepause heights around 9-10 km. These show ozone maxima around 30 km at lower altitudes than the tropical and midlatitude profiles.

This day is a good example of the advantage of classifying profiles by meteorological regime. All of the HALOE measurements seen in Figures 5.3 and 5.4 are located within ~2 degrees latitude of each other, as all of them fall between approximately 43° and 45°N, yet they show distinctly different profile shapes in the lower to mid stratosphere. Thus, if a zonal average over this very small latitude band was done at 15 km, it would contain both upper tropospheric and lower

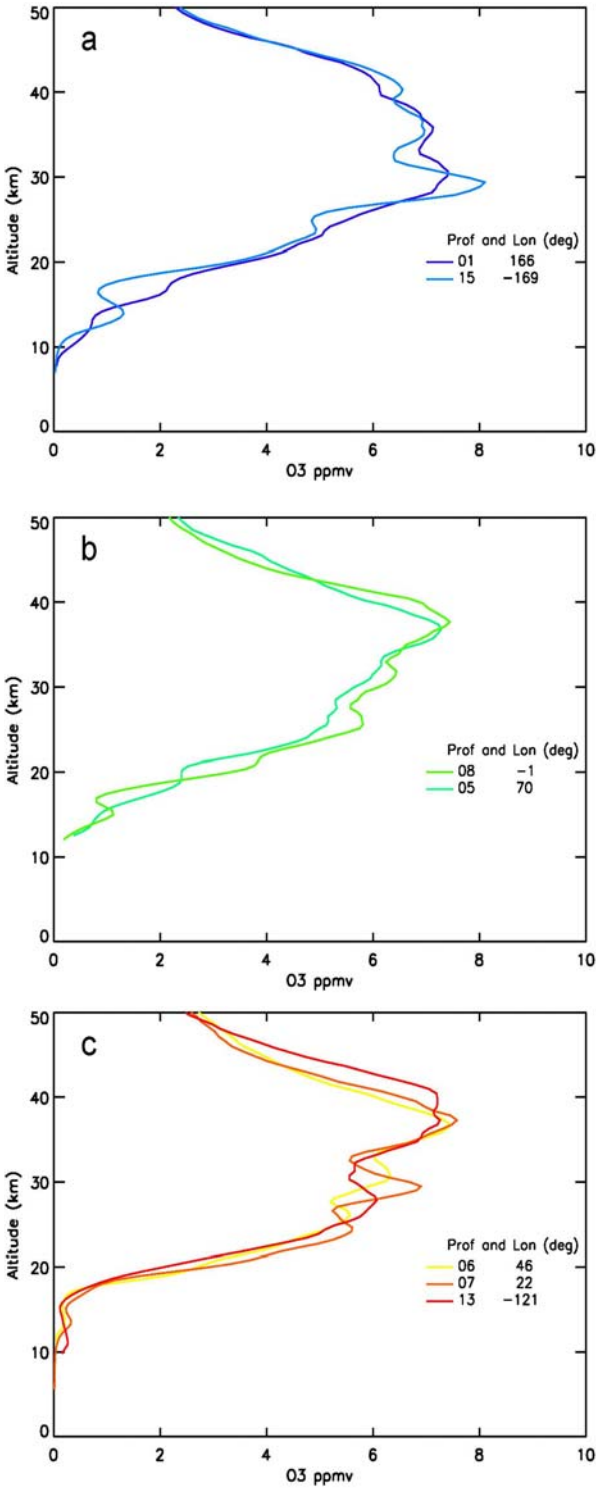

Figure 5.5 HALOE ozone profiles that correspond to the colored X's on Figure 5.3 for January 8, 2001 for the a) polar regime, b) midlatitude regime, and c) tropical regime. The profile numbers and longitudes are also listed.

stratospheric air. By classifying these profiles by meteorological regime, the lower stratosphere can be isolated. This is essential for the examination of ozone trends in the lower stratosphere.

5.5 Ozone Profile Separation – Climatology

As expected, ozone profiles separate well by regime. Next, data from both HALOE and SAGE were used to calculate monthly climatologies for each regime over the time period 1997 – 2004. Only profiles between 25° and 60°N were included in this analysis. Figures 5.6 and 5.7 show the March and June, and September and December ozone profile climatologies, respectively, calculated using data from the HALOE instrument for the subtropical (red), midlatitude (green), and polar (blue) regimes. The one-sigma standard deviations are shown as dashed lines on either side of the mean, and the number of points used to calculate the mean is shown on the right side of each plot. Both the number of points and the standard deviations have the same color scheme as the mean profiles.

In the lower stratosphere, the climatological profiles show distinct ozonepause heights within each regime for every month, except for September, which will be discussed below. In the region of the tropopause the distributions barely overlap, if at all. The largest ozone mixing ratio values are seen in the tropical regime in June coinciding with a maximum in ozone production. The lowest ozone values and ozonepause heights are seen in December. The polar regime consistently has the lowest number of points, owing to the fact that it is the smallest in area.

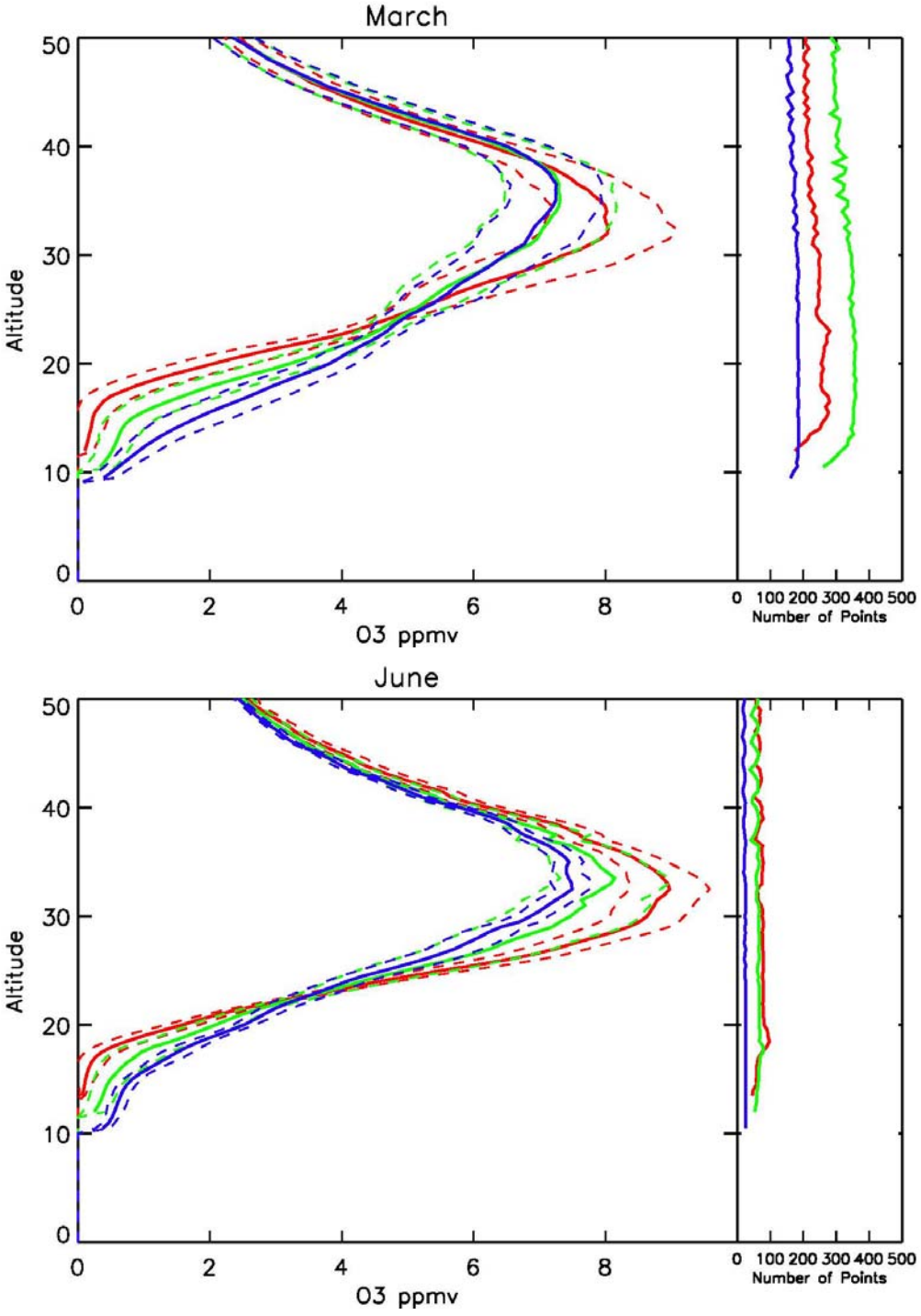

Figure 5.6 HALOE ozone profile climatologies calculated from 1997-2004 between 25° and 60°N for March (top) and June (bottom). The one-sigma standard deviations are shown as dashed lines, and the number of points is shown on the right. The color scheme is: red – tropical, green – midlatitude, and blue – polar.

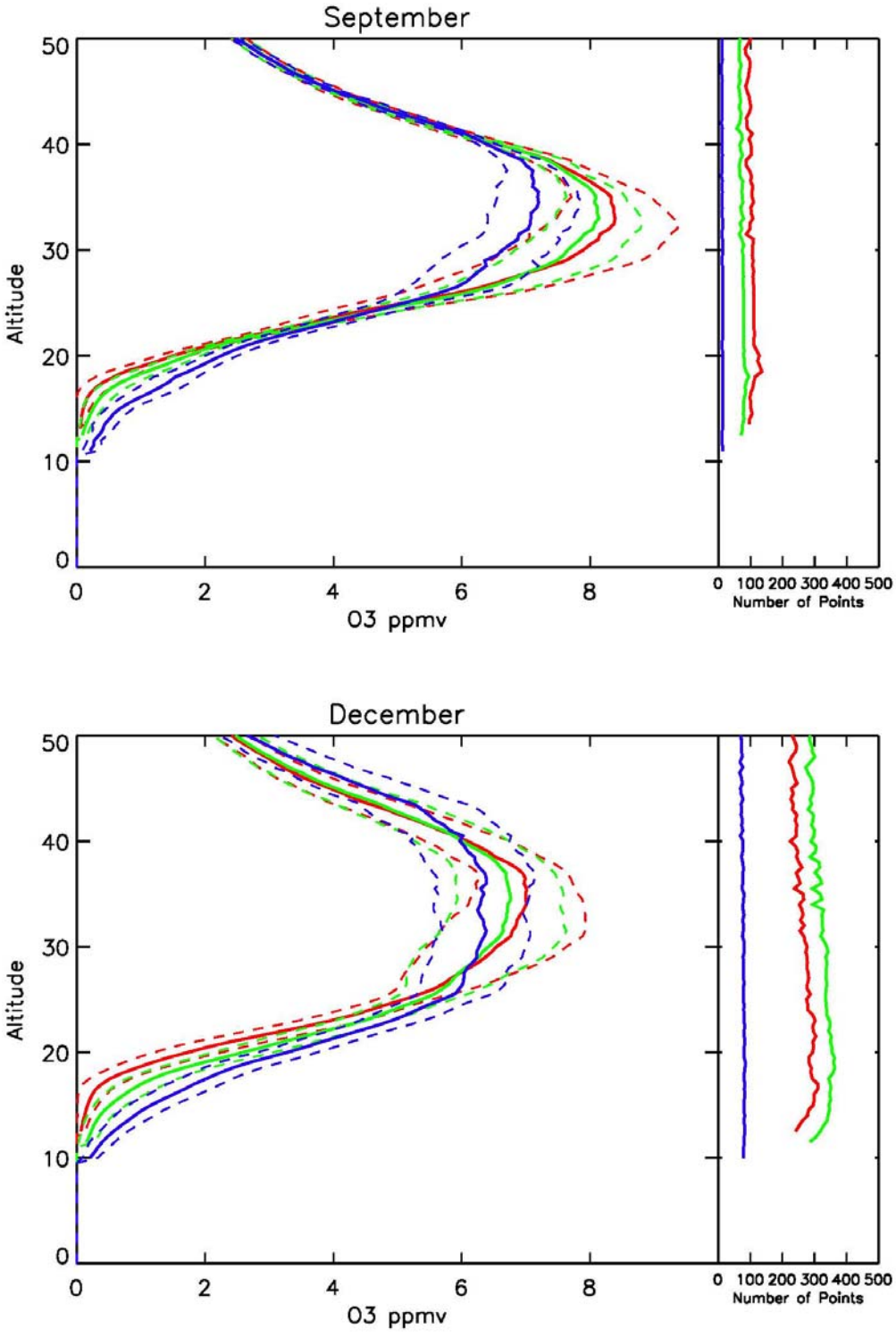

Figure 5.7 HALOE ozone profile climatologies calculated from 1997-2004 between 25° and 60°N for September (top) and December (bottom). Color scheme and line designation same as Figure 5.6.

As discussed in Section 4.2, the total ozone is at its "flattest" in August and September, meaning the difference in DU from one regime to the next is at a minimum, as is the difference in tropopause height. During this time of year persistent and weak weather patterns are prevalent. These months are therefore most susceptible to misclassification errors. An increase in tropospheric pollution could add to the column amount and cause a region that would otherwise be tropical, to be classified as midlatitude. An example of the homogeneity of the total ozone field during these months is given in Figure 5.8. This figure shows the total ozone field for September 5, 2001, and is similar to Figure 5.3. There are six tropical profiles and three midlatitude profiles on this day. They are plotted on Figure 5.9, similar to Figure 5.4. There is little difference in the profiles seen here

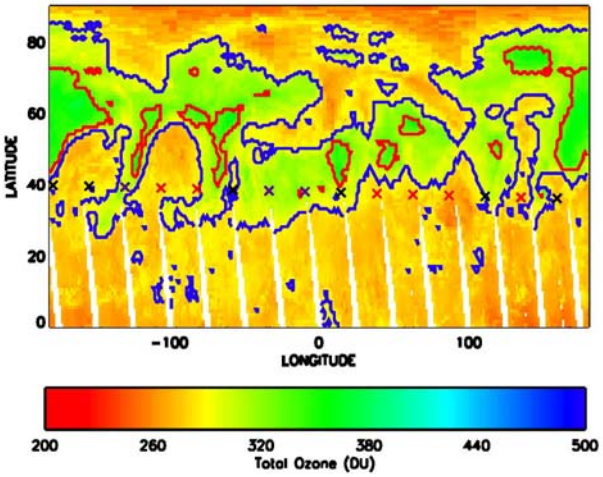

Figure 5.8 EP TOMS total ozone field for September 5, 2001. The subtropical, polar, and arctic boundaries are shown as blue, red, and black lines, respectively. Each X represents a HALOE sunrise measurement for this day. The color of each X corresponds to its classification: red – tropical, purple – midlatitude, blue – polar, and black – boundary.

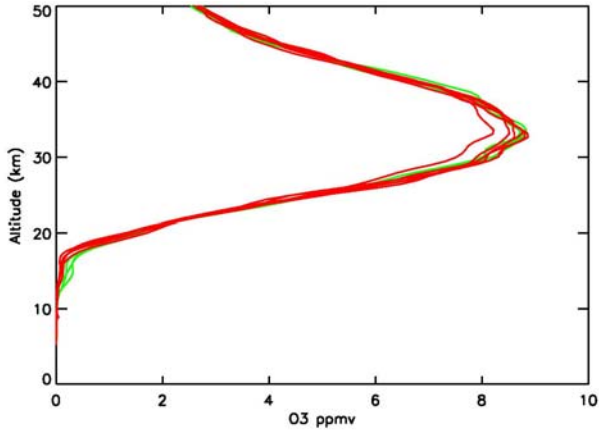

Figure 5.9 HALOE ozone profiles that correspond to the X's on Figure 5.8 for September 5, 2001. Profiles that were classified into the tropical regime are shown in red, and midlatitude is shown as green.

despite being classified into different regimes. They show similar shapes and ozonepause heights. These figures show that a combination of interference from tropospheric pollution and a flatter total ozone field can lead to both misclassification and a reduced distinction between regime profiles.

The March and June, and September and December ozone profile climatologies calculated using data from SAGE are shown in Figures 5.10 and 5.11, respectively. Similar to the HALOE figures, the one-sigma standard deviation in addition to the number of points within each regime is shown. As anticipated, the same features seen for the HALOE climatologies are also observed here, namely, distinct ozonepause heights and lower profile shapes in the lower stratosphere. The climatologies calculated by the two different instruments are shown in Figures 5.12 and 5.13. On these figures, the solid lines represent the data from HALOE, the dashed lines represent the SAGE data, and the tropical regime, midlatitude regime, and polar regime are red, green, and blue, respectively. The one-sigma standard deviations for each regime and the zonal data between 25° and 60°N (shown as a black solid line for HALOE and a black dashed line for SAGE) have also been included on these figures. It should be noted that below about 20 km for SAGE and about 23 km for HALOE, the standard deviation within each regime is smaller than that for the zonal data. This indicates a reduction in lower stratospheric variability when separating by regime.

The climatologies agree well in the lower stratosphere for every regime, and every month. Though the month of September shows the worst agreement between the two instruments, they still agree within experimental error. As described above, these two instruments use the solar occultation technique to infer vertical profiles of several

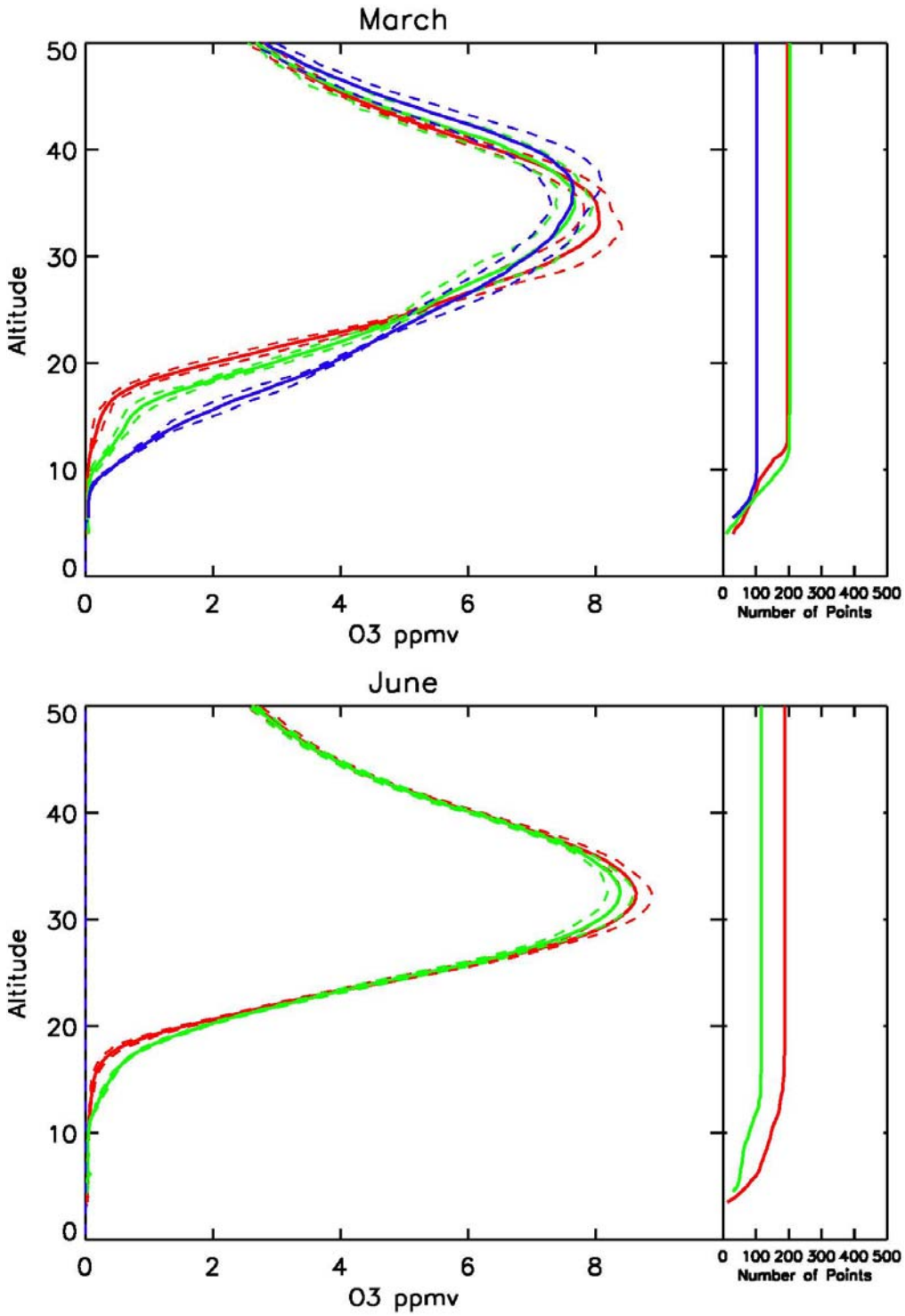

Figure 5.10 SAGE ozone profile climatologies calculated from 1997-2004 between 25° and 60°N for March (top) and June (bottom). Color scheme and line designation same as Figure 5.6.

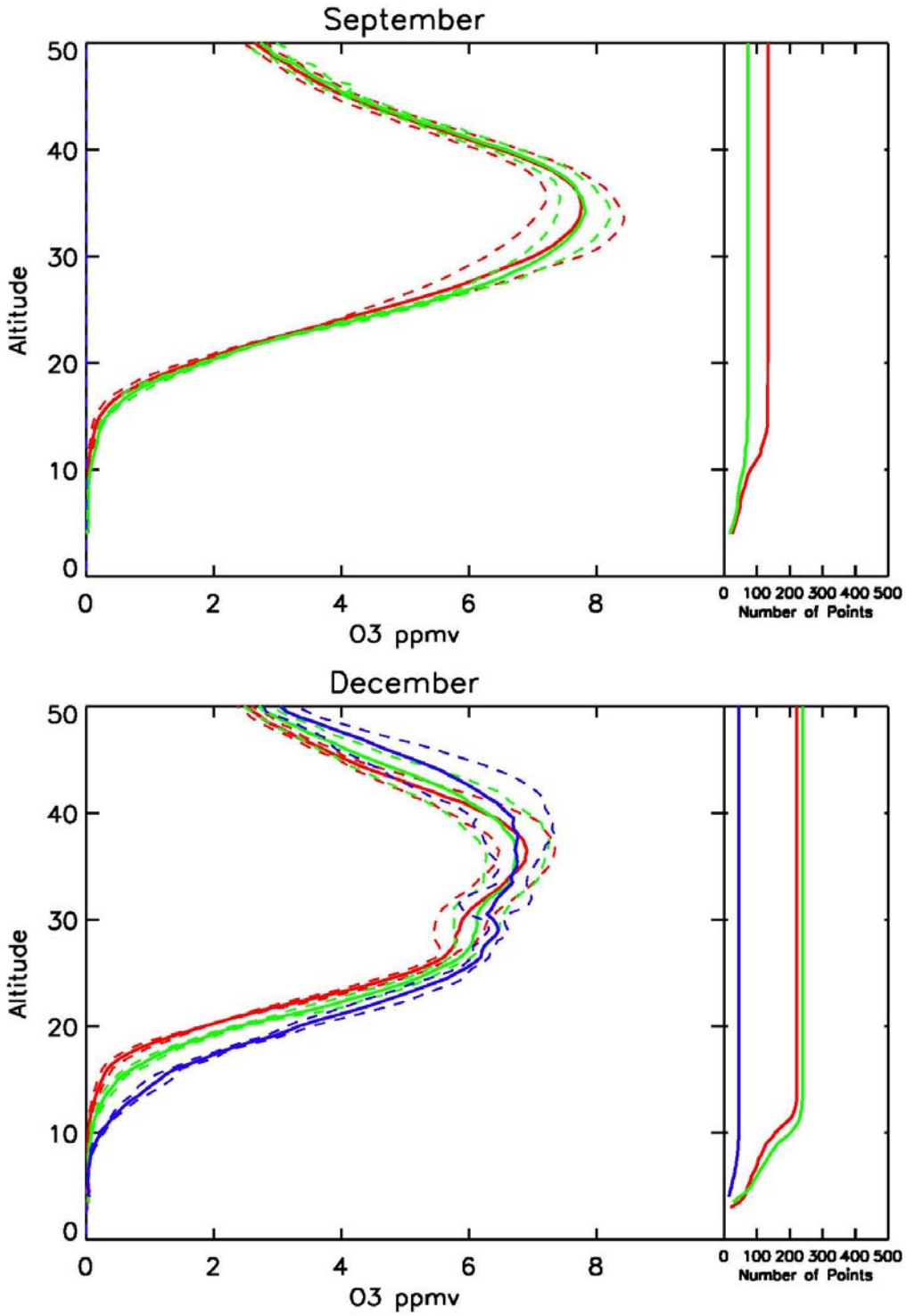

Figure 5.11 SAGE ozone profile climatologies calculated from 1997-2004 between 25° and 60°N for September (top) and December (bottom). Color scheme and line designation same as Figure 5.6.

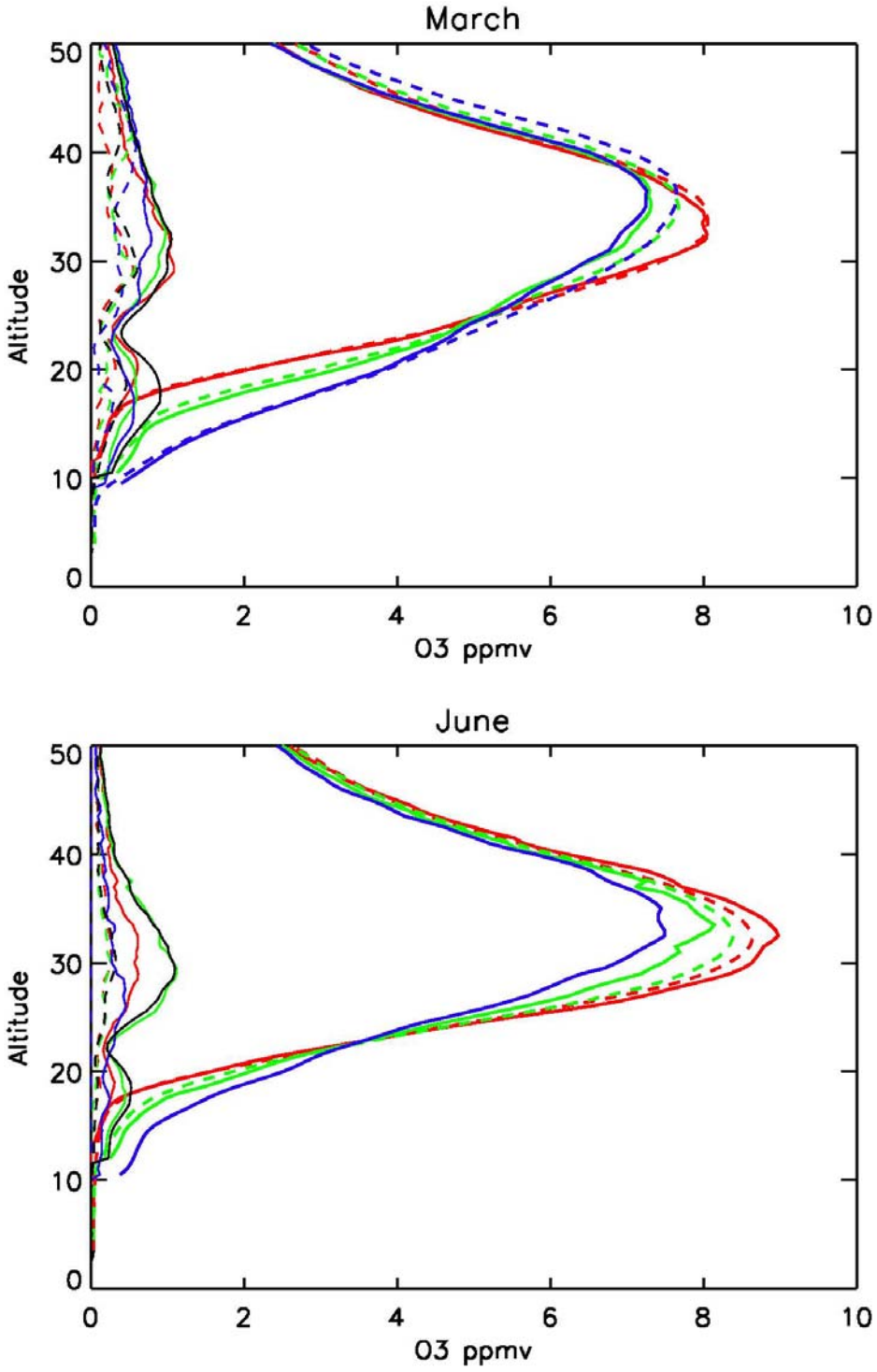

Figure 5.12 HALOE and SAGE ozone profile climatologies calculated from 1997-2004 between 25° and 60°N for March (top) and June (bottom). HALOE data is shown as solid lines, and SAGE data is shown as dashed lines. The one-sigma standard deviations are shown on the left. The color scheme is: red – tropical, green – midlatitude, and blue – polar. The zonal standard deviations between 25° and 60°N for both instruments have also been plotted in black (HALOE-solid, SAGE-dashed).

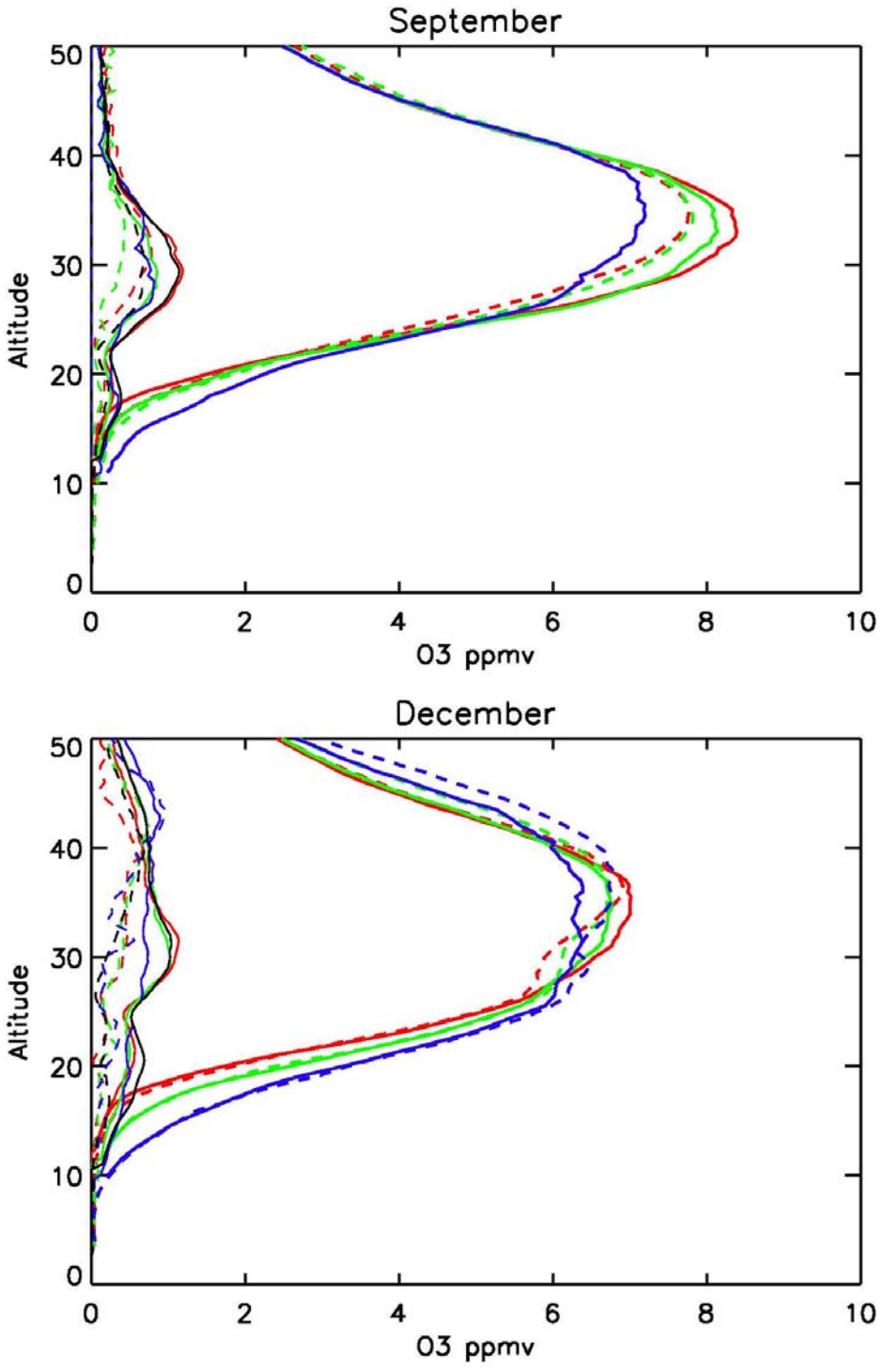

Figure 5.13 HALOE and SAGE ozone profile climatologies calculated from 1997-2004 between 25° and 60°N for September (top) and December (bottom). Color scheme and line designation same as Figure 5.12.

chemical species. As such, they have very similar orbits and sampling patterns. However, there are a number of differences between the two. The sampling patterns of the two satellites do not coincide with one another. In fact, the number of coincident measurements between the two instruments is small (Morris et al. 2002). Figure 5.14 show histograms of the latitude distributions of the SAGE and HALOE satellites. Again, HALOE is shown by solid lines and SAGE is shown by dashed lines. Each satellite has been normalized to itself for these figures. In March, the latitude distributions of each regime are similar. However, the distributions of June, September, and December show

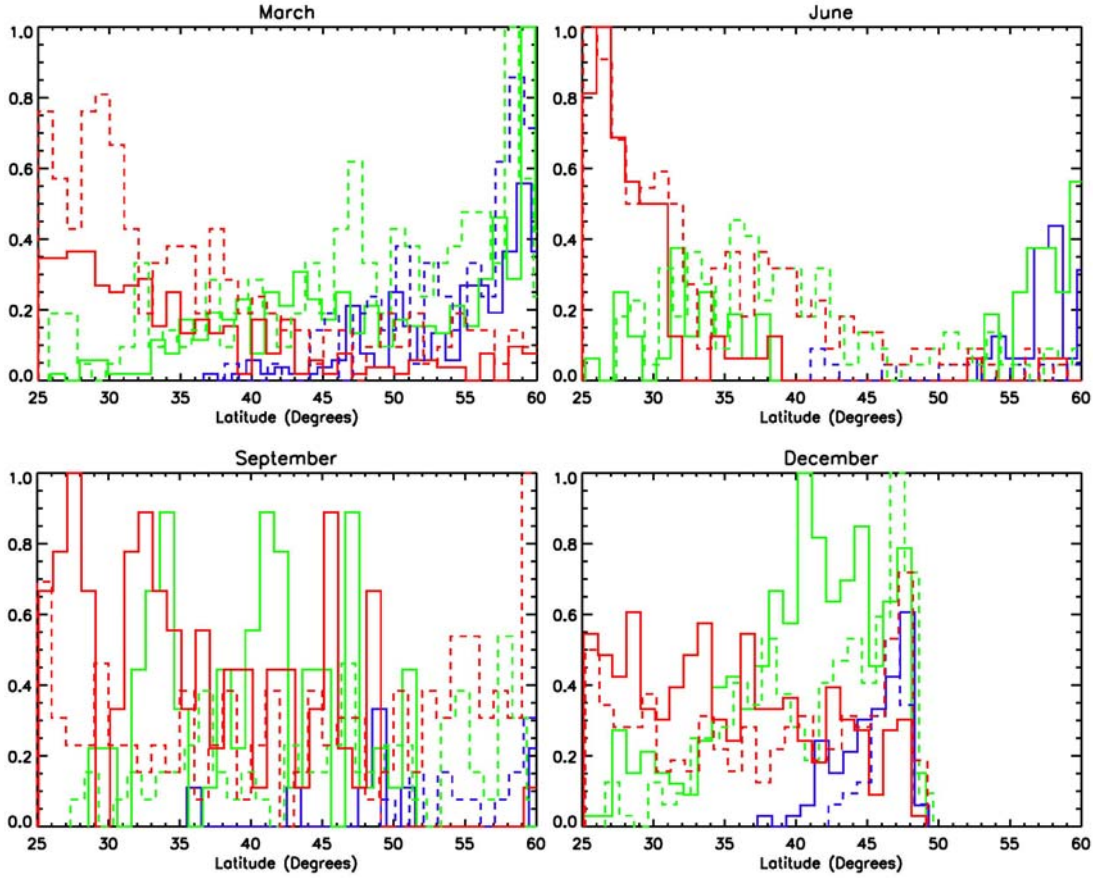

Figure 5.14 Latitude distribution histograms for March, June, September, and December for 1997-2004. HALOE is shown as solid lines and SAGE is shown as dashed lines. The color scheme is: red – tropical, green – midlatitude, and blue – polar. Each instrument has been normalized to itself.

significant differences. For example, the tropical profiles in June from HALOE are primarily located south of ~40°N, whereas the SAGE tropical profiles are located throughout the 25°-60°N latitude zone. Another difference between the two instruments is the region where ozone absorption is measured. HALOE measures ozone in the infrared region of the spectrum (9.6 μm), whereas SAGE measures in the visible (0.6 μm). These differences make the agreement seen in Figures 5.12 and 5.13 all the more impressive.

The agreement between the two climatologies appears to deteriorate above approximately 25 km. This corresponds to the region where photochemistry begins to dominate the distribution of ozone. This can also been seen in the overlap of the climatologies in the mid and upper stratosphere. If the profiles from 25°-60°N were separated into latitude bands, and not meteorological regimes, there would be little to no overlap in the mid and upper stratosphere. Figure 5.15 shows three climatological profiles for March. The red represents the low-latitude profiles

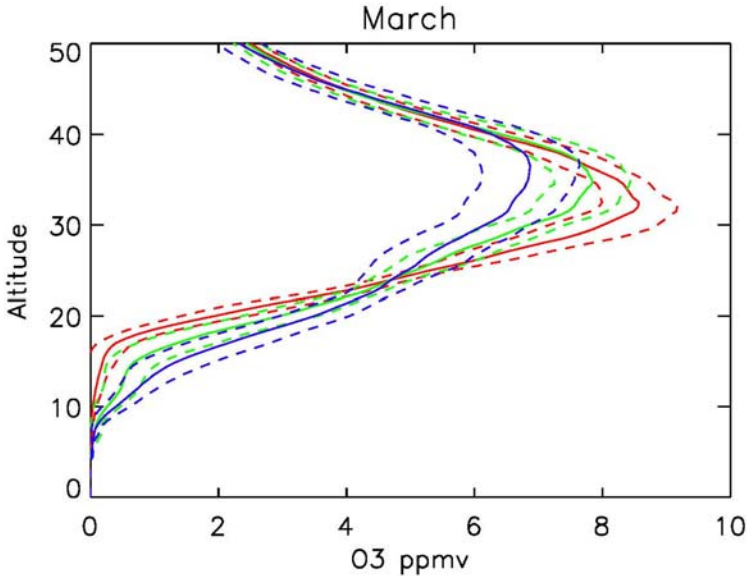

Figure 5.15 HALOE ozone profile climatologies calculated from 1997-2004 between 25° and 60°N for March. The red indicates the low latitude (25°-33°N) climatology, the green indicates the middle latitude (38°-46°N) climatology, and the blue indicates the high latitude (51°-60°N) climatology. The dashed lines are the one-sigma standard deviation.

(25°-33°N), the green represents mid-latitude profiles (38°-46°N), and the blue represents high-latitude profiles (51°-60°N). The dashed lines are the one-sigma standard deviation. The chemistry-dominated region above ~30 km shows three different ozone peak altitudes and values. The lower stratosphere shows three different tropopause heights. However, in contrast to the March climatologies shown in Figures 5.6 and 5.10, these overlap in error significantly. This indicates that the meteorological regime influence extends up to approximately 25 km, above which, ozone tends to follow a more zonal structure.

5.6 Water Vapor

5.6.1 Characteristics and Distribution

Water vapor makes up only a small fraction of the mass of the Earth's atmosphere. Out of this small fraction, only a few percent is liquid water in the form of clouds. However, though it is not present in abundance, water vapor is very important for the study of the atmosphere. It is one of the atmosphere's most variable components; it is affected by both large-scale circulations and convection, and is the most effective greenhouse gas. Water vapor absorbs energy at various wavelengths in the infrared. This absorption is essential to the energy balance of the planet, thus a better understanding of its interannual variability is essential for predicting future climate change.

The primary source of water vapor in the atmosphere is evaporation from the ocean surface (Brasseur and Solomon 1984). Consequently, water vapor values decrease from these low altitudes up, reaching a minimum around the tropopause. Water vapor is

also the source of the hydroxyl radical, OH, in both the troposphere and stratosphere. OH directly affects many chemical cycles, controls the oxidizing capacity of the atmosphere for short-lived species, and regulates the lifetimes of longer-lived species (Kley et al. 2000). For this reason, it is important to identify the dynamics that affect the concentration and distribution of water vapor

Water vapor in the stratosphere is controlled by several factors, and is still the source of much debate (Kley et al. 2000). One of the most important processes , the oxidation of methane, produces 1.6-2 molecules of H_2O per molecule of CH_4 (Letexier et al. 1988) such that the quantity $2 \times CH_4 + H_2O$ is usually used to approximate the water budget of the atmosphere. Exceptions to this are regions that experience dehydration, such as in the Arctic and Antarctic ozone holes (Kley et al. 2000, and references therein).

Water vapor distribution is influenced by atmospheric dynamics, but can also be an influence on atmospheric dynamics. An example of the latter is the condensation of water vapor that serves as an atmospheric heat reservoir, providing energy for storm development. The major dynamical pathway for water vapor to enter the stratosphere is through cross-isentropic transport across the tropical tropopause as part of the Brewer-Dobson circulation (Brewer, 1949). Since water vapor and temperature decrease with altitude in the troposphere, the amount that passes into the stratosphere through this mechanism is controlled to a certain degree by the temperature of the tropical tropopause (Holton et al. 1995). The intensity of the Brewer-Dobson circulation therefore also has an effect on the interannual variability of water vapor in the stratosphere (Randel et al. 2006). Evidence for this is in the fact that water vapor in the tropical lower stratosphere

shows variability corresponding to the seasonal cycle of the tropopause temperature, even retaining a "tape recorder" memory of past seasons (Mote et al. 1996).

Other processes that possibly affect the stratospheric distribution of water vapor are: A) direct injection through subtropical deep convection (Poulida et al. 1996; Stenchikov et al. 1996), and B) isentropic transport from the upper troposphere to the lower stratosphere (Dessler et al. 1995; Kley et al. 2000). Although these processes are known to affect stratospheric water vapor, the mechanisms and the contributions made have not been quantified. For example, regarding pathway A, overshooting cloud tops penetrating the tropopause might increase lower stratospheric water vapor, but also could dehydrate this region (Brasseur and Solomon 1984). Pathway B occurs during tropopause folding events (Kley et al. 2000 and references therein).

Water vapor in the lower stratosphere will be a combination of air that has higher mixing ratios that has subsided from the upper stratosphere and air with relatively low mixing ratios that has traveled across the tropopause. In addition, water vapor in this region of the atmosphere has a long chemical lifetime. For these reasons, water vapor is considered to be an excellent tracer of motion and transport in the lower stratosphere (Brasseur and Solomon 1984; Rosenlof 2002; Chiou et al. 2006), and should therefore show similar results as ozone when separated into meteorological regimes.

5.6.2 Measurements

Both SAGE and HALOE measure vertical profiles of water vapor. The water vapor channel on the HALOE instrument is a broadband channel. It measures solar infrared radiation at 6.6 μm. At this wavelength, other species are unlikely to

contaminate the signal, although absorption by aerosols can have an affect. After the eruption of Mt. Pinatubo, this channel was opaque below 35 km near the equator (Harries et al. 1996). For water vapor profiles, the combined systematic and random errors in the lower stratosphere are 14-24% (Grooβ and Russell 2006). Kley et al. (2000) did an extensive validation, and found that HALOE v19 water vapor profiles agreed with correlative measurements within ~10% throughout most of the stratosphere. Differences increase however, in the upper stratosphere and near the tropopause.

SAGE began measuring water vapor absorption at 0.94 μm, using a method similar to that described above for SAGE ozone profiles. However, it soon became obvious that the retrieval was very sensitive to aerosols at even moderate levels (Chu et al. 1993) and a significant dry bias of as high as 40% in the region of the hygropause was detected (Taha et al. 2004, and references therein). The hygropause is defined as the minimum water vapor mixing ratio level (Kley et al. 1979). In addition, the data did not resolve the well-known tropical tape recorder (Mote et al. 1996). As a result, the water vapor retrieval was revised. The primary source of error was found to be a significant drift in the filter used to define the spectral characteristics of the water vapor channel (Thomason et al. 2004). Through sensitivity studies on the effects of changing the spectral channel's center and width, a modified band pass filter was chosen with its center at 0.945 μm with a full width at half maximum (FWHM) of .033 μm. A new aerosol model was also introduced to better eliminate the effects of aerosols, and a correction was applied for the temperature data used to calculate the effects of Rayleigh scattering. These changes were subsequently introduced into the SAGE water vapor retrieval. Though still affected by the presence of aerosols, the sensitivity has been

reduced in version 6.2. The dry bias with respect to the HALOE water vapor profiles was effectively eliminated, and the tropical tape recorder signal was observed in the data set (Thomason et al. 2004). When SAGE water vapor profiles were compared with both ground-based and satellite correlative measurements, good agreement of within 10% was seen from 15-40 km. The agreement was best for comparisons with HALOE and from balloon-borne frost-point hygrometers. These agreed with SAGE within 5% over the same altitude range (Taha et al. 2004). Comparison between data sets in the region of the hygropause is more difficult, given the increase in atmospheric variability and differences in the techniques and ability of each platform in resolving this region. However, SAGE comparisons with balloon-borne frost-point hygrometers and MkIV interferometers showed agreement around the hygropause to within 10% (Taha et al. 2004).

5.7 Water Vapor Profile Separation – One day

Similar to the ozone profiles above, water vapor profiles from January 8, 2001 were classified into meteorological regimes. Figure 5.3 shows the total ozone field, boundaries, and location of each sunset measurement taken. Figure 5.16 shows all of the water vapor profiles for this day. Each profile that has been classified into a regime is in color, and the key indicates the profile's number and longitude. All of the profiles show a minimum below 20 km, and then increasing mixing ratios with increasing altitude, corresponding to the formation of water vapor through the oxidation of methane. The variability around the hygropause is much larger than the variability seen around the ozonepause region in Figure 5.4. This is most likely due to noise introduced by the injection of water vapor into the stratosphere through deep convection (Poulida et al.

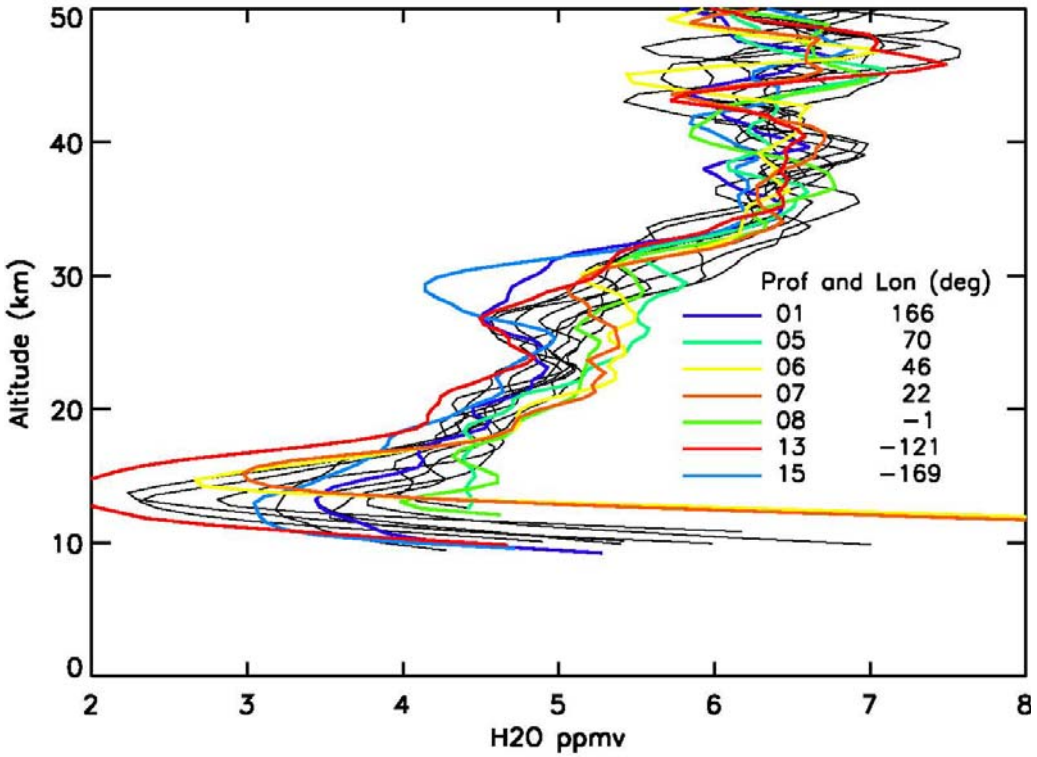

Figure 5.16 HALOE water vapor profiles that correspond to the X's on Figure 5.3 for January 8, 2001. Profiles that were classified into a meteorological regime are shown in color and listed on the figure. Profiles that fell within a pixel of the boundary are shown in black.

1996; Stenchikov et al. 1996). Figures 5.17a-c show the individual profiles that have been classified into the polar, midlatitude, and tropical regimes, respectively. The two polar profiles in Figure 5.17a have similar hygropause heights, but the hygropause of profile 15 is 0.5 ppmv lower. Figure 5.17b shows the two midlatitude profiles. These, like the midlatitude ozone profiles seen in Figure 5.5b, stop around 12 km, and do not show a definitive hygropause. They still differ substantially from the two tropical profiles located between them and seen in Figure 5.17c. Profiles 06 and 07 show very similar shapes and hygropause heights, and slightly different minimum values. Profile 13 has a similar hygropause height to profiles 06 and 07, but shows a much drier minimum value, below 2 ppmv.

Water vapor profiles appear to separate by regime. The hygropause height seen for the tropical profiles is ~15 km, and about 12-13 km for the polar profiles. However, these heights are much closer to each other than for tropical and polar ozone. There is much larger variability in this region in addition to greater instrument uncertainty. Therefore, while the water vapor profiles classified by meteorological regime do show distinction from one another, this distinction is less than for the ozone profiles.

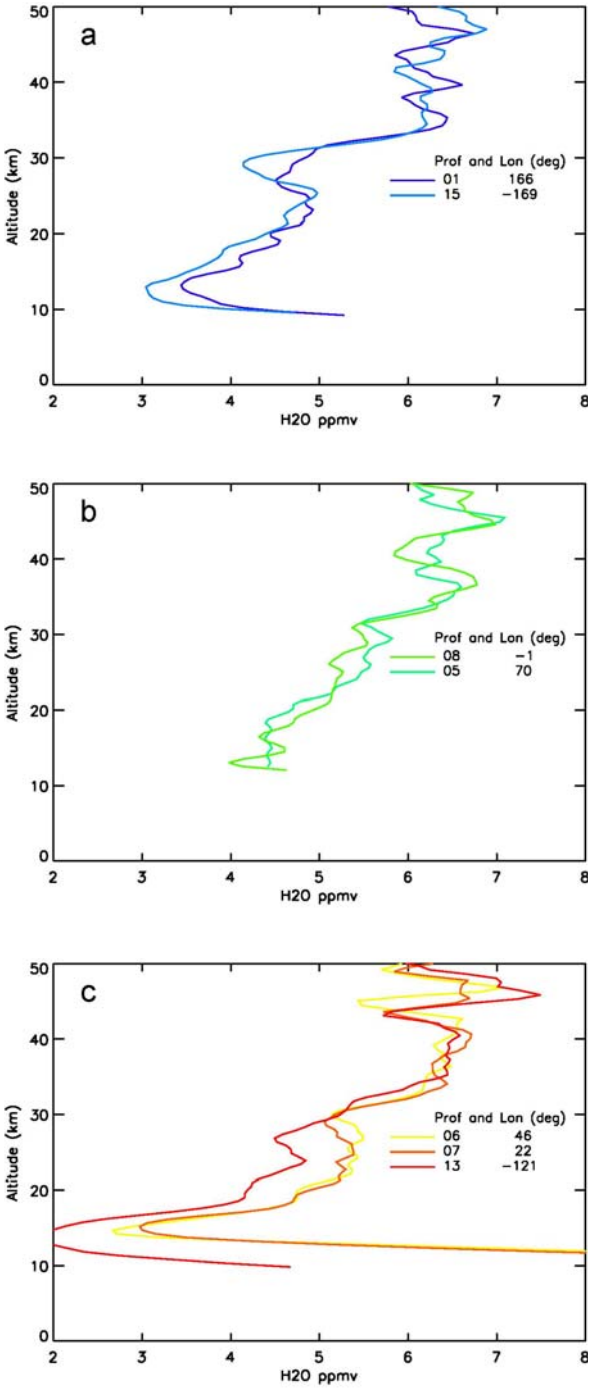

Figure 5.17 HALOE water vapor profiles that correspond to the colored X's on Figure 5.3 for January 8, 2001for the a) polar regime, b) midlatitude regime, and c) tropical regime. The profile numbers and longitudes are also listed.

5.8 Water Vapor Profile Separation – Climatology

Monthly water vapor climatologies were calculated using data from both SAGE and HALOE for the period 1997-2004 between 25° and 60°N. Figures 5.18 and 5.19 show the

March and June, and September and December monthly water vapor climatologies, respectively, calculated using data from HALOE. The one-sigma standard deviations are shown as dashed lines, and the number of points is shown in the right. The subtropical, midlatitude, and polar regimes are shown as red, green, and blue lines, respectively.

As seen in section 5.7, the variability in the hygropause region is large compared to the variability of ozone around the region of the ozonepause. The climatologies for each month show a minimum below 20 km, with increasing water vapor value with increasing altitude. The month of March shows excellent separation. Three distinct hygropause values and heights are seen for each regime. The driest hygropause is seen here: the tropical climatology shows a minimum value of ~2.7 ppmv. June displays a different height within each regime, but all around the same value, ~3.5 ppmv. September and December do not show as much distinction. In September, the tropical and midlatitude climatologies come close to overlapping. This is due to the reasons discussed in section 5.5. In December the same happens, the midlatitude and polar practically overlap, although the polar shows a broader hygropause.

The March and June, and September and December monthly climatologies calculated using data from SAGE are shown in Figures 5.20 and 5.21, respectively. The color scheme and line designations are the same as in Figure 5.18. The results seen here are similar to the results using the HALOE data. March shows the most distinction between regimes, again showing different hygropause heights and values for each regime. Curiously, June and September show similar results. This could be the result of misclassification as discussed in section 5.3. The SAGE December climatologies look similar to those of HALOE in that the midlatitude and polar overlap somewhat.

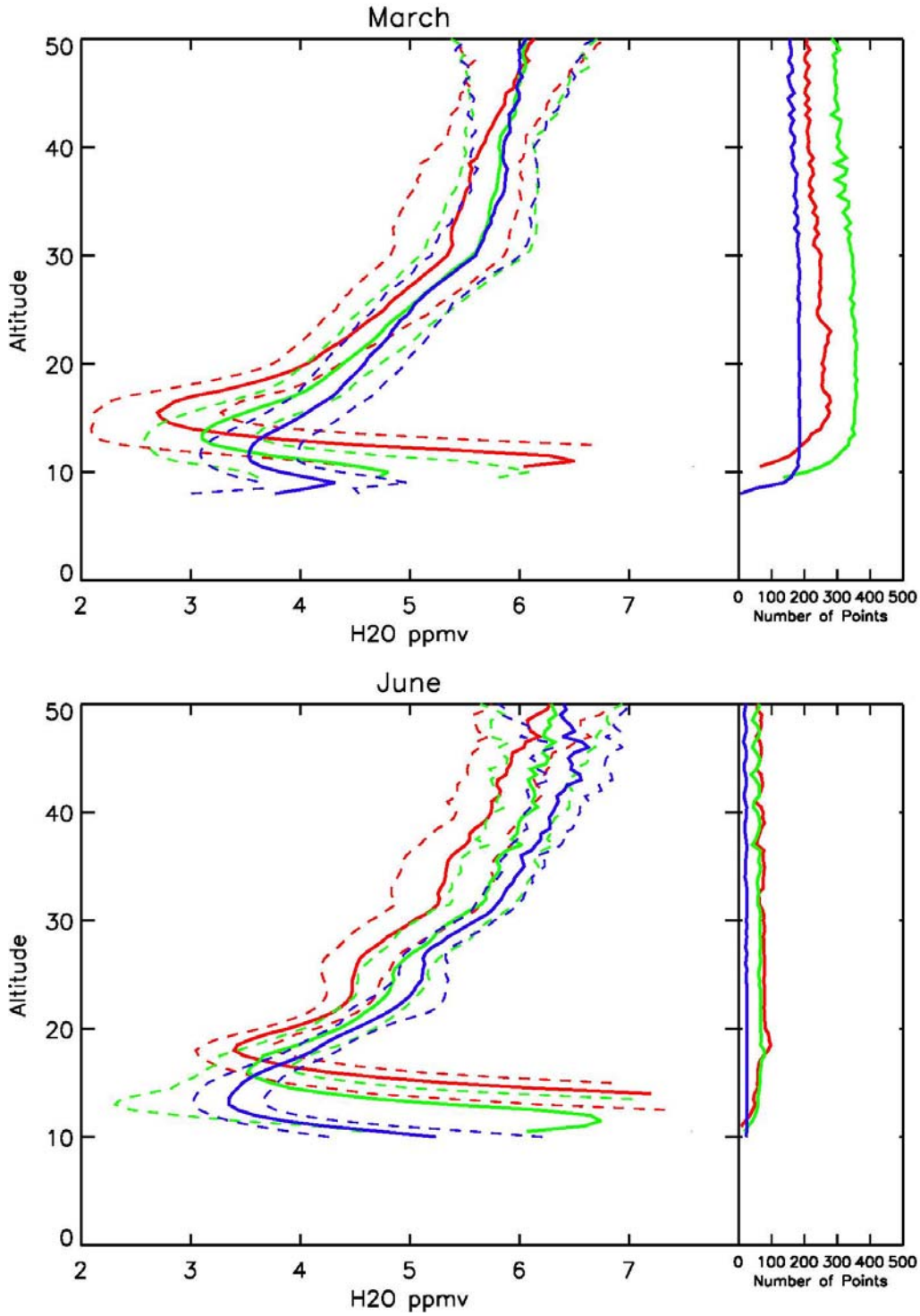

Figure 5.18 HALOE water vapor profile climatologies calculated from 1997-2004 between 25° and 60°N for March (top) and June (bottom). The one-sigma standard deviations are shown as dashed lines, and the number of points are shown on the right. The color scheme is: red – tropical, green – midlatitude, and blue – polar.

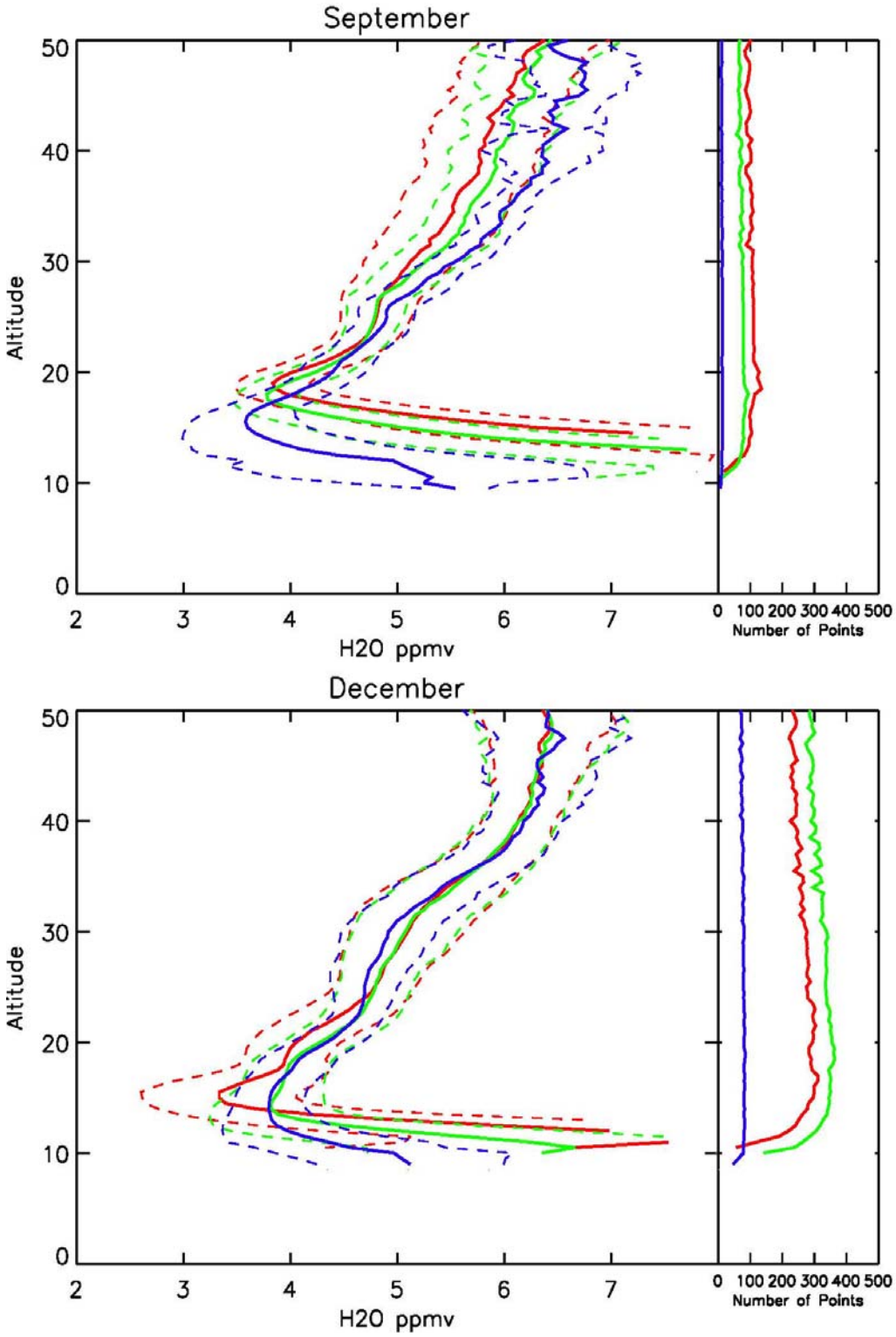

Figure 5.19 HALOE water vapor profile climatologies calculated from 1997-2004 between 25° and 60° for September (top) and December (bottom). Color scheme and line designation same as Figure 5.18.

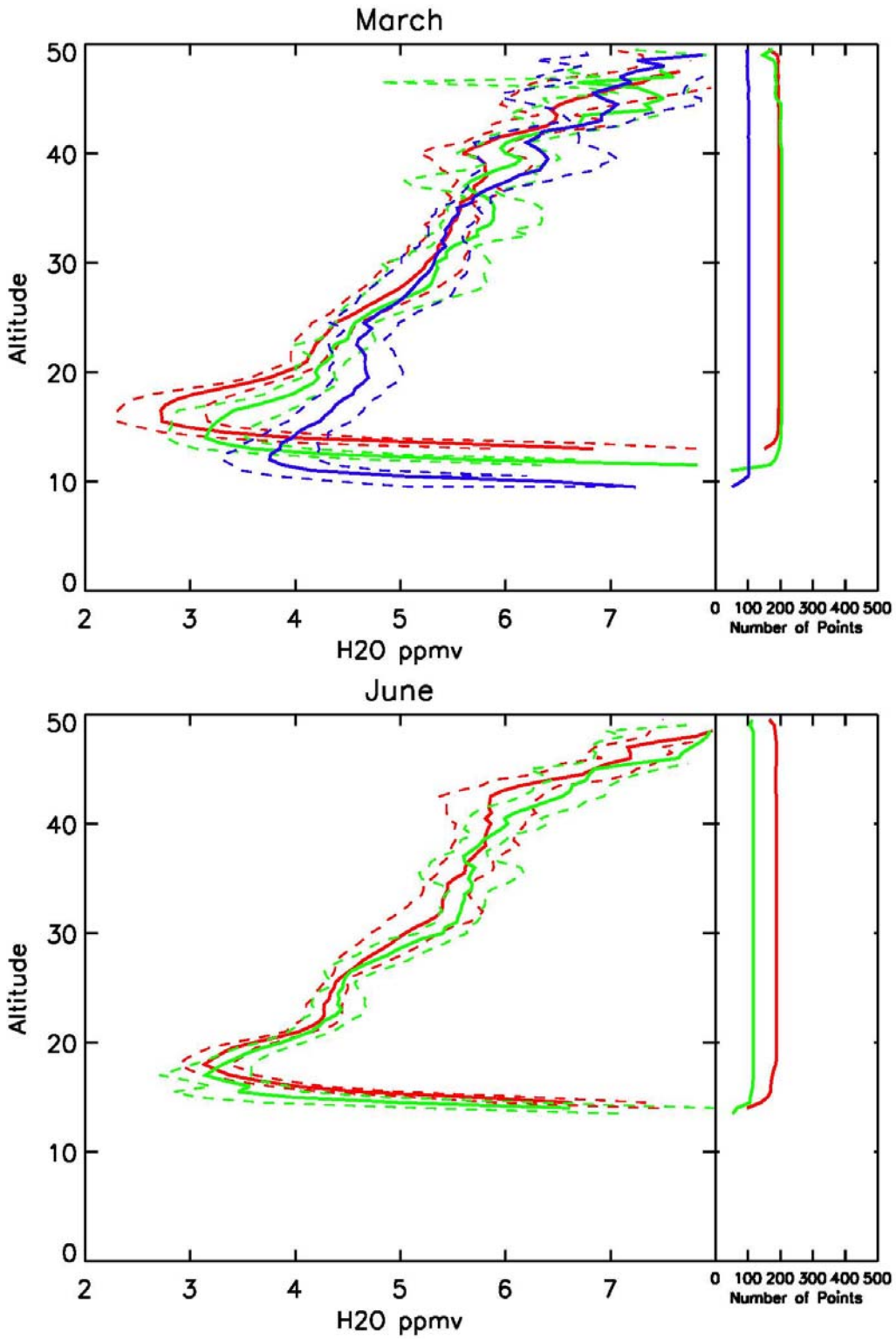

Figure 5.20 SAGE water vapor profile climatologies calculated from 1997-2004 between 25° and 60°N for March (top) and June (bottom). Color scheme and line designation same as Figure 5.18.

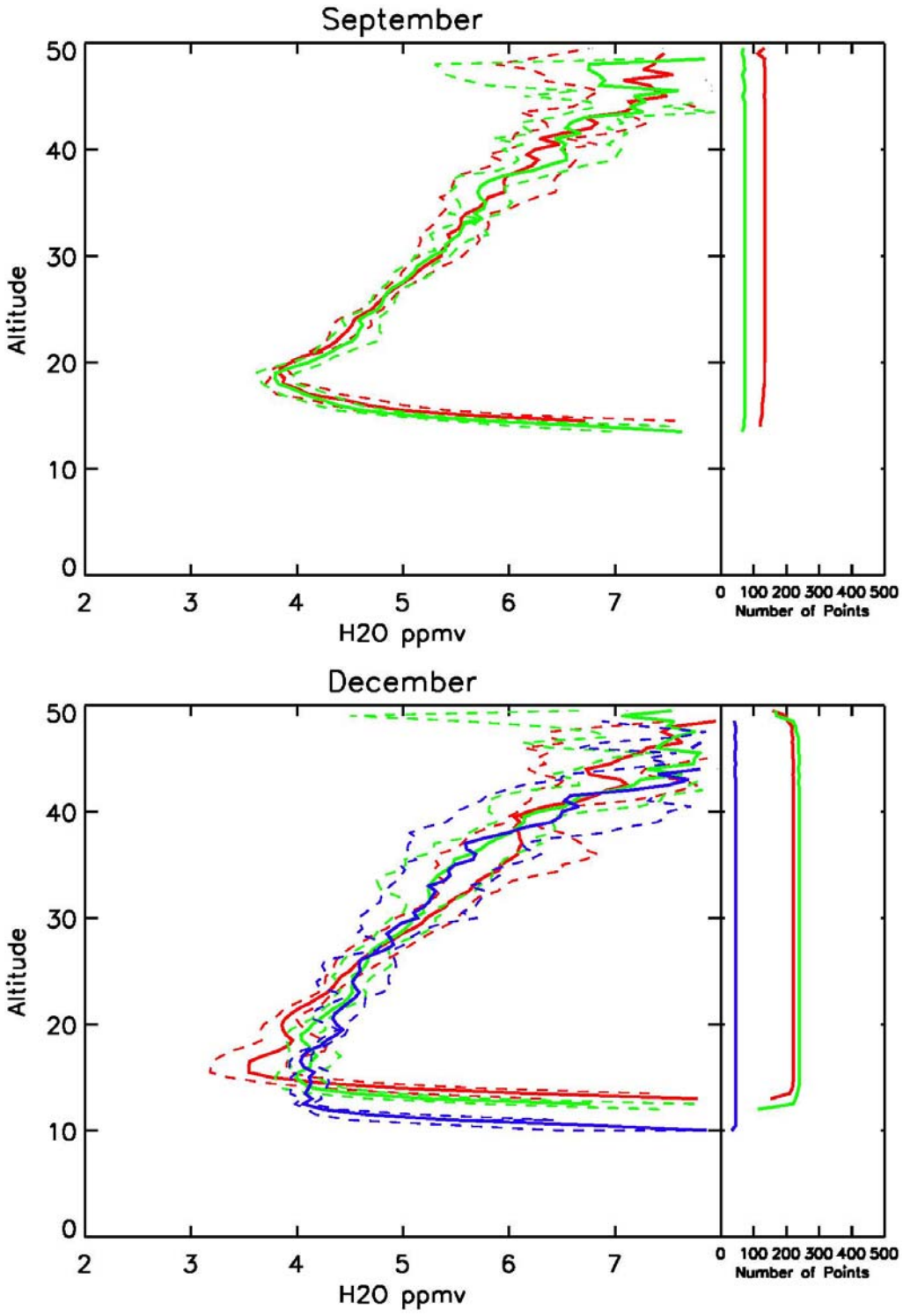

Figure 5.21 SAGE water vapor profile climatologies calculated from 1997-2004 between 25° and 60° for September (top) and December (bottom). Color scheme and line designation same as Figure 5.18.

However, the polar December climatology has the least amount of data points for the SAGE data, as evidenced by its jagged mean.

The HALOE and SAGE climatologies plotted in Figures 5.18-21 are seen in Figures 5.22 and 5.23. On these figures, the solid lines represent the HALOE data, the dashed lines represent the SAGE data, and the color scheme is the same as the previous four figures. The one-sigma standard deviations for each regime and the zonal data between 25° and 60°N (shown as a black solid line for HALOE and a black dashed line for SAGE) have also been included on these figures. The water vapor climatologies do not show the same decrease in lower stratospheric variability when separated by regime. The variability in this region within each regime, and the zonal data, increase below about 15 km, corresponding to an increase in instrument uncertainty (Thomason et al. 2004).

The water vapor climatologies do not show as good agreement as the ozone climatologies do, but they still agree within experimental error throughout the stratosphere. The differences seen are most likely the result of instrument differences in resolving the hygropause and atmospheric variability (Taha et al. 2004). In the upper stratosphere, above about 40 km, SAGE shows a much sharper water vapor increase with altitude with respect to HALOE. In general, the hygropause measured by HALOE tends to be lower in altitude, and drier than SAGE, but at times both are located at the same altitude. The one exception to this is seen in the June climatologies, when SAGE shows a drier tropical hygropause than HALOE. However, despite the large uncertainties, the same general features are seen in the two sets of climatologies. For example, the tropical regime has the highest mean hygropause height, followed by the midlatitude, and then the

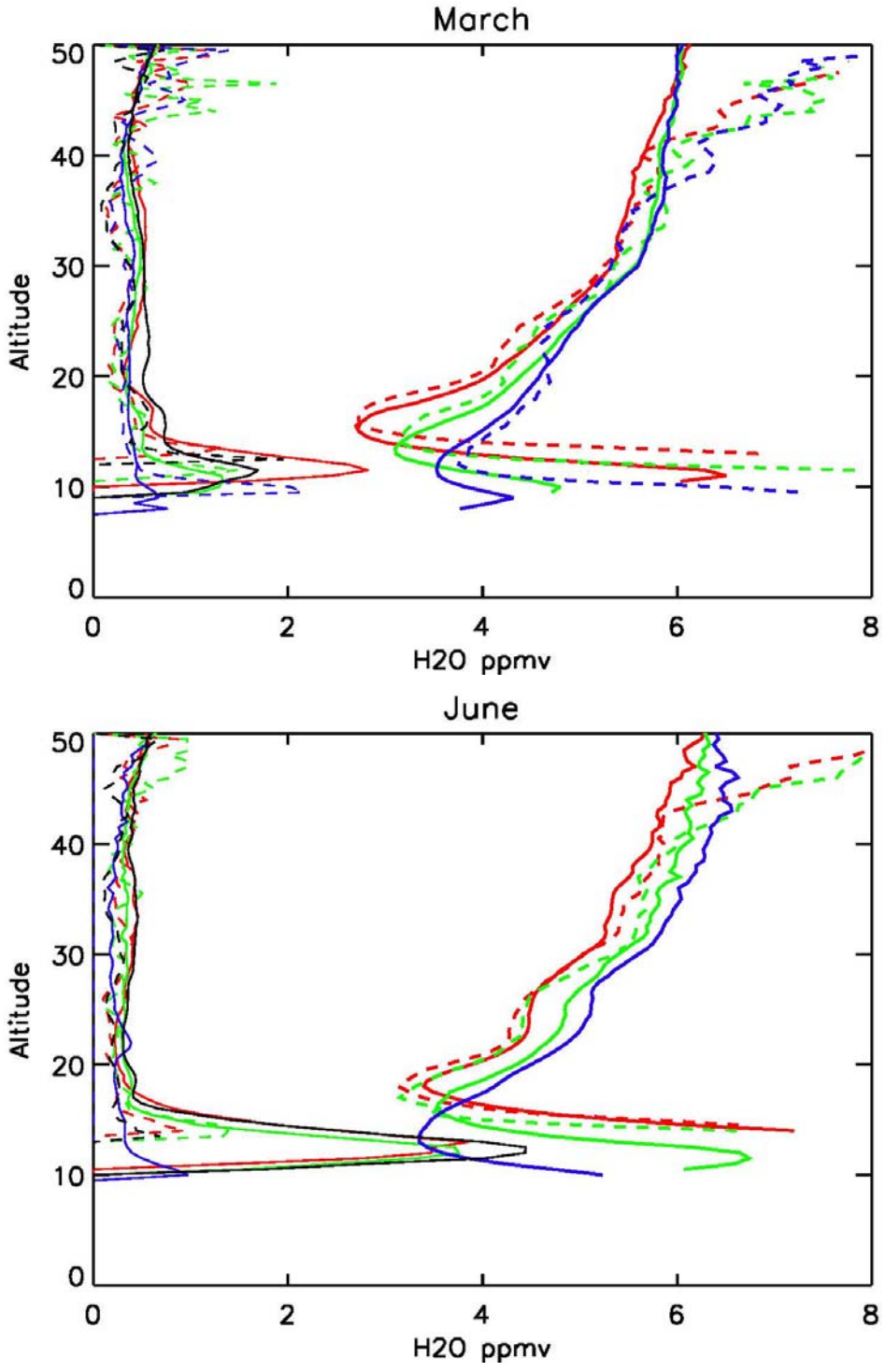

Figure 5.22 HALOE and SAGE water vapor profile climatologies calculated from 1997-2004 between 25° and 60°N for March (top) and June (bottom). HALOE data is shown as solid lines, and SAGE data is shown as dashed lines. The one-sigma standard deviations are shown on the left. The color scheme is: red – tropical, green – midlatitude, and blue – polar. The zonal standard deviations between 25° and 60°N for both instruments have also been plotted in black (HALOE-solid, SAGE-dashed).

polar regime. Overall, good agreement is obtained between the climatologies calculated by the two instruments.

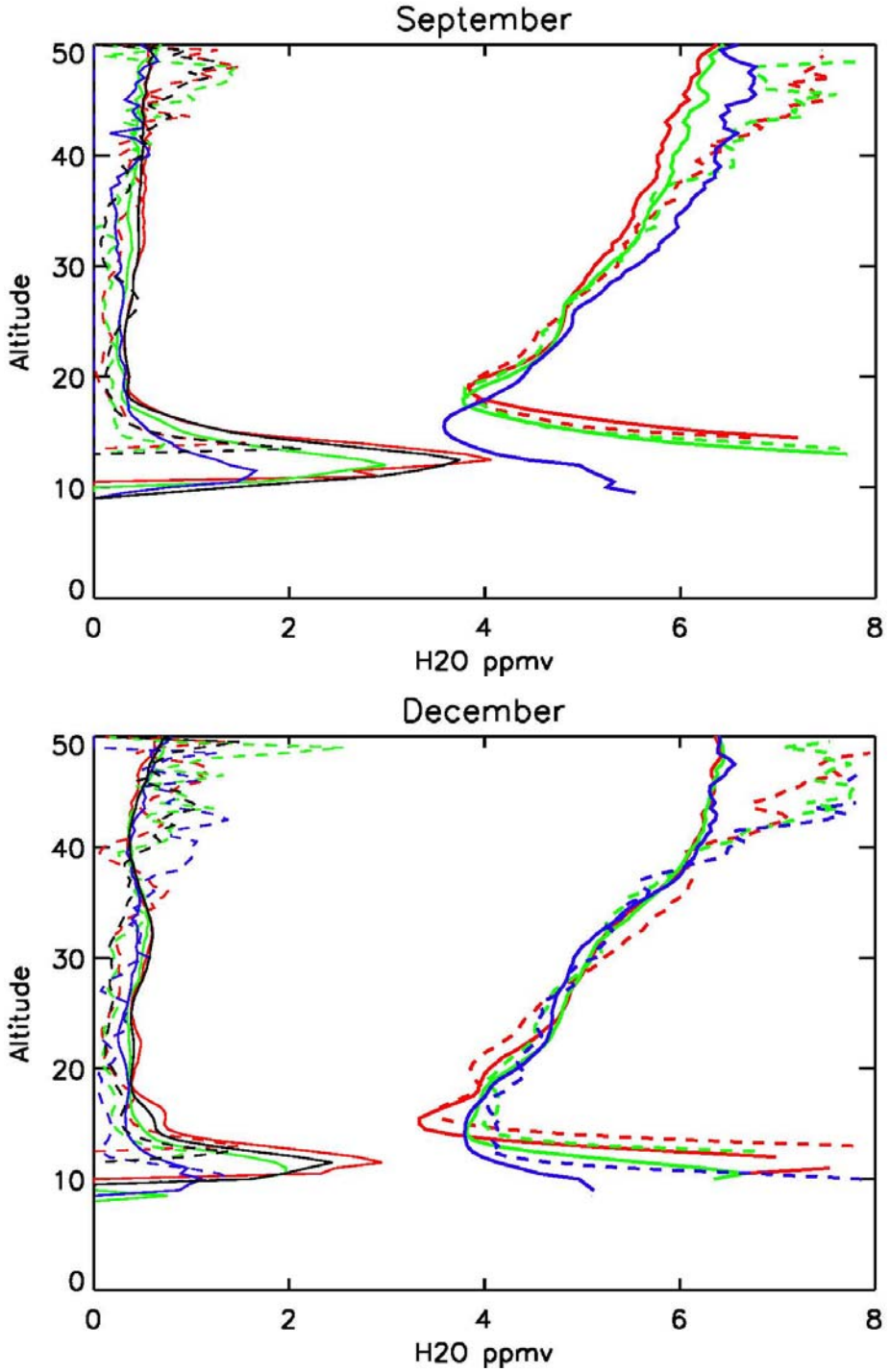

Figure 5.23 HALOE and SAGE water vapor profile climatologies calculated from 1997-2004 between 25° and 60°N for September (top) and December (bottom). Color scheme and line designation same as Figure 5.22.

Chapter 6: Vertical Trends

In Chapter 4, it was shown that the zonal ozone trend between 25° and 60°N from January 1979 to May 1991 was due to both changes in total ozone within the meteorological regimes defined by Hudson et al. (2003) and changes in the relative weighting of these regimes over time. In Chapter 5, ozone and water vapor profiles within this latitude range were classified by regime. Below approximately 25 km, each regime was characterized by distinct profile shapes, and ozonepause and hygropause heights for ozone and water vapor, respectively. Less distinction between regimes was seen above this altitude. Since each regime has a unique profile shape in the lower stratosphere, a zonal trend at these altitudes will include both tropospheric and stratospheric values, leading to inaccuracies. Thus, similar to trends in total ozone, changes in this region will also be the result of changes within each regime and changes in the contributions made by each regime over time. Changes in the zonal profile, as well as within each regime, will be examined over two time periods.

6.1 Past vertical trends

WMO (1998) conducted an evaluation of the vertical distribution of ozone trends from 1979-1996. A variety of ozone measuring platforms were used for this study, such as ground-based Umkehr measurements and balloon-borne sondes. Data from SAGE I, II, and the solar backscatter ultraviolet (SBUV) instrument were also used. When these data were combined, they showed statistically significant negative trends between 10 and 45 km from 1979-1996 for 40°-50°N. This combined trend has two negative minima,

one at 40 km of -7.2 ± 2.0 %/decade, and another of -7.3 ± 4.6 %/decade at 15 km. There is a minimum of -2.0 ± 1.8 %/decade at 30 km (Randel et al. 1999). When WMO (2003) updated the analysis done by WMO (1998) they found similar trend patterns with reduced magnitudes in the upper and lower stratosphere. However Newchurch et al. (2003), using data from HALOE and SAGE II, report a global slowdown of ozone depletion at 35-45 km starting in 1997 due to decreasing chlorine levels at these altitudes.

Long-term changes in stratospheric water vapor have been widely reported on and are difficult to quantify. Differences in instrumentation, scattered data records, complications involved with the measurements, and the non-linearity of its changes have made it difficult to quantify any trend. Oltmans et al. (2000) analyzed data from Climate Monitoring and Diagnostics Laboratory (CMDL) frost-point hygrometers in Boulder, CO (40°N, 105°W) from 1980-2000 and Washington, D.C. (39ºN, 77ºW) from 1964-1976 and found a 1.0-1.5%/yr increase above 16 km. Rosenlof et al. (2001) conducted an analysis based on 10 different datasets spanning 1954-2000 for ~30º-50ºN and confirmed a 1%/year increase throughout the stratosphere from 1954-2000. This corresponds to a 2 ppmv increase in water vapor over the past 45 years. Randel et al. (2004) reported low and persistent water vapor anomalies throughout the lower stratosphere from 2001-2003 using data from HALOE, POAM III, and CMDL hygrometers. However, the HALOE and Boulder, CO CMDL time series agree well until 1997, after which the two time series diverge. Both show the post-2001 decrease, but the balloon measurements show overall higher values than HALOE. Therefore, a vertical trend calculated for HALOE from 1992-2002 will show negative values in the lower stratosphere; the same trend for the Boulder balloon measurements will show positive values to the mid stratosphere. In

addition, the reported decrease in water vapor after 2001 makes calculating linear trends difficult for short time periods (Randel et al. 2004). SAGE water vapor shows reasonable agreement with HALOE, including the decreases after 1996 (Chiou et al. 2006).

6.2 1997-2004

6.2.1 Ozone

Figure 6.1 shows the vertical zonal trend between 25° and 60°N from 1997-2004 for SAGE (left) and HALOE (right). This will be the convention through the rest of the chapter. The dashed lines indicate the two-sigma trend error. This trend was calculated using a simple linear fit to the data. Linear fits, rather than Equation 4.5, were used because of the short time period analyzed. As shown below in section 6.3.1, the 11-year solar cycle signal in the total ozone regression is large from 1979-2004; however, it would be incorrect to fit an 11-yr cycle to a seven year period. Therefore, the data was first deseasonalized, and then a linear fit was calculated. No significant trends are seen throughout the stratosphere,

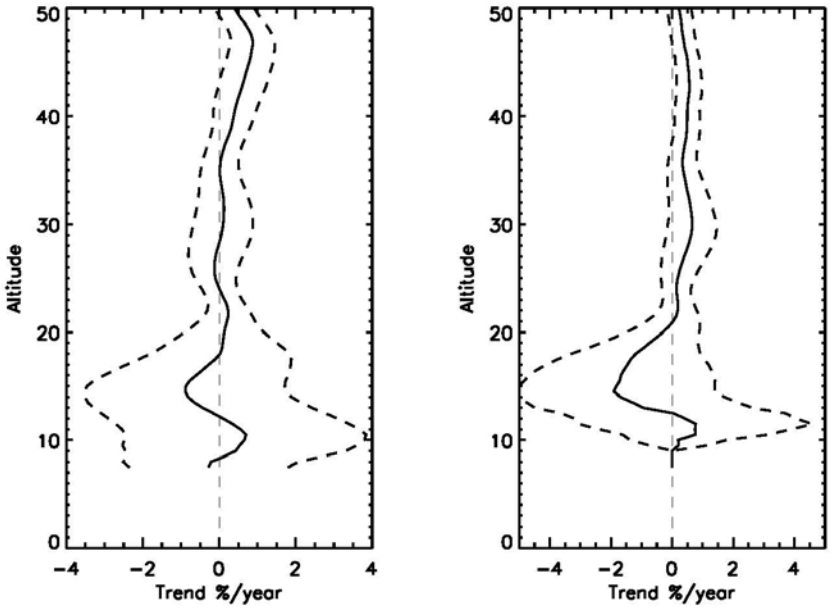

Figure 6.1 SAGE (left) and HALOE (right) zonal ozone trends in percent per year calculated for 1997-2004 between 25° and 60°N. The gray dashed line is the zero line. The dark dashed lines are the two-sigma trend error.

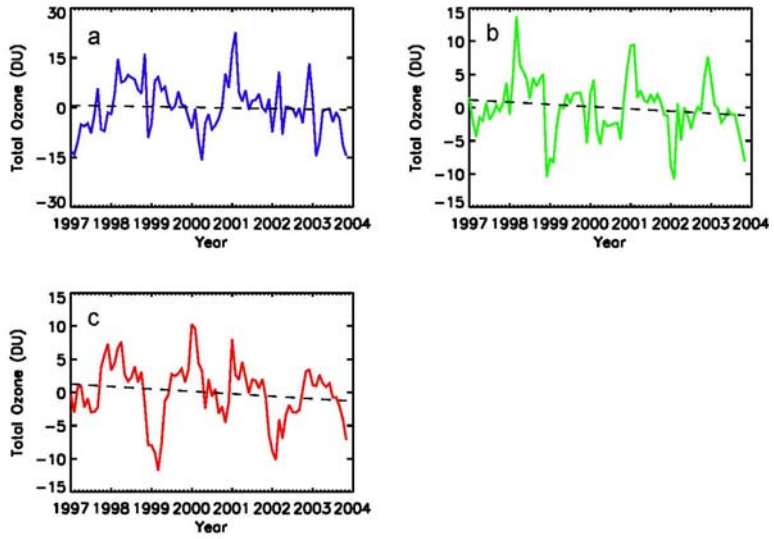

Figure 6.2 Deseasonalized monthly total ozone for the a) polar, b) midlatitude, and c) tropical regime, taken from the TOMS analysis discussed in Chapter 4, from 25°-60°N for 1997-2004. The deseasonalization was calculated by subtracting the monthly mean climatology from 1997-2004. The dashed line in each plot is a simple linear fit to the data.

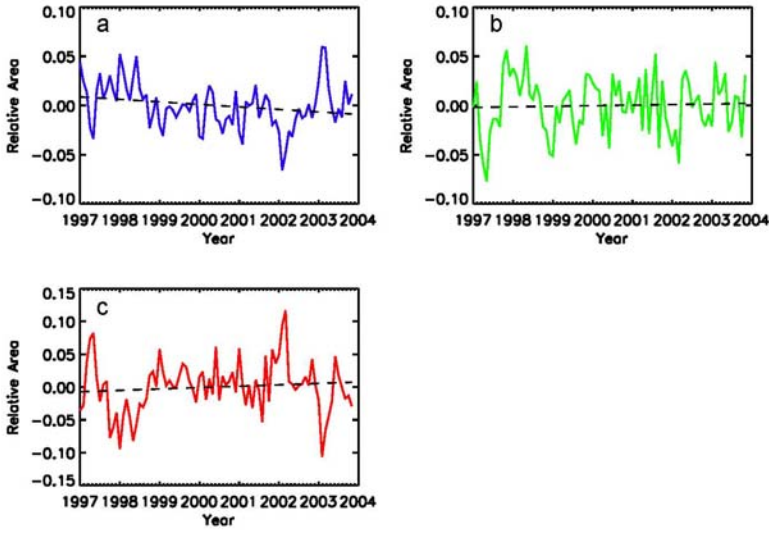

Figure 6.3 Deseasonalized monthly relative areas for the a) polar, b) midlatitude, and c) tropical regime, taken from the TOMS analysis discussed in Chapter 4, from 25°-60°N for 1997-2004. The deseasonalization was calculated by subtracting the monthly mean climatology from 1997-2004. The dashed line in each plot is a simple linear fit to the data.

except a slight positive trend in the upper stratosphere at about 47 km, and 43 km for SAGE and HALOE, respectively. The trend uncertainty increases rapidly below 20 km for both instruments.

As stated above, the zonal trends in the lower stratosphere are the result of both changes within each regime, and changes in the relative area weighting of these regimes over time. Figures 6.2 and 6.3 show the deseasonalized total ozone and relative areas from 25° and 60°N for 1997-2003, taken from the analysis in Chapter 4. On each plot, the dashed line represents a simple linear fit to the data. The zonal trends in Figure 6.1 show little significance over this time period. This is

confirmed by looking at the total ozone in Figure 6.2, where each regime shows a decreasing slope, however, they are not statistically significant. The linear fits seen in Figure 6.3 are also not statistically significant, indicating that changes in the relative areas will not have a substantial effect on the zonal trend for this time period.

Figures 6.4, 6.5, and 6.6 show the vertical ozone trends, for both the SAGE and HALOE instruments, for the tropical, midlatitude, and polar regimes, respectively. Trends were not calculated at altitudes below the ozonepause due to inaccuracies in retrieving tropospheric ozone. As expected by the lack of significant zonal trends, little to no significant trends are seen in each of the regimes, and the trends calculated for the two instruments agree within two sigma. The trends within each regime also show increased errors below ~20 km. Interestingly, the only regime that shows a positive trend in the upper stratosphere is the tropical regime, indicating that this increase is primarily at lower latitudes. This positive trend is seen in both satellites, and is over a larger altitude range than that seen in the zonal trends.

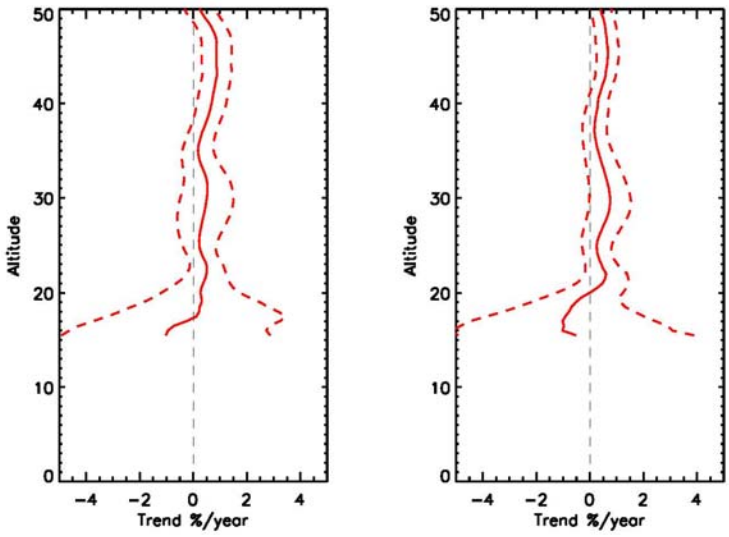

Figure 6.4 SAGE (left) and HALOE (right) tropical ozone trends in percent per year calculated for 1997-2004 between 25° and 60°N. Line designations are as in Figure 6.1.

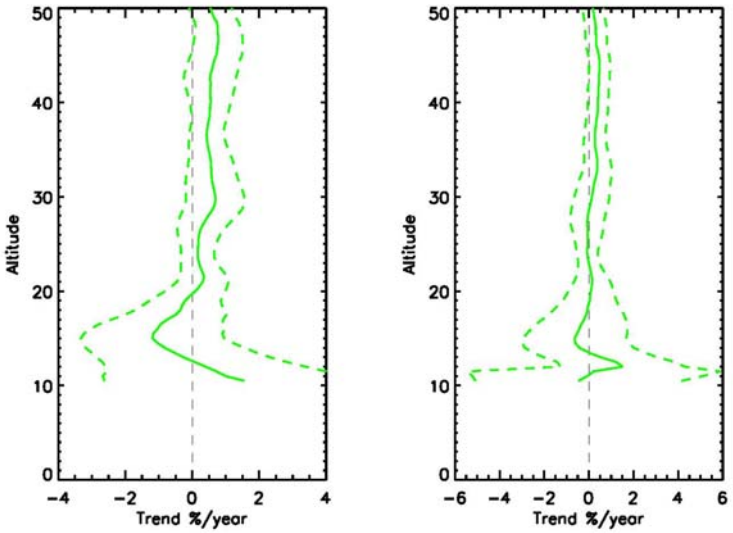

Figure 6.5 SAGE (left) and HALOE (right) midlatitude ozone trends in percent per year calculated for 1997-2004 between 25° and 60°N. Line designations are as in Figure 6.1.

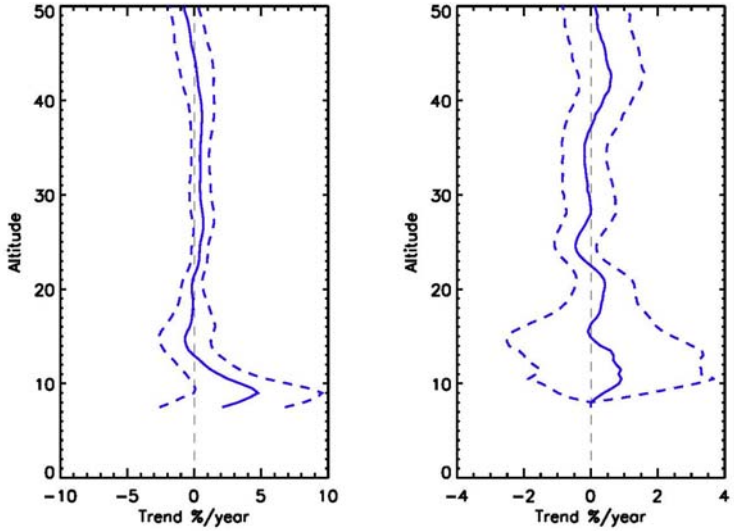

Figure 6.6 SAGE (left) and HALOE (right) polar ozone trends in percent per year calculated for 1997-2004 between 25° and 60°N. Line designations are as in Figure 6.1.

6.2.2 Water vapor

The HALOE and SAGE zonal water vapor trends between 25° and 60°N for 1997-2004 are seen in Figure 6.7. The SAGE zonal trend is largely statistically insignificant, except for a small negative trend at ~16 km, and a small positive trend at

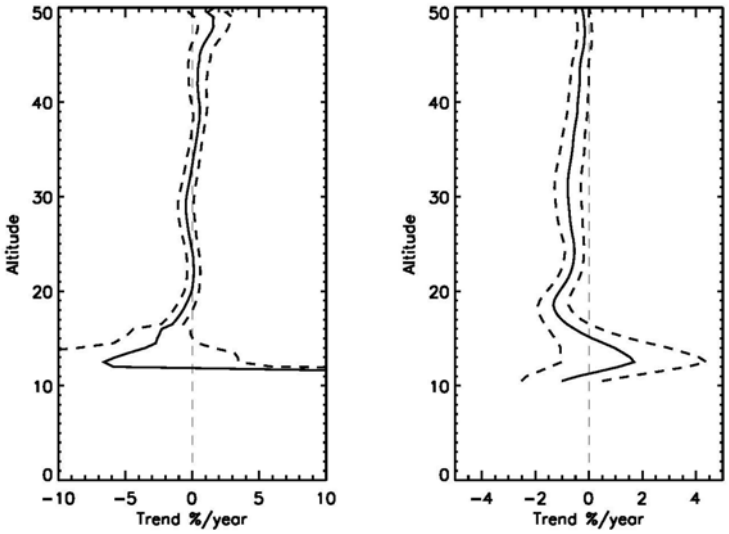

Figure 6.7 SAGE (left) and HALOE (right) zonal water vapor trends in percent per year calculated for 1997-2004 between 25° and 60°N. The gray dashed line is the zero line. The dark dashed lines are the two-sigma trend error.

~48 km. HALOE shows statistically significant negative trends from 16-36 km, with a minimum of -1%/year at 19 km. This agrees with the results of Randel et al. (2004). Figures 6.8, 6.9, and 6.10 show the vertical trends for both instruments for the tropical, midlatitude, and polar regimes, respectively. The SAGE trends show little to no statistical significance throughout the stratosphere. However, the small negative trend seen at ~16 km in the zonal trend is also seen at that altitude in the tropical and midlatitude regimes, and is seen at ~14 km in the polar regime. Thus, this feature could be real.

The vertical trends within each regime for HALOE all show statistically significant negative trends over different altitude ranges. The tropical regime shows negative trends from 17-40 km with a minimum of ~1.8 %/yr at about 18 km, and the midlatitude regime shows negative trends from 16-35 km, with a minimum of ~1 %/yr at about 18 km. The trends within these two regimes resemble that of the zonal, but in the tropical regime, the magnitude of the trend is greater. The polar regime only shows

statistically significant negative trends from ~10-16km, with a minimum of ~1.5 %/yr at about 12km. Thus, the zonal trend seems to be dominated by contributions from the midlatitude and tropical regimes.

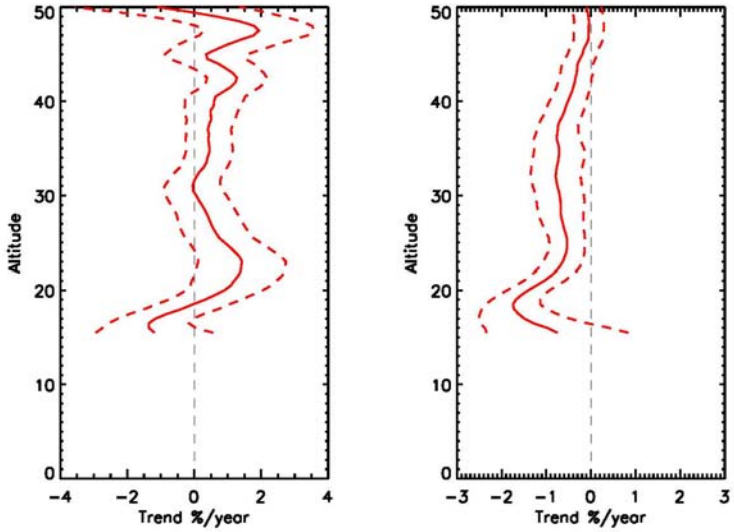

Figure 6.8 SAGE (left) and HALOE (right) tropical water vapor trends in percent per year calculated for 1997-2004 between 25° and 60°N. Line designations are as in Figure 6.7.

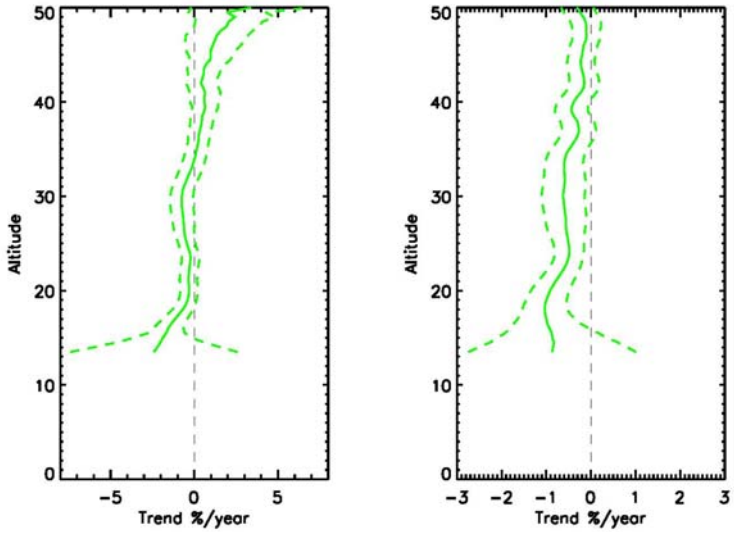

Figure 6.9 SAGE (left) and HALOE (right) midlatitude water vapor trends in percent per year calculated for 1997-2004 between 25° and 60°N. Line designations are as in Figure 6.7.

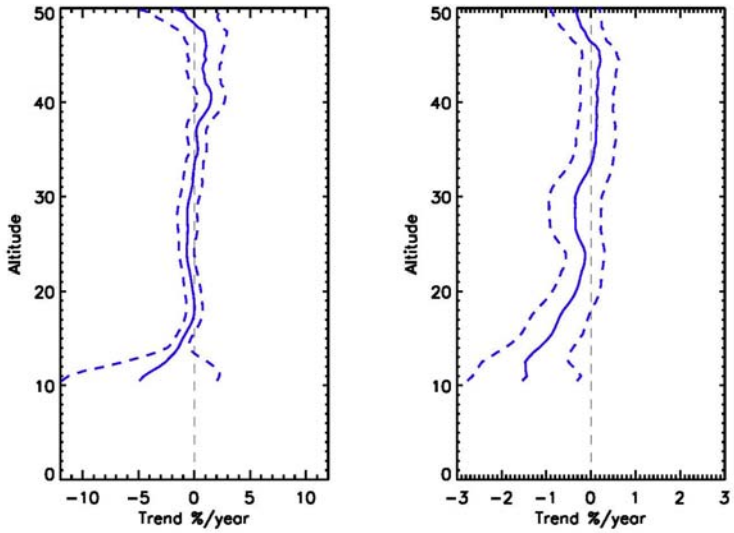

Figure 6.10 SAGE (left) and HALOE (right) polar water vapor trends in percent per year calculated for 1997-2004 between 25° and 60°N. Line designations are as in Figure 6.7.

6.3 October 1984 – May 1991

The first time period analyzed did not show many statistically significant trends in ozone. Thus, a second time period was chosen for analysis, October 1984 to May 1991. This is a period of known negative total ozone trends at mid-latitudes due to depletion by homogeneous and heterogeneous chemistry, and transport through dynamical processes (Salby and Callaghan 1993; Solomon 1999; WMO 1999; Staehelin et al. 2001; Randel et al. 2002; Hudson et al. 2006). The starting point corresponds to the month in which SAGE began making measurements, and the endpoint was chosen to avoid effects from the eruption of Mt. Pinatubo in June 1991. Volcanic aerosols from this eruption contaminated retrievals in both ozone and water vapor in the lower stratosphere, making them unreliable for trend analyses (Wang et al. 2002; Taha et al. 2004).

Figures 6.11 and 6.12 show the deseasonalized monthly mean total ozone and relative areas for the polar, midlatitude, and tropical regimes from 25°-60°N for October

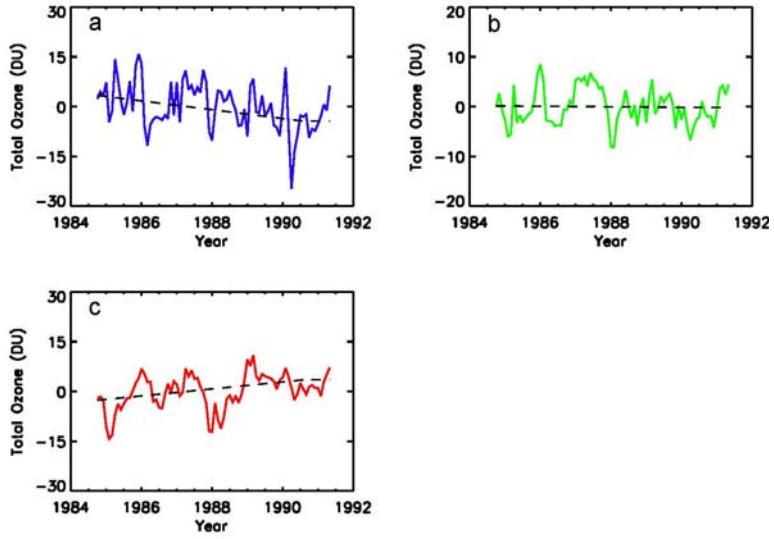

Figure 6.11 Deseasonalized monthly total ozone for the a) polar, b) midlatitude, and c) tropical regime, taken from the TOMS analysis discussed in Chapter 4, from 25°-60°N for October 1984 to May 1991. The deseasonalization was calculated by subtracting the monthly mean climatology from 1985-1990. The dashed line in each plot is a simple linear fit to the data.

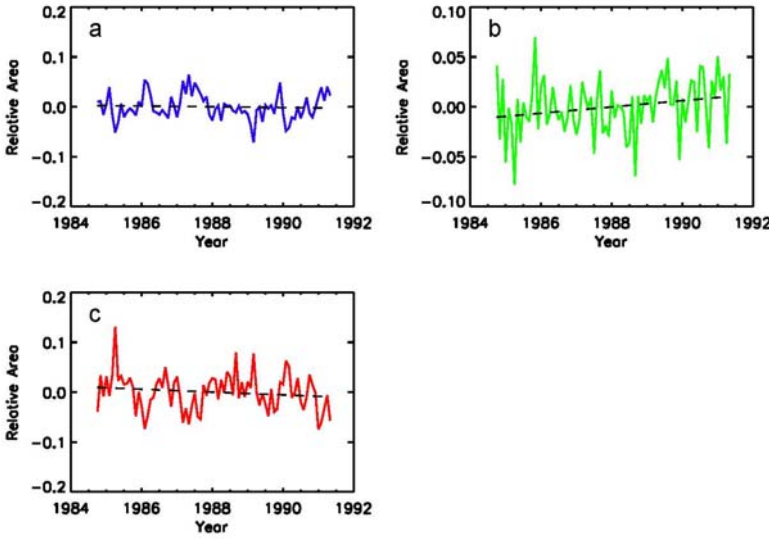

Figure 6.12 Deseasonalized monthly relative areas for the a) polar, b) midlatitude, and c) tropical regime, taken from the TOMS analysis discussed in Chapter 4, from 25°-60°N for October 1984 to May 1991. The deseasonalization was calculated by subtracting the monthly mean climatology from 1985-1990. The dashed line in each plot is a simple linear fit to the data.

1984-May 1991. The dashed lines in these plots represent simple linear fits to the data. The polar total ozone seen in Figure 6.11a shows a statistically significant decreasing slope. The midlatitude total ozone shows no statistically significant slope. The tropical regime has an increasing slope during this period that appears to contradict the previous analyses. However, Figure 6.13 shows the contribution from the 11-year solar cycle to the total ozone regression in section 4.1 (equation 4.5) for the zonal data, polar, midlatitude, and tropical regimes. Figure 6.13 shows that the year 1985 corresponds to a solar minimum, and 1990 to a solar maximum. Therefore, the tropical regime shows an increasing slope

because of the increase in ozone production over this time period, as explained in Section 4.5.

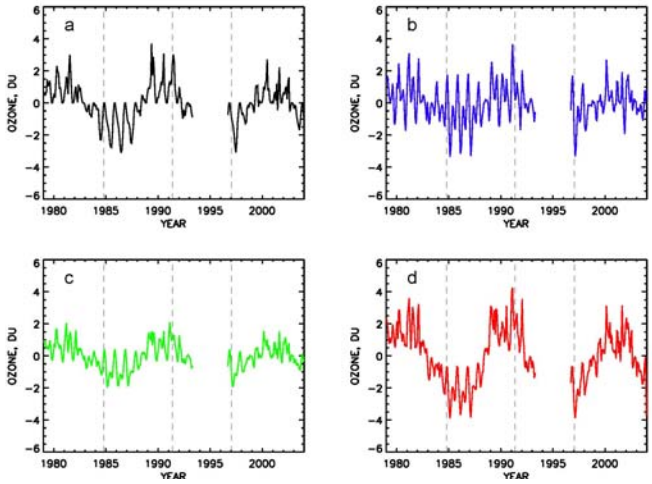

Figure 6.13 Contribution from the solar cycle to total ozone for the a) zonal data, b) polar, c) midlatitude, and d) tropical regimes, taken equation 4.5 from 25°-60°N for 1979-2004. The grey dashed lines represent the beginning and end of the two time periods discussed here: October 1984 – May 1991, and January 1997 – December 2003.

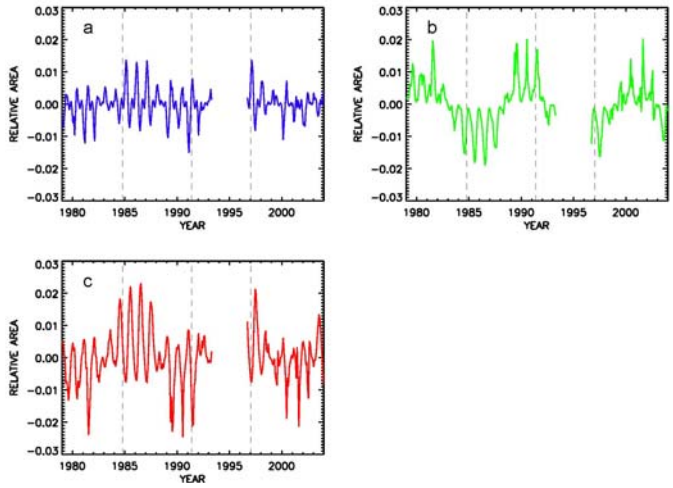

Figure 6.14 Contribution from the solar cycle to relative area for the a) polar, b) midlatitude, and c) tropical regimes, taken equation 4.5 from 25°-60°N for 1979-2004. The grey dashed lines are as in Figure 6.13.

None of the slopes seen in Figure 6.12 are statistically significant, indicating that, similar to the 1997-2004 period, changes in the relative areas will not have a substantial effect on the zonal trend for this time period. Figure 6.14 shows the contribution from the 11-year solar cycle to the relative area regression in section 4.2 (equation 4.5) for the polar, midlatitude, and tropical regimes. The solar maximum around 1990 contributes negatively to the tropical and polar relative area, and positively to the midlatitude relative area. Therefore, the lack of a significant trend in the

relative areas of the tropical and polar regime over this short time period does not contradict the relative area trends calculated in Chapter 4.

6.3.1 Ozone

Figure 6.15 shows the SAGE zonal ozone trend for October 1984-May 1991 from 25°-60°N. As in the previous figures, the dashed lines are the two-sigma trend error. There is a small positive trend at about 37 km, and negative trends from 8-17 km, with a minimum of -4 %/yr at 10 km. The vertical ozone trends for the tropical, midlatitude, and polar trends are shown in Figure 6.16, 6.17, and 6.18, respectively. The tropical regime also shows a small positive trend at ~37 km, but no statistically significant trends in the lower stratosphere. This makes sense considering the altitudes at which the zonal trend showed significance are in the troposphere for the tropical regime. The midlatitude trend in Figure 6.16 again shows the small positive trend at ~37 km. The negative trends for the midlatitude regime are found from 10-19 km with magnitudes of -0.5 to -4.0 %/yr. The polar trends show statistically significant negative trends from 9-17 km, with magnitudes of ~3.0 %/yr. Since, as seen in Figure 6.12, changes in the relative areas of each regime over time are expected to have no substantial effect on the zonal trend, it is therefore concluded that the negative trend seen in the lower stratosphere in the zonal trend is the result of ozone depletion around and just above the ozonepause regions of the midlatitude and polar regimes.

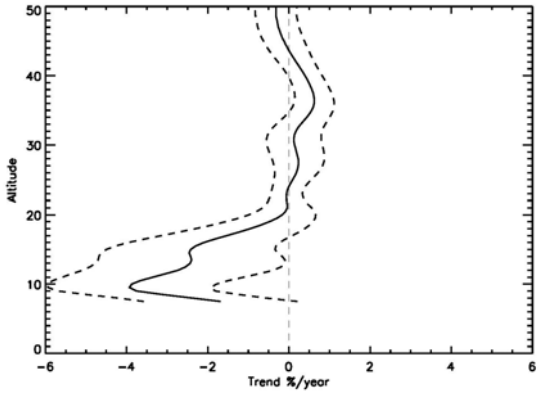

Figure 6.15 SAGE zonal ozone trend in percent per year calculated for October 1984 to May 1991 between 25° and 60°N. The gray dashed line is the zero line. The dark dashed lines are the two-sigma trend error.

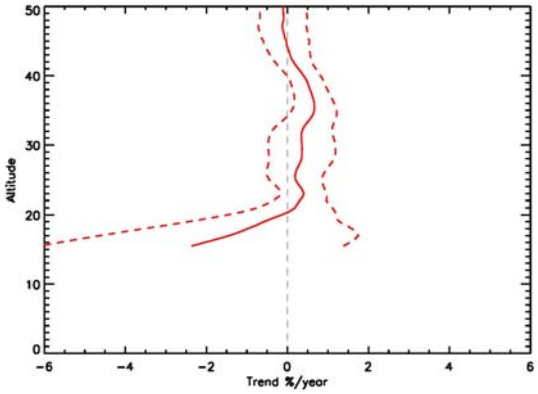

Figure 6.16 SAGE tropical ozone trend in percent per year calculated for October 1984 to May 1991 between 25° and 60°N. Line designations are as in Figure 6.15.

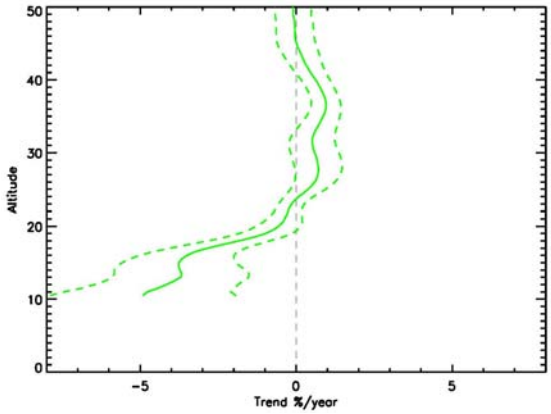

Figure 6.17 SAGE midlatitude ozone trend in percent per year calculated for October 1984 to May 1991 between 25° and 60°N. Line designations are as in Figure 6.15.

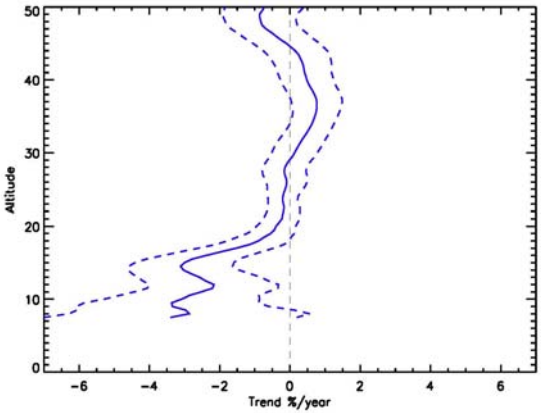

Figure 6.18 SAGE polar ozone trend in percent per year calculated for October 1984 to May 1991 between 25° and 60°N. Line designations are as in Figure 6.15.

6.3.2 Water vapor

The zonal water vapor trend is seen in Figure 6.19. There is a small negative trend at 38 km, a larger negative trend of ~-1.5 %/yr from 25-32 km, and another negative trend of ~-2.0 %/yr at about 18 km below which the two-sigma trend error becomes unreasonably large. The vertical water vapor trends for the tropical, midlatitude, and polar trends are shown in Figure 6.20, 6.21, and 6.22, respectively. The

small negative trend seen in Figure 6.18 at 38 km is also seen in the midlatitude trend at the same altitude. The trend in the middle stratosphere from 25-32 km is seen over similar altitude ranges, with similar magnitudes, in the trends of all three regimes. The lower stratospheric trend around 18 km is seen in the tropical and midlatitude regimes, with larger magnitudes than the zonal trend.

As shown here, zonal vertical trends in the lower stratosphere are a combination of tropospheric and stratospheric air; how much of each will depend of the relative

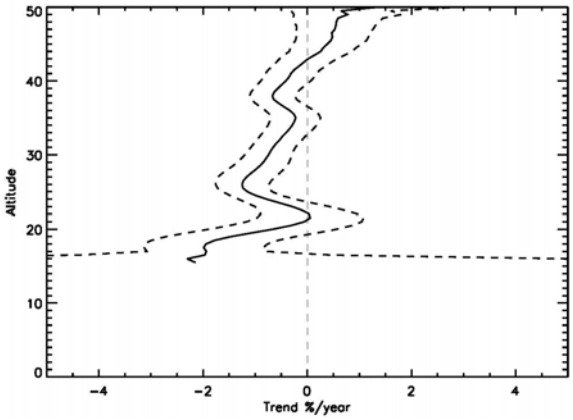

Figure 6.19 SAGE zonal water vapor trend in percent per year calculated for October 1984 to May 1991 between 25° and 60°N. The gray dashed line is the zero line. The dark dashed lines are the two-sigma trend error.

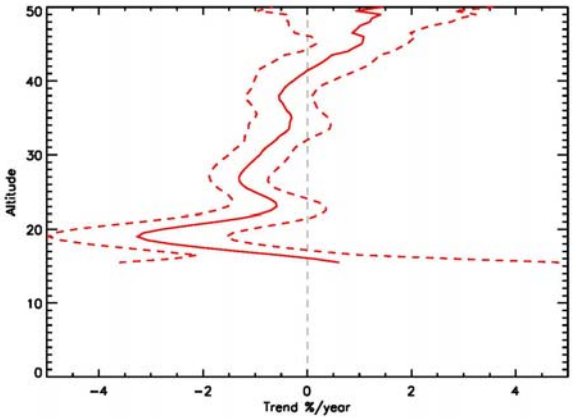

Figure 6.20 SAGE tropical water vapor trend in percent per year calculated for October 1984 to May 1991 between 25° and 60°N. Line designations are as in Figure 6.19.

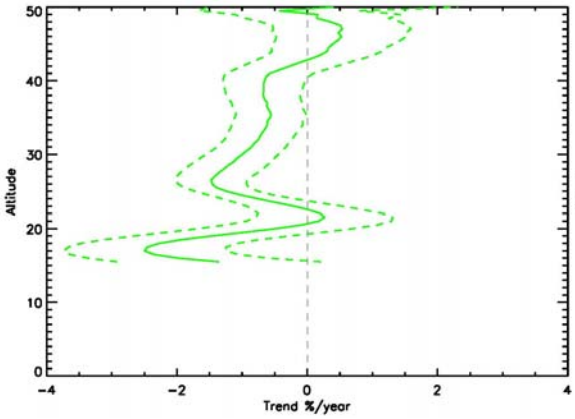

Figure 6.21 SAGE midlatitude water vapor trend in percent per year calculated for October 1984 to May 1991 between 25° and 60°N. Line designations are as in Figure 6.19.

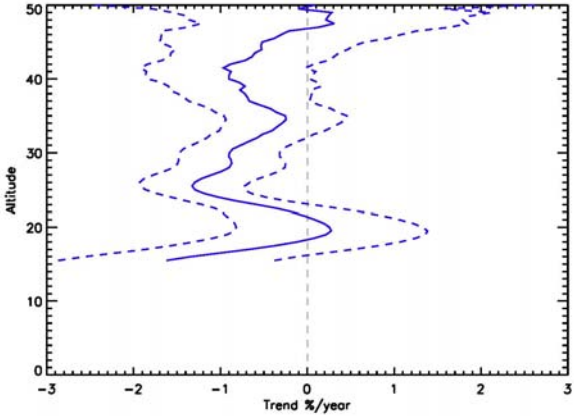

Figure 6.22 SAGE polar water vapor trend in percent per year calculated for October 1984 to May 1991 between 25° and 60°N. Line designations are as in Figure 6.19.

weighting of each meteorological regime. For example, because the relative areas of each regime did not significantly change over the time period from October 1984 to May 1991, changes within the regimes must dominate the zonal ozone trend. Upon examination of the ozone trends within each regime, it is concluded that ozone depletion in the lower stratosphere of the midlatitude and polar regimes was responsible for the zonal decrease observed.

The trends here were calculated over very short time periods due to lack of data and the eruption of Mt. Pinatubo, and should therefore be viewed with caution. The example given just above covers only about six years and shows no significant trend in the relative areas of each regime. However, if the relative area trends are taken from January 1979 to May of 1991, as they are in Chapter 4, the overall picture becomes different because the trends over this time period are significant. Thus, care should be taken not only when choosing the time period over which a trend will be calculated, but also in the interpretation of those trends. Nevertheless, the examples presented here are consistent with the idea of meteorological regimes and reinforce the conclusion that a true understanding of trends in the lower stratosphere involves understanding both changes within each regime and changes in the relative weighting of each regime over time.

Chapter 7: Summary, Conclusions, and Future Work

7.1 Summary and Conclusions

In the preceding chapters I have shown that the Northern Hemisphere total ozone field can be divided into meteorological regimes, separated by the subtropical and polar upper troposphere fronts, as defined by Hudson et al. (2003). The upper troposphere fronts are characterized by large gradients in wind speed, temperature, tropopause height, potential vorticity, and total ozone (Bluestein 1993; Reed 1955; Shalamyanskiy and Romashkina 1980; Shapiro et al. 1982). The regions away from the fronts are characterized by small gradients in tropopause height and total ozone (Defant and Taba 1957; Karol et al. 1987).

In this work, the subtropical and polar fronts were initially defined using ozone contours to represent the gradients in total ozone across the fronts (Hudson et al. 2003). Using data adapted from Karol et al. (1987) and from TOMS, these contours were obtained using an iterative process that calculated new boundary values by taking the average of the neighboring regimes' mean total ozone. This method was validated using rawinsondes, ozonesondes, and 200 mb winds from the NCEP reanalysis (Hudson et al. 2003; Andrade 2004). Using these data, it was determined that the boundaries calculated as ozone contours corresponded well to regions of high winds. In addition, relatively constant total ozone, tropopause heights and ozonepause heights were found within each regime. However, the total ozone within each regime displayed a latitude dependence unaccounted for by the ozone-contour method. Thus I developed a new method to allow the boundary values to vary with latitude. This method was applied to the TOMS data

from 1979-2004. Relatively constant total ozone was again found within each regime, despite large overlaps in latitude. In other words, within a regime, total ozone and tropopause height were found to be fairly homogeneous. Abrupt changes were only observed when crossing a boundary, i.e. upper troposphere front. The new boundaries calculated agree well with those calculated previously, such that the validation performed for the old boundaries in Hudson et al. (2003) and Andrade (2004) should be valid for the new method as well.

Though this method was applied to every day TOMS data was available, the period January 1979- May 1991 was chosen to examine in detail because it has been the subject of previous study (WMO 1999, 2003) and because it is a period of known ozone depletion (Staehelin et al. 2001). WMO 1999 reported a -3.15 %/decade decrease in total ozone from 25°-60°N over this time period. When the monthly mean total ozone within each regime was examined, statistically significant negative trends of -1.4 ± 1.0 %/decade, -2.3 ± 0.5 %/decade, and -3.0 ± 0.7 %/decade were observed within the tropical, midlatitude, and polar regimes, respectively. The monthly mean relative areas of each regime showed an increase in the relative area of the tropical regime over this time period, and a decrease in the area of the polar regime. Since the tropical/polar regime has the lowest/highest values of total ozone, an increase/decrease in the relative area of the tropical regime could contribute to a negative trend. Upon examining the overall contribution by each regime over this time period it was found that despite a negative trend in total ozone, the tropical regime had a positive contribution. This implies that the area of the tropical regime is increasing faster than the rate of decay of its mean ozone. Therefore based on this analysis, I conclude that total ozone changes within

a zonal band are the result of changing ozone within each regime as well as changes in the relative areas of each regime.

Using equation 4.7, the portion of the zonal trend that arises from changes in the total ozone within each regime was separated from the portion arising from changes in the relative areas in order to estimate their relative roles. From this analysis, I conclude that 35% of the zonal trend between 25°-60°N from January 1979 – May 1991 can be ascribed to movement of the upper troposphere fronts. The remaining 65% could have both chemical and/or dynamical origins. For example, ozone depletion by homogeneous and heterogeneous chemistry and an overall weakening of the Brewer-Dobson circulation over this time period would both cause a negative total ozone trend within a regime.

The increase in the area of the tropical regime and decrease in the area of the polar regime imply a net poleward movement of the subtropical and polar upper troposphere fronts. To quantify this, I used the relative areas to calculate the mean latitudes of these fronts. A linear fit through the resulting mean latitudes yields a poleward shift of the subtropical front of 1.1 degrees per decade, and 1.2 degrees per decade for the polar front from January 1979 to May 1991. I repeated the procedure for the entire TOMS period from 1979-2004. The trend for the subtropical front was one degree per decade and the trend for the polar front was 0.5 degrees per decade. This poleward movement is consistent with other works (McCormack and Hood 1997; McCabe et al. 2001; Fu et al. 2006), and represents a climate change, as storm tracks tend to follow the upper troposphere fronts.

In order to estimate the robustness of the boundaries for trend analysis, I conducted an experiment using two runs from the NASA-GSFC 3D FCTM. The first run

contained observed aerosol and source gas concentrations. The second held source gases to their 1979 level. The dynamics for the two runs were calculated offline, and were thus identical. If the positions of the subtropical and polar fronts are the same in both runs, then there should be no difference in the calculated relative areas of each regime, despite the large and latitudinally dependent changes in ozone in the former model run.

The calculated boundaries were plotted on top of one another for four days in 1994 and 2003. The year 1994 was chosen because it is after a period of ozone depletion by chlorine (WMO 1999, Solomon 1999). The year 2003 was chosen to establish that there was no drift in the boundaries calculated, as it is late in the time period studied. Excellent agreement between the two was obtained. In order to establish possible trend bias, trends were calculated from January 1983 – May 1991, and January 1983 – December 2003. These time periods were chosen for the reasons listed above. No statistically significant trends in the relative areas were found, and the trends calculated were not statistically different from one another. Therefore, I found no biases in the relative area trends as a result of long term changes in total ozone were found and thus I conclude that the trends reported in this analysis can be considered reliable and robust.

Hudson et al. (2003) used data from ozonesondes to show that each regime was characterized by a unique ozonepause height and lower stratospheric profile shape. The upper troposphere / lower stratosphere region is one characterized by complex interactions between dynamics, chemistry, microphysics, and radiation. As explained in Chapter 5, ozone and water vapor are two essential chemical species affected by all of these processes. More accurate assessments of the budgets of these two species, how

they are affected by stratosphere-troposphere exchange, and their impact on the radiative balance in this region are essential for reliable predictions of climate change.

Using the results of the improved method of separating the Northern Hemisphere into meteorological regimes, I classified ozone profiles from the HALOE and SAGE satellite instruments by regime from 1997-2004. HALOE and SAGE are limb-scanning instruments that use the solar occultation technique to infer vertical profiles of various chemical species. Most limb-scanning retrieval algorithms assume a homogeneous atmosphere along the slant path for their calculations (Chu et al. 1993). However, the upper troposphere fronts are regions of profile inhomogeneity, due to the tropopause height change across them (Bluestein 1993), and this is not accounted for in the retrieval. The subtropical, polar, and arctic boundaries were subsequently widened by one pixel in latitude and longitude so as to ensure that the measurements included in this analysis were along a homogeneous slant path, i.e. within a meteorological regime.

When ozone profiles from HALOE for January 8, 2001 were classified by regime, similar results to Hudson et al. (2003) were obtained. The HALOE measurements on this day were taken over ~2 degrees latitude, but cover a wide range of longitudes. Despite being over a narrow latitude band, each regime showed a distinct ozonepause height and profile shape in the mid and lower stratosphere. Thus, if a zonal average was taken over this narrow latitude band at about 15 km of altitude, it would contain both tropospheric and stratospheric air, contaminating the average. By classifying profiles into meteorological regimes, the lower stratosphere and upper troposphere can be isolated, which is essential for the calculation of trends in these regions.

Monthly ozone profile climatologies were calculated for both SAGE and HALOE and for each regime from 1997-2004 for 25°-60°N. The climatologies showed distinct ozonepause heights and lower stratospheric profile shapes within each regime. In addition, below ~23 km the standard deviation of the zonal data with no classification is larger than the standard deviations of each regime for both instruments. This indicates a reduction in variability in the lower stratosphere when separating by regime. There was also excellent agreement between the two instruments in spite of the differences in the latitude distributions of the measurements, chosen wavelengths, and retrieval techniques.

The agreement between the climatologies deteriorates above ~25 km, as does the regime separation. This corresponds to the region where photochemistry begins to dominate the distribution of ozone. When the March profiles for 1997-2004 from 25°-60°N were separated into low, middle, and high latitude bands, a clear separation in the mid to upper stratosphere was obtained, whereas the distributions in the lower stratosphere overlapped. This indicated that the meteorological regime influence extends up to approximately 25 km, above which, the ozone distribution tends to be photochemically dominated.

Both SAGE and HALOE also measure vertical profiles of water vapor. When water vapor profiles measured on January 8, 2001 were separated into meteorological regimes, they showed similar hygropause heights within a regime. The mixing ratio value at the hygropause varied within a regime, however. In addition, the difference in hygropause heights between regimes was smaller than the difference in ozonepause heights. Thus I concluded that while water vapor profiles appeared to show distinction when classified into meteorological regimes, this distinction was less than that for ozone.

Monthly ozone profile climatologies were calculated for both SAGE and HALOE and for each regime from 1997-2004 from 25°-60°N. The larger variability within a regime seen in the one day separation was also seen in the monthly climatologies. The variability for each regime and the zonal data increases below ~15 km for both instruments, corresponding to a known increase in instrument uncertainty and increased atmospheric variability (Thomason et al. 2004). Despite these large uncertainties, the same general features are seen in the two sets of climatologies. For example, the tropical regime has the highest mean hygropause height, followed by the midlatitude, and then the polar. March shows the clearest separation between regimes, displaying distinct hygropause heights, and mixing ratios for each regime. Other months show overlap between climatologies for the reasons discussed in sections 5.5 and 5.8. While the agreement between the two climatologies is not as good as for ozone, they agree within experimental error. Overall, water vapor does appear to separate by regime, however large uncertainties in the lower stratosphere make it difficult to conclude in terms of statistical significance.

I have shown here that, below ~25 km, each regime is characterized by a unique ozone and water vapor profile shape. Therefore, zonal averages, and as a result, zonal trends, calculated at mid-latitudes in the lower stratosphere and upper tropospheric are erroneous and misleading. By first classifying profiles into meteorological regimes, the lower stratosphere and upper troposphere can be isolated, which is essential for quantification of both chemical and transport processes in these regions. Thus, similar to trends in total ozone, changes in this region will also be the result of changes within each regime and changes in the contributions made by each regime over time.

Two time periods were examined, October 1984 – May 1991 and 1997-2004. The latter time period did not show any statistically significant total ozone or relative area trends within each regime between 25° and 60°N. Therefore, any changes seen in the vertical profile over this time period must be the result of changes within each regime. There are no statistically significant ozone trends in the lower stratosphere of each regime. There is a positive trend in the upper stratosphere of the tropical regime that appears inconsistent with the lack of a trend in total ozone. As previously mentioned in Chapter 3, TOMS data after 2003 is questionable for trend analysis. Since the positive trend in the upper stratosphere is consistent with previous results (Newchurch et al. 2003), it is possible the TOMS data is inaccurate.

The HALOE zonal trend in water vapor shows negative trends from 16-35 km. Again, zonal trends over this time period must be the result of changes within each regime, and as expected, negative trends over similar altitude ranges were observed in the tropical and midlatitude regimes. The polar regime only showed negative trends from ~10-16 km, indicating that contributions from the tropical and midlatitude regimes dominated the zonal trend over this time period.

The period October 1984 – May 1991 was chosen because it is a period of known ozone depletion by homogeneous and heterogeneous chemistry, and transport through dynamical processes (Salby and Callaghan 1993; Solomon 1999; WMO 1999; Staehelin et al. 2001; Randel et al. 2002; Hudson et al. 2006). Only SAGE data was available for this analysis. The zonal ozone profile trend shows negative trends in the lower stratosphere. Looking at the changes in total ozone within each regime, the polar total ozone shows a statistically significant negative slope, the midlatitude shows no trend, and

the tropical shows a positive slope. The tropical regime increase is most likely the result of the transition from solar minimum to solar maximum over this time period. Again, the relative areas of this time period show no statistically significant trend. It should be emphasized that this does not contradict the previously calculated relative area trends from January 1979 – May 1991. The trends here were calculated over very short time periods due to lack of data and the eruption of Mt. Pinatubo, and should therefore be viewed with caution. Care should be taken not only when choosing the time period over which a trend will be calculated, but also in the interpretation of those trends.

The ozone profile trends are consistent with the total ozone trends. The tropical regime shows a positive trend in the upper stratosphere, the midlatitude shows a positive trend in the upper stratosphere and a negative trend in the lower stratosphere, and the polar only shows a negative trend in the lower stratosphere. The lower stratospheric trends in the midlatitude and polar regimes are similar in altitude range and magnitude as the zonal trend. Thus it is concluded that ozone depletion in the lower stratosphere of the midlatitude and polar regimes was responsible for the zonal decrease observed from October 1984 – May 1991.

The zonal water vapor trend shows negative trends at 38 km, from 25-32 km, and at about 18 km below which the two-sigma trend error becomes large. The trend in the middle stratosphere from 25-32 km is seen over similar altitude ranges, with similar magnitudes, in the trends of all three regimes. The lower stratospheric trend around 18 km is seen in the tropical and midlatitude regimes, with larger magnitudes than the zonal trend, and is not seen in the polar trend.

Though over short time periods, the examples presented here are consistent with the idea of meteorological regimes and reinforce the major conclusion of my work. A true understanding of zonal trends in either the column or in the lower stratosphere involves understanding both changes within each regime and changes in the relative weighting of each regime over time.

In summary, the main conclusions of my work are:

- The Northern Hemisphere can be separated into meteorological regimes, characterized by relatively constant total ozone and tropopause height.
- Total ozone changes within a zonal band are the result of changing ozone within each regime as well as changes in the relative areas of each regime.
- 35% of the zonal trend between 25°-60°N from January 1979 – May 1991 can be ascribed to a net poleward movement of the subtropical and polar upper troposphere fronts. The remaining 65% is the result of changes in total ozone within each regime.
- A linear fit yields a poleward shift of the subtropical front of 1.1 degrees per decade, and 1.2 degrees per decade for the polar front from January 1979 to May 1991. From 1979-2004, the trend for the subtropical front was 1.0 degrees per decade and the trend for the polar front was 0.5 degrees per decade. These frontal movements represent a climate change.
- Each regime shows distinct ozonepause heights and profile shapes in the mid and lower stratosphere.
- The meteorological regime influence extends up to approximately 25 km, above which, the ozone distribution tends to be photochemically dominated.

- Overall, water vapor profiles separate by regime, however, the distinction between regimes is less than that for ozone, and large uncertainties in the lower stratosphere make it difficult to conclude in terms of statistical significance.
- I have shown here that, below ~25 km, each regime is characterized by a unique ozone and water vapor profile shape. Therefore, zonal averages, and as a result, zonal trends, calculated at mid-latitudes in the lower stratosphere and upper tropospheric are erroneous and misleading.
- Similar to trends in total ozone, changes in this region will also be the result of changes within each regime and changes in the contributions made by each regime over time.
- Ozone depletion observed in the lower stratosphere between 25° and 60°N from October 1984 – May 1991 was the result of depletion in the lower stratosphere in the midlatitude and polar regimes.
- A true understanding of zonal trends in either the column or in the lower stratosphere involves understanding both changes within each regime and changes in the relative weighting of each regime over time.

7.2 Future Work

By using this method of classification into meteorological regimes, the lower stratosphere can be uniquely isolated. Thus, the logical next step in this work is to examine the time series of ozone and water vapor in the lower stratosphere and refine the trends calculated. This will be done by lengthening the time period observed (as discussed below) and applying a multivariate regression. Only linear fits to the data were

used here, however as explained earlier, ozone within a regime is affected by both the 11-yr solar cycle and the QBO. Thus, a similar regression analysis as was done on the column should be done on various levels in the vertical.

In order to calculate reliable trends, the time period over which they are calculated must be extended. The gap in the TOMS data prevents this. However, TIROS Operational Vertical Sounder (TOVS) data can be used. The TOVS series of instruments measures ozone in the lower stratosphere using infrared and microwave emissions, specifically using the suppression of surface emission at 9.7 μm. The total ozone is calculated by holding the mid- and upper-stratospheric components as constants that vary as a function of latitude (Neuendorffer 1996). Studies have been done comparing TOVS to other total ozone measurements (Neuendorffer 1996; Corlett and Monks 2001). It was found that TOVS overestimates total ozone by ~20 DU at high latitudes, and underestimates total ozone by ~10-15 DU at equatorial latitudes with respect to TOMS. This is not very good agreement; however, TOVS measures lower stratospheric ozone and will reflect the changes in total ozone across the upper troposphere fronts. These gradients in total ozone are what are used to locate the positions of the upper tropospheric fronts, not the total ozone values themselves. Therefore the relative accuracy of TOVS is more important than the absolute accuracy.

TOVS also allows the analysis to extend up to 90°N because it is not affected by polar night. By calculating the relative areas from 25-90°N a clearer picture of their trends can be obtained. For example, the decrease in the polar relative area from January 1979 – May 1991 could also be the result of a change in the amplitude of the polar front over time. If the amplitude increases, less of the polar regime could reside below 60°N,

resulting in a decrease in relative area. Therefore, in order to accurately determine the evolution of the polar front, a complete hemispheric picture is needed.

Preliminary results show good agreement between the TOVS- and TOMS-calculated boundaries, but more analysis is needed before the TOVS boundaries can be used for relative area trends. They should however, be adequate for classification of profiles. Since the boundaries must be widened in order to accurately separate profiles into regimes, they are less sensitive to differences between the TOVS- and TOMS-calculated boundaries. Thus, classifying profiles from HALOE and SAGE using the TOVS boundaries can also be used as further validation, in addition to providing more years for profile trend analysis.

References

Ackerman, S. A., and J. A. Knox, 2003: *Meteorology: Understanding the Atmosphere*. Thompson Learning Inc., Pacific Grove, CA, 486pp.

Andrade, M. F., 2004: *Stratospheric ozone trends as determined by regime analysis: The Southern Hemisphere*. Dissertation, Department of Atmospheric and Oceanic Science, University of Maryland, College Park, MD, 146pp.

Appenzeller, C., A. K. Weiss, and J. Staehelin, 2000: North Atlantic Oscillation modulates total ozone winter trends, *Geophys. Res. Lett.*, **27**, 1131-1134.

Baldwin, M. P., and Coauthors, 2001: The quasi-biennial oscillation. *Rev. Geophys.*, **39**, 179-229.

Bethan, S., G. Vaughan, and S. J. Reid, 1996: A comparison of ozone and thermal tropopause heights and the impact of tropopause definition on quantifying the ozone content of the atmosphere. *Q. J. Roy. Meteor. Soc.*, **122**, 929-944.

Bhatt, P. P., E. E. Remsberg, L. L. Gordley, J. M. McInerney, V. G. Brackett, and J. M. Russell III, 1999: An evaluation of the quality of Halogen Occultation Experiment ozone profiles in the lower stratosphere. *J. Geophys. Res.*, **104**, 9261-9275.

Bluestein, H. B., 1993: *Synoptic-dynamic meteorology in midlatitudes: Vol II*. Oxford University Press, New York, NY, 594 pp.

Brasseur, G., 1993: The response of the middle atmosphere to long-term and short-term solar variability: A two-dimensional model. *J. Geophys. Res.*, **98**, 23 079-23 090.

Brasseur, G. and S. Solomon, 1984: *Aeronomy of the middle atmosphere*. D. Reidel Publishing Company, Dordrecht, Holland, 441pp.

Brewer, A. W., 1949: Evidence for a world circulation provided by measurements of helium and water vapor distribution in the stratosphere. *Q. J. Roy. Meteor. Soc.*, **75**, 351-363.

Brönnimann, S., and L. L. Hood, 2003: Frequency of low-ozone events over northwestern Europe in 1952-1963 and 1990-2000. *Geophys. Res. Lett.*, **30**, doi:10.1029/2003GL018431.

Brühl, C., and Coauthors, 1996: Halogen Occulation Experiment ozone channel validation. *J. Geophys. Res.*, **101**, 10 217-10 240.

Chandra, S., and R. D. McPeters, 1997: The solar cycle variation of ozone in the stratosphere inferred from Nimbus 7 and NOAA 11 satellites. *J. Geophys. Res.*, **90**, 20 665-20 671.

Chiou, E. W., L. W. Thomason, and W. P. Chu, 2006: Variability of stratospheric water vapor inferred from SAGE II, HALOE, and Boulder (Colorado) balloon measurements. J Climate, 19, 4121-4133.

Chu, W. P., M. P. McCormick, J. Lenoble, C. Brogniez, and P. Pruvost, 1989: SAGE II inversion algorithm. *J. Geophys. Res.*, **94**, 8339-8351.

Chu, W. P., E. W. Chiou, J. C. Larsen, L. W. Thomason, D. Rind, J. J. Buglia, S. Oltmans, M. P. McCormick, and L. M. McMaster, 1993: Algorithms and sensitivity analyses for Stratospheric Aerosol and Gas Experiment II water vapor retrieval. *J. Geophys. Res.*, **98**, 4857-4866.

Corlett, G.K, and P.S. Monks, 2001: A comparison of total column ozone values derived from the Global Ozone Monitoring Experiment (GOME), the Tiros Operational

Vertical Sounder (TOVS), and the Total Ozone Mapping Spectrometer (TOMS). *J. Atmos. Sci.*, **58**, 1103-1116.

Cunnold, D. M., W. P. Chu, R. A. Barnes, M. P. McCormick, and R. E. Veiga, 1989: Validation of SAGE II ozone measurements. *J. Geophys. Res.*, **94**, 8447-8460.

Danielsen, E. F., 1968: Stratospheric-tropospheric exchange based on radioactivity, ozone and potential vorticity. *J. Atmos. Sci.*, **25**, 502-518.

Danielsen, E. F., R. Bleck, J. Shedlovsky, A. Wartburg, P. Haagenson, and W. Pollock, 1970: Observed distribution of radioactivity, ozone, and potential vorticity associated with tropopause folding. *J. Geophys. Res.*, **75**, 2353-2361.

Danielsen, E. F., and R. S. Hipskind, 1980: Stratospheric-tropospheric exchange at polar latitudes in summer. *J. Geophys. Res.*, **85**, 393-400.

Danielsen, E. F., R. S. Hipskind, S. E. Gaines, G. E. Sachse, G. L. Gregory, and G. F. Gills, 1987: Three-dimensional analysis of potential vorticity associated with tropopause folds and observed variations of ozone and carbon monoxide. *J. Geophys. Res.*, **92**, 2103-2111.

Defant, F., and H. Taba, 1957: The threefold structure of the atmosphere and the characteristics of the tropopause. *Tellus*, **9**, 259-274.

Dessler, A.E., E.J. Hintsa, E.M. Weinstock, J.G. Anderson, and K.R. Chan, 1995: Mechanisms controlling water vapor in the lower stratosphere: "A tale of two stratospheres". *J. Geophys. Res.*, **100**(D11), 23,167-23,172.

Dhomse, S., M. Weber, I. Wohltmann, M. Rex, and J. P. Burrows, 2006: On the possible causes of recent increases in northern hemispheric total ozone from a statistical analysis of satellite data from 1979 to 2003. *Atmos. Chem. Phys.*, **6**, 1165-1180.

Djuric, D., 1994: *Weather Analysis*. Prentice Hall, Englewood Cliffs, NJ, 304 pp.

Dobson, G. M., D. N. Harrison, and J. Lawrence, 1929: Measurements of the amount of ozone in the Earth's atmosphere and its relation to other geophysical conditions – Part III. *Proc. Roy. Soc. Lond.*, **A122**, 456-486.

Dobson, G. M., 1956: Origin and distribution of polyatomic molecules in the atmosphere. *Proc. Roy. Soc. Lond.*, **A236**, 187-193.

Douglass, A. R., C. J. Weaver, R. B. Rood, and L. Coy, 1996: A three-dimensional simulation of the ozone annual cycle using winds from a data assimilation system. *J. Geophys. Res.*, **101**, 1463-1474.

Finlayson-Pitts, B. J., and J. N. Pitts, 2000: *Chemistry of the upper and lower atmosphere: Theory, experiments, and applications*. Academic Press, San Diego, CA, 968 pp.

Fu, Q., C. M. Johanson, J. M. Wallace, and T. Reichler, 2006: Enhanced mid-latitude tropospheric warming in satellite measurements. *Science*, **312**, 1179.

Fusco, A. C., and M. L. Salby, 1999: Interannual variations of total ozone and their relationship to variations in planetary wave activity. *J. Climate*, **12**, 1619-1629.

Grooβ, J. -U., and J. M. Russell, 2005: Technical note: A stratospheric climatology for O_3, H_2O, CH_4, NO_x, HCl and HF derived from HALOE measurements. *Atmos. Chem. Phys.*, **5**, 2797-2807.

Hadjinicolau, P., J. A. Pyle, N. R. P. Harris, 2005: The recent turnaround in stratospheric ozone over northern middle latitudes: A dynamical modeling perspective. *Geophys. Res. Lett.*, **32**, L12821, doi:10.1029/2005GL022476.

Harries, J. E., and Coauthors, 1996: Validation of measurements of water vapor from the Halogen Occultation Experiment (HALOE). *J. Geophys. Res.*, **101**, 10 205-10 216.

Hartmann, D. L., 1994: *Global Physical Climatology*. Academic Press, San Diego, CA, 411 pp.

Heath, D., and B. Schlesinger, 1986: The Mg 280 nm doublet as a monitor of changes in solar ultraviolet irradiance, *J. Geophys. Res.*, **91**, 8672-8682.

Herman, J. R., and Coauthors, 1996: Meteor-3 Total Ozone Mapping Spectrometer (TOMS) data product user's guide. NASA reference publication, No. 1393, 61pp.

Hervig, M. and M. McHugh, 1999: Cirrus detection using HALOE measurements. *Geophys. Res. Lett.*, **26**, 719-722.

Hoerling, M. P., T. K. Schaak, and A. J. Lenzen, 1991: Global objective tropopause analysis. *Mon. Wea. Rev.*, **119**, 1816-1831.

Hoinka, K. P., H. Claude, and U. Köhler, 1996: On the correlation between tropopause pressure and ozone above central Europe. *Geophys. Res. Lett.*, **23**, 1753-1756.

Hoinka, K. P., 1998: Statistics of the global tropopause pressure. *Mon. Wea. Rev.*, **126**, 3303-3325.

Holton, J. R., 1992: *An introduction to dynamic meteorology.* Academic Press, San Diego, CA, 511pp.

Holton, J. R., P. H. Haynes, M. E. McIntyre, A. R. Douglass, R. B. Rood, and L. Pfister, 1995: Stratosphere-troposphere exchange. *Rev. Geophys.*, **33**, 403-440.

Hood, L. L., S. Rossi, and M. Beulen, 1999: Trends in lower stratospheric zonal winds, Rossby wave breaking behavior, and column ozone at northern midlatitudes. *J. Geophys. Res.*, **104**, 24 321-24 339.

Hood, L. L., B. E. Soukharev, M. Fromm, and J. P. McCormack, 2001: Origin of extreme ozone minima at middle to high northern latitudes. *J. Geophys. Res.*, **106**, 20 925-20 940.

Hood, L. L., and B. E. Soukharev, 2005: Interannual variations of total ozone at northern midlatitudes correlated with stratospheric EP flux and potential vorticity. J. Atmos. Sci., 62, 3724-3740.

Hoskins, B. J., M. E. McIntyre, and A. W. Robertson, 1985: On the use and significance of isentropic potential vorticity maps. *Q. J. Roy. Meteor. Soc.*, **111**, 877-946.

Hudson, R. D., A. D. Frolov, M. F. Andrade, and M. B. Follette, 2003: The total ozone field separated into meteorological regimes. Part I: Defining the regimes. *J. Atmos. Sci.*, **60**, 1669-1677.

Hudson, R. D., M. F. Andrade, M. B. Follette, and A. D. Frolov, 2006: The total ozone field separated into meteorological regimes. Part II: Northern Hemisphere mid-latitude total ozone trends. Accepted to *Atmos.Chem. Phys.*.

James, P. M., 1998: A climatology of ozone mini-holes over the Northern Hemisphere. *Int. J. Climatol.*, **18**, 1287-1303.

Kalnay, E., and Coauthors, 1996: The NCEP/NCAR 40-Year reanalysis project. *Bull. Amer. Meteor. Soc.*, **77**, 437–471.

Keyser, D., and M. A. Shapiro, 1986: A review of the structure and dynamics of upper-level frontal zones. *Mon. Wea. Rev.*, **114**, 452-499.

Kistler, R., and Coauthors, 2001: The NCEP–NCAR 50-Year reanalysis: Monthly means CD-ROM and documentation. *Bull. Amer. Meteor. Soc.,* **82,** 247–267.

Kley, D., E. J. Stone, W. R. Henderson, J. W. Drummond, W. J. Harrop, A. L. Schmeltekopf, T. L. Thompson, and R. H. Winkler, 1979: In situ measurements of the mixing ratio of water vapor in the stratosphere. *J. Atmos. Sci.*, **36**, 2513-2524.

Kley, D., and Coauthors, 2000: SPARC assessment of upper tropospheric and stratospheric water vapor. WCRP 113, WMO/TD-1043, SPARC Rep. 2, World Clim. Res. Program, Geneva, 312 pp.

Krzyścin, J. W., M. Degórska, and B. Rajewska-Więch, 2001: Impact of interannual meteorological variability on total ozone in northern middle latitudes: A statistical approach. *J. Geophys. Res.*, **106**, 17 953-17960.

Lee, S., and H. Kim, 2003: The dynamical relationship between subtropical and eddy-driven jets. *J. Atmos. Sci.*, **60**, 1490-1503.

Letexier, H., S. Solomon, and R.R. Garcia, 1988: The role of molecular hydrogen and methane oxidation in the water vapor budget of the stratosphere. *Quart. J. Roy. Meteor. Soc.*, **114**, 281-295.

Lutgens, F. K., E. J. Tarbuck, 1998: *The atmosphere*. Prentice Hall Inc., Upper Saddle River, New Jersey, 434pp.

McCabe, G. J., M. P. Clark, M. C. Serreze, 2001: Trends in Northern Hemisphere surface cyclone frequency and intensity. *J. Climate*, **14**, 2763-2768.

McCormack, J. P., and L. L. Hood, 1997: The frequency and size of ozone “mini-hole” events at northern midlatitudes in February. *Geophys. Res. Lett.*, **24**, 2647-2650.

McPeters, R. D., and Coauthors, 1996: Nimbus-7 Total Ozone Mapping Spectrometer (TOMS) data product user's guide. NASA reference publication, No. 1384, 73pp.

McPeters, R. D., and Coauthors, 1998: Earth Probe Total Ozone Mapping Spectrometer (TOMS) data product user's guide. NASA reference publication, No. 1998-206895, 70pp.

Mote P. W., and Coauthors, 1996: An atmospheric tape recorder: The imprint of tropical tropopause temperatures on stratospheric water vapor. *J. Geophys. Res.*, **101**, 3989-4006.

Morris G. A., J. F. Gleason, J. M. Russell, M. R. Schoeberl, and M. P. McCormick, 2002: A comparison pf HALOE v19 with SAGE II V6.00 ozone observations using trajectory mapping. *J. Geophys. Res.*, **107**, 4177, doi:10.1029/2001JD000847.

Nash, E. R., P. A. Newman, J. E., Rosenfield, M. R. Schoeberl, 1996: An objective determination of the polar vortex using Ertel's potential vorticity. *J. Geophys. Res.*, **101**, 9471-9478.

Neuendorffer, A.C., 1996: Ozone monitoring with TIROS-N operational vertical sounders. *Geophys. Res.*, **101**, 18 807-18 828.

Oltmans, S. J., H. Vömel, D. J. Hofmann, K. H. Rosenlof, and D. Kley, 2000: The increase in stratospheric water vapor from balloonborne, frostpoint hygrometer measurements at Washington, D.C., and Boulder, Colorado. *Geophys. Res. Lett.*, **27**, 3453-3456.

Petzoldt, K., B. Naujokat, and K. Neugebohren, 1994: Correlation between stratospheric temperature, total ozone, and tropospheric weather systems. *Geophys. Res. Lett.*, **21**, 1203-1206.

Poulida, O., R. R. Dickerson, and A. Heymsfield, 1996: Stratosphere-troposphere exchange in a midlatitude mesoscale convective complex: 1. Observations. *J. Geophys. Res.*, **101**, 6823-6836.

Randall, C. E., and Coauthors, 2003: Validation of POAM III ozone: Comparisons with ozonesondes and satellite data. *J. Geophys. Res.*, **108**, 4367, doi:10.1029/2002JD002944.

Randel, W. J., R. S. Stolarski, D. M. Cunnold, J. A. Logan, M. J. Newchurch, and J. M. Zawodny, 1999: Trends in the vertical distribution of ozone. *Science*, **285**, 1689-1692.

Randel , W. J., F. Wu, and R. S. Stolarski, 2002: Changes in column ozone correlated with the stratospheric EP flux. *J. Meteorol. Soc. Japan*, **80**, 849-862.

Randel, W. J., F. Wu, S. J. Oltmans, K. Rosenlof, G. E. Nedoluha, 2004: Interannual changes in stratospheric water vapor and correlations with tropical tropopause temperatures. *J. Atmos. Sci.*, **61**, 2133-2148.

Randel, W.J., F. Wu, H. Vömel, G. Nedoluha, and P. Forster, 2006: Decreases in stratospheric water vapor after 2001: Links to changes in the tropical tropopause and the Brewer-Dobson circulation. *J. Geophys. Res.*, **111**, D12312, doi:10.1029/2005JD006744.

Reed, R., 1955: A study of a characteristic type of upper-level frontogenesis. *J. Meteorol.*, **12**, 226-237.

Reid, S. J., A. F. Tuck and G. Kiladis, 2001: On the changing abundance of ozone minima at northern midlatitudes. *J. Geophys. Res.*, **105**, 12 169-12180.

Reinsel, G. C., A. J. Miller, E. C. Weatherhead, L. E. Flynn, R. M. Nagatani, G. C. Tiao, and D. J. Wuebbles, 2005: Trend analysis of total ozone data for turnaround and dynamical contributions. *J. Geophys. Res.*, **110**, D16306, doi:10.1029/2004JD004662.

Reiter, E. R., 1975: Stratospheric-tropospheric exchange processes. *Rev. Geophys. Space Phys.*, **13**, 459-474.

Rosenlof, K. H., and Coauthors, 2001: Stratospheric water vapor increases over the past half-century. *Geophys. Res. Lett.*, **28**, 1195-1198.

Rosenlof, K. H., 2002: Transport changes inferred from HALOE water and methane measurements. *J. Meteorol. Soc. Japan*, **80**, 831-848.

Russell, J. M., and Coauthors, 1993: The halogen occultation experiment. *J. Geophys. Res.*, **98**, 10 777-10 797.

Salby, M. L., and P. F. Callaghan, 1993: Fluctuations of total ozone and their relationship to stratospheric air motions. *J. Geophys. Res.*, **98**, 2715-2727.

Salby M. L., and P. F. Callaghan, 2004: Systematic changes of Northern Hemisphere ozone and their relationship to random interannual changes. *J. Climate*, **17**, 4512-4521.

Schubert, S. D., and M.J. Munteanu, 1988: An analysis of tropopause pressure and total ozone correlations. *Mon. Wea. Rev.*, **116**, 569-582.

Seidel, D., R. J. Ross, J. K. Angell, and G. C. Reid, 2001: Climatological characteristics of the tropical tropopause as revealed by radiosondes. *J. Geophys. Res.*, **106**, 7857-7878.

Shalamyanskiy, A. M., and A. K. Romashkina, 1980: Distribution and variation in the total ozone concentration in various air masses. *Izv. Acad. Sci. USSR, Atmos. Oceanic Phys.*, **16**, 931-937.

Shapiro, M. A., 1978: Further evidence of the mesoscale and turbulent structure of upper level jet stream-frontal zone systems. *Mon. Wea. Rev.*, **106**, 1100-1111.

Shapiro, M. A., 1980: Turbulent mixing within tropopause folds as a mechanism for the exchange of chemical constituents between the stratosphere and troposphere. *J. Atmos. Sci.*, **37**, 994-1004.

Shapiro, M. A., A. J. Krueger, and P. J. Kennedy, 1982: Nowcasting the position and intensity of jet streams using a satellite-borne Total Ozone Mapping Spectrometer, *Nowcasting*. Academic Press, San Diego, CA,137-145.

Shapiro, M. A., 1985: Dropwinsonde observations of an Icelandic low and a Greenland mountain-lee wave. *Mon. Wea. Rev.*, **113**, 680-683.

Shapiro M. A., T. Hampel, and A. J. Krueger, 1987: The arctic tropopause fold. *Mon. Wea. Rev.*, **115**, 444-454.

Solomon, S., R. W. Portmann, R. R. Garcia, L. W. Thomason, L. R. Poole, and M. P. McCormick, 1996: The role of aerosol variations in anthropogenic ozone depletion at northern midlatitudes. *J. Geophys. Res.*, **101**, 6713-6727.

Solomon, S., and Coauthors, 1998: Ozone depletion at mid-latitudes: Coupling of volcanic aerosols and temperature variability to anthropogenic chlorine. *Geophys. Res. Lett.*, **25**, 1871-1874.

Solomon, S., 1999: Stratospheric ozone depletion: A review of concepts and history. *Rev. Geophys.*, **37**, 275-316.

Staehelin, J., N.R.P. Harris, C. Appenzeller, and J. Eberhard, 2001: Ozone trends: A review. *Rev. Geophys.*, **39**, 231-290.

Steinbrecht, W., H. Claude, U. Köhler, and K. P. Hoinka, 1998: Correlations between tropopause height and total ozone: Implications for long-term changes. *J. Geophys. Res.*, **103**, 19 183-19 192.

Stenchikov, G., R. Dickerson, W. Ellis Jr., B. Doddridge, S. Kondragupta, O. Poulida, J. Scala, W.-K. Tao, 1996: Stratosphere-troposphere exchange in a midlatitude mesoscale convective complex: 2. Numerical simulations. *J. Geophys. Res.*, **101**, 6837-6852.

Stolarski, R., R. Bojkov, L. Bishop, C. Zerefos, J. Staehelin, J. Zawodny, 1992: Measured trends in stratospheric ozone. *Science*, **256**, 342-349.

Stolarski, R, S., and S. M. Frith, 2006: Search for evidence of trend slow-down in the long-term TOMS/SBUV total ozone data record: the importance of instrument drift uncertainty. *Atmos. Chem. Phys.*, **6**, 4057–4065.

Taha, G., L. W. Thomason, S. P. Burton, 2004: Comparison of Stratospheric Aerosol and Gas Experiment (SAGE) II version 6.2 water vapor with balloon-borne and space-based measurements. *J. Geophy. Res.*, **109**, D18313, doi:10.1029/2004JD004859.

Thomason, L. W., S. P. Burton, N. Iyer, J. M. Zawodny, and J. M. Anderson, 2004: A revised water vapor product for the Stratospheric Aerosol and Gas Experiment (SAGE) II version 6.2 data set. *J. Geophy. Res.*, **109**, D06312, doi:10.1029/2003JD004465.

Varotsos, C., C. Cartalis, A. Vlamakis, C. Tzanis, I. Keramitsoglou, 2004: The long-term coupling between column ozone and tropopause properties. *J. Clim.*, **17**, 3843-3854.

Wang, H. J., D. M. Cunnold, L. W. Thomason, J. M. Zawodny, and G. E. Bodeker, 2002: Assessment of SAGE version 6.1 ozone data quality. *J. Geophy. Res.*, **107**, 4691, doi:10.1029/2002JD002418.

Wellemeyer, C. G., P. K. Bhartia, R. D. McPeters, S. L. Taylor, and Ch. Ahn, 2004: A new release of data from the Total Ozone Mapping Spectrometer (TOMS), *SPARC Newsletter*, **22**, 37-38, available at www.aero.jussieu.fr/~sparc.

Wohltmann, I., M. Rex, D. Brunner, and J. Mäder, 2005: Integrated equivalent latitude as a proxy for dynamical changes in the ozone column. *Geophy. Res. Lett.*, **32**, L09811, doi:10.1029/2005GL022497.

World Meteorological Organization (WMO), 1957: Definition of the thermal tropopause. *WMO Bull*. **6**,136.

WMO, 1986: Atmospheric ozone 1985: Global ozone research and monitoring report. Report 16, World Meteorological Organization, Geneva, Switzerland, 392 pp.

WMO, 1998: SPARC/IOC/GAW Assessment of trends in the vertical distribution of ozone: 1998, Ozone Research and Monitoring Project, Rep. 43, 289 pp.

WMO, 1999: Scientific assessment of ozone depletion: 1998, Global Research and Monitoring Project, Rep. 44, Geneva, Switzerland, 496 pp.

WMO, 2003: Scientific assessment of ozone depletion: 2002, Global Research and Monitoring Project, Rep. 47, Geneva, Switzerland, 498 pp.